POWER SYSTEM STABILITY ASSESSMENT USING MEASUREMENT BASED MODAL ANALYSIS

by

© SAKTHIVEL RAJMURUGAN

A thesis submitted to the

School of Graduate Studies

in partial fulfilment of the

requirements for the degree of

Master of Engineering

Faculty of Engineering and Applied Science

Memorial University of Newfoundland

October 2018

St. John's Newfoundland

Abstract

Stability analysis of larger power system can be challenging and difficult. This is mainly due to the effect of several power system phenomena which are no longer negligible when the analysis is made on larger and complex power systems. The modelling of these unknown number of power system phenomena increases the overall model complexity. This causes the simulation more time consuming which does not help in improving stability of the system in the event of disturbance. Although, reduced order modelling of larger power system is considered as temporary solution, there is always a risk of producing different results than the actual power system response.

In this thesis, various types of measurement based modal analysis is studied in detail as an alternate approach to the conventional model based modal analysis. This is based on the fact that any disturbance given to the system excites a particular eigenvalue pair/s causing significant reduction in damping ratio and thereby moving the system towards instability. These eigenvalue pair/s of each generator can be extracted directly from obtained system response using various mathematical techniques.

Both time domain and frequency domain techniques are analyzed and compared with the results of model based modal analysis. Different IEEE test cases are considered based on the type of domain in which the data is analyzed.

Acknowledgements

At first, I like to thank my supervisor Dr. Benjamin Jeyasurya for his advice, guidance and constant support during my research.

Special appreciation is given to Natural Sciences and Engineering Research Council of Canada(NSERC), School of graduate studies and Memorial University of Newfoundland for providing financial support throughout my master's program.

Also, I like to thank Dr. Leonard Lye, Dr. Siu O'young and Dr. Cecilia Moloney for the graduate course they taught which helped me to fulfill my course requirements for this master's program.

Special thanks and appreciation to my parents, Rajmurugan Ganapathy and Devi Rajmurugan for giving moral support, without which this work is not possible.

Lastly, I like to thank all my friends and colleagues who supported me during my master's program.

Contents

List of Tables

List of Figures

Chapter 1

Introduction

1.1 Background of the research

In 1901, the concept of co-generation and distribution was adopted to meet the overall demand with the generation. This made the interconnection of power system present in various areas/ regions. The term tie-line was coined and has been highly monitored especially in the tie lines connecting power system of two countries. With time, more and more interconnection of power systems have been carried out and the system as a whole became more complex. This made it difficult for analyzing the stability of the power system causing risk in ensuring reliable power delivery to the consumers. Use of high processing units for solving the inter-connected power system reduced the processing times but the simulated results using a model proved to be different than that produced by the actual system. The western north-American blackout on 10^{th} August 1996 [1] and Northern India blackout on 30^{th} July 2012 [2] are some classic examples of power system instability due to effect of dynamic cascading.

1.2 Objective of the research

The main objectives of this research are listed as follows:

- To study about various types of instability and power system stability problems in power systems.
- To study about the modelling of various power system components for stability studies.
- To understand about the conventional method of modal analysis in power system for stability purposes and difficulties in extending it to a large power system.
- To study about the importance of system operating parameters, network parameters and gains of control system used to calculate the model of the power system for stability studies.
- To analyze measurement based modal analysis as an alternative approach to model based modal analysis.
- To study about various types of time and frequency domain techniques based on actual system measurement.
- To compare the realized system model from measured system response with that of full order model of the power system.
- To tune/ re-tune power system stabilizer(PSS) using the obtained modal parameters from measurement based techniques.

1.3 Organization of the thesis

This thesis has been organized such that power system stability problems and conventional modal analysis are discussed in early chapters and measurement based modal analysis is discussed in later chapters. In Chapter 2, various types of power system instability and its stability problems are demonstrated. In Chapter 3, dynamic modelling of various power system components are discussed and the sensitivity of the exciter parameters on stability is analyzed using single machine infinite bus(SMIB) system. In Chapter 4, conventional method of modal analysis in power system is discussed and sensitivity of various system parameters is analyzed to show how the different parameters affect the stability estimation of the system using model based modal analysis. In Chapter 5, an alternative approach to modal analysis is discussed using 3 types of time domain techniques. In Chapter 6, frequency domain based modal identification is discussed and its advantages and disadvantages are discussed. In Chapter 7, the method of measurement based PSS tuning/ re-tuning is discussed and demonstrated on IEEE 39 bus system. Chapter 8 concludes the thesis by highlighting the key contribution of this research and presenting various suggestions for future work.

Chapter 2

Power System Stability

2.1 Introduction

In this chapter, an overview of the various power system stability problems and different disturbances that excite local and control modes are studied in terms of transient/ small signal stability. In Section 2.2, the basis of power system operation and the characteristics of power system during a transient followed by a disturbance are discussed. In Section 2.3, classification of power system stability is briefly discussed. In Section 2.4, various types of power system stability problems are discussed and the difference between a transient stability and small signal stability is shown. In Section 2.5, various types of oscillatory modes observed in power system and their adverse effects are discussed. In Section 2.6, a single machine infinite bus (SMIB) system is simulated and various modes present in the oscillation are analyzed with and without exciter. Section 2.7 concludes this chapter.

2.2 Overview of power system stability

Power system stability refers to the ability of the system reaching an equilibrium after a disturbance. The operation of power system can be broadly divided into two types [3]:

1. Steady state operation

   The steady state operation deals with power flow in the power system to meet the load demands with the available generation capability. It refers to the analysis of the system neglecting any minute changes in the power system properties.

2. Transient Operation

   The dynamic state analysis of the power system deals with the stability of the power system after a disturbance occurs. It takes into account the changes in system properties due to the disturbance. It also involves modelling the power system under study to obtain its oscillatory characteristics for any future contingencies.

When a power system operating in steady state when experiences a disturbance either severe or weak for a long or short duration, it enters into a transient state causing it to oscillate around the equilibrium point. After the oscillation, a stable system attains a new equilibrium position. It is said to be stable even if it attains a new equilibrium point than it was before the disturbance. Stability is the ability of the system to remain in synchronism during the post disturbance period.

A power system is said to be unstable if oscillations during the transient period are undamped and sustained. A poorly damped oscillation occurring for a time period

large enough can cause the separation of generators or progressive reduction of bus voltage leading to failure of the operation of the power system. A different kind of instability which even occur without losing synchronism is due to the collapse of voltage due to the presence of large induction motor in the bus.

The dynamic modelling of power system has always been a challenging task because of nature of the system as described below [4]:

1. Non-linear and unpredictable nature.
2. Drifting of system parameters with time.
3. Higher order due to complexity of the system.

2.3 Classification of power system stability

A need for having a classification for stability arised with the variety of ways a disturbance might occur which leads to different types of the oscillation causing instability [5]. The stability of power system is broadly classified based on the three main power system parameters as follows:

- active power support: known as *frequency stability*
- reactive power support: known as *voltage stability*
- maintenance of synchronism: known as *rotor angle stability*

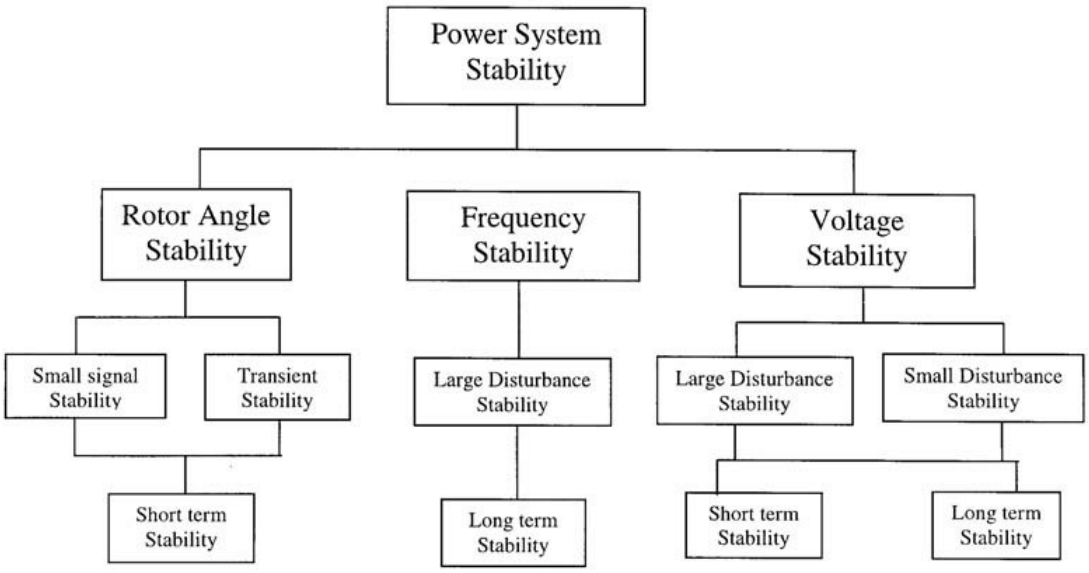

Figure 2.1: Classification of power system stability [5]

Figure (2.1) shows the overall classification of power system stability. It is broadly divided into rotor angle, frequency and voltage stability based on synchronism, active and reactive power support in power system which are three important operation parameters for the power system to function. Each type of stability can be affected either small disturbance or large disturbance indicative of the severity of the disturbance and also classified based on the time duration of each type of disturbance. Thus the classification covers almost every type of disturbance that a power system might experience.

2.4 Rotor angle stability

The rotor angle stability deals with the maintenance of synchronism with all the generators present in the power system. The system is stable if the rotor angle of one of the machines deviates from the steady state value due to any disturbance, attains

the equilibrium/ steady state after the disturbance is eliminated.

The power output of the synchronous machine highly depends upon the rotor angle and if one of the synchronous generator runs in higher speed, then the rotor of that machine gets advanced than that of the other machines in the power system. This leads to a load shift towards the machine which has the advanced rotor angle. The magnitude of the load shift depends upon the non-linear power angle characteristics of the machine. The relation indirectly relates to sufficient amount of torque to return back the rotor to a new or previous equilibrium point. Insufficient electrical torque will result in rotor drifting away from the equilibrium point causing instability.

The electro-mechanical torque of a synchronous machine consists of two components which are in quadrature with each other.

1. Synchronizing torque: in-phase with the change in rotor angle. An insufficient synchronizing torque will cause aperiodic instability without any oscillation.

2. Damping torque: in-phase with the change in rotor speed. An insufficient damping torque causes a periodic or oscillatory instability.

2.4.1 Small signal stability

Small signal stability of the power system defines the ability of the power system to return back to its equilibrium position when subjected to a small disturbance. The small disturbance can be a minor change in loads, change in set-point voltage of voltage regulator or even due to weakly coupled static var compensator (SVC) or high voltage dc converters (HVDC). Small signal instabilities are highly dependent on initial states and might be both oscillatory and aperiodic. In modern power system,

the aperiodic instabilities are eliminated by the use of automatic voltage regulators with rotating exciters. But due to saturation effects and limits of the exciter, such instabilities cannot be totally eliminated for small disturbances.

2.4.2 Transient stability

Transient Stability defines the ability of the power system to return back to its equilibrium position when subjected to a large disturbance. The large disturbance might be a short circuit in the transmission line. A large disturbance causes a change in rotor angle so large that there is insufficient synchronizing torque. Therefore, the instability is always aperiodic.

2.4.3 Contrasts between transient and small signal stability

The contrast between a transient stability and small signal stability is the analysis method used. The time frame of interest for a small signal stability studies is 10-15 seconds, whereas for transient stability studies it might be 3-5 seconds after the disturbance. In small signal stability analysis, the differential equations governing the non-linearity are linearized due to shorter time scales in small disturbances. For transient stability studies, the dynamic equations are solved directly using trapezoidal integration since linearization of the dynamic equations are not made for severe faults or faults with longer duration. Small signal disturbances are prone to occur more frequently than the transient disturbances in a practical power system [6].

2.5 Small signal stability problems on power system

The frequency range of each type of oscillation arising from variety of sources is termed as mode. The following are a few common modes of oscillations related to small signal stability [7]:

1. **Intra-plant modes:** The machines within a power plant oscillate. Here the frequency range of oscillation is 2-3 Hz.

2. **Local modes:** Local modes are associated with swinging of units at a generating station with respect to the rest of the power system. The oscillations are localized at one station. Here frequency range of oscillation is 1-2 Hz.

3. **Inter-area modes:** Inter area modes are associated with the swings of many machines in one part of the system against a group of machines in the other parts. As the number of machines involved here is more, frequency of oscillation is less compared to intra-plant modes. Here the frequency range of oscillation is 0.1-0.9 Hz.

4. **Control modes:** Control modes are associated with generating units and other control units like poorly tuned exciters, speed governors, HVDC converters and SVC. The nonlinear interaction between exciter and loads leads to oscillatory response in bus voltage.

5. **Torsional modes:** Torsional modes relate to oscillation of various stages of

steam turbine shaft system with the electrical network. Instability in torsional modes may be caused by interaction with excitation controls, speed governors, HVDC controls, and series capacitor compensated lines. Here the frequency range of oscillation is 10-46 Hz.

2.6 Case study: SMIB system

In order to demonstrate the various types of oscillation modes associated in power system, a single machine infinite bus (SMIB) system is used as shown in Figure (2.2). The parameter values for the generator, exciter system and system operating conditions are given in Appendix A. To study the different types of the modes as explained in Section 2.4, the system is perturbed with a 3 phase to ground fault at bus 3 which is applied at $t = 1$s and the fault is cleared at $t = 1.1$s. The simulation is carried out using PowerWorld [8] for 10s with and without the exciter model and the eigenvalues of the system model is studied to obtain the modes present in the oscillation.

It can be seen the simulation results of Figures (2.3) and (2.4) that the system is totally stable since the system attains an equilibrium position after the disturbance. It is to be noted that although the power system with and without exciter is stable, the response of the system with the exciter model is less damped due to the addition of control modes in the SMIB power system.

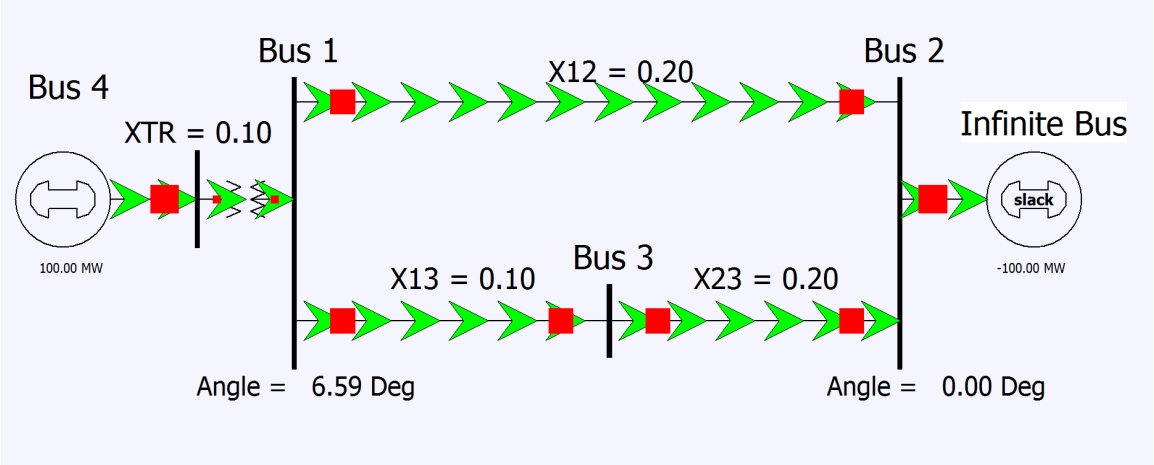

Figure 2.2: Single machine infinite bus system

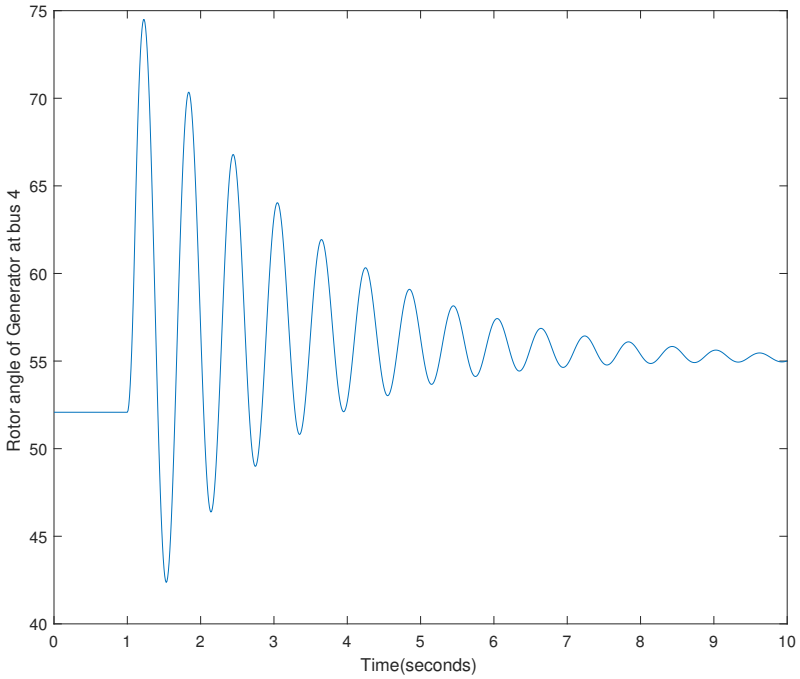

Figure 2.3: Rotor angle oscillation of generator at bus 4 without exciter system

2.6.1 Various modes of oscillations

Eigenvalue analysis gives an estimate of number of modes,the frequency associated with each mode and the damping ratio. The SMIB system consists of 4^{th} order model

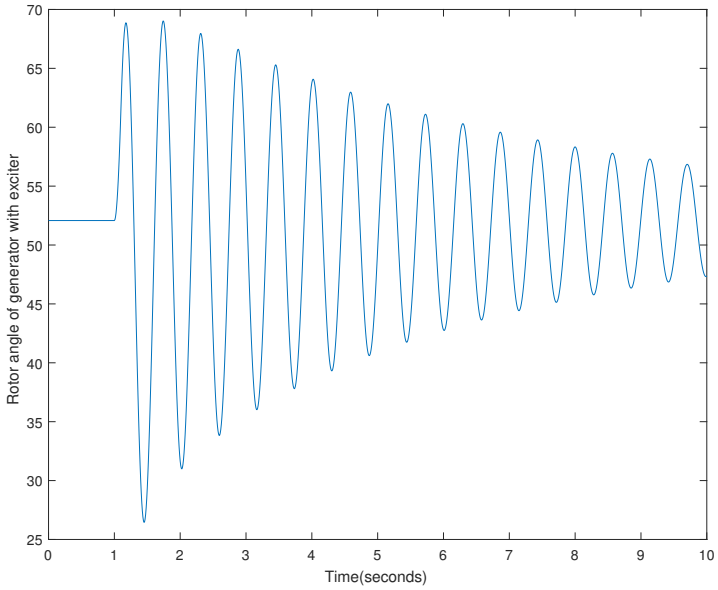

Figure 2.4: Rotor angle oscillation of generator at bus 4 with exciter system

for generator and 3^{th} order model for the exciter. Therefore, it results in 4 and 7 modes with and without exciter respectively.

Table 2.1: Eigenvalue of SMIB system without exciter model

Eigenvalue no.	Most Associated States	Real part	Imag Part	Frequency
1	δ, ω	-0.5893	11.2576	1.7917
2	δ, ω	-0.5893	-11.2576	-1.7917
3	E_d	-3.508	0	0.55
4	E_q	-0.2832	0	0.0451

Table 2.2: Eigenvalue of SMIB system with exciter model

Eigenvalue	Most Associated States	Real part	Imag Part	Frequency
1	V_e, V_r	-4.8236	15.467	2.461
2	V_e, V_r	-4.8236	-15.467	-2.461
3	ω, δ	-0.1654	11.058	1.758
4	ω, δ	-0.1654	-11.058	-1.758
5	E_q, E_d	-5.9311	0	0
6	V_f, E_q	-1.708	1.707	0.2719
7	V_f, E_q	-1.708	1.707	0.2719

Tables (2.1) and (2.2) show the most associated states based on the highest participation factor of the state on that eigenvalue for the two cases of without and with an exciter calculated using PowerWorld [8]. The method of calculating participation factors of each eigenvalue on state variables will be discussed in Chapter 3. The eigenvalues corresponding to eigenvalue 6 and 7 in Table (2.2) is the control mode due to exciter showing the highest participation factor for V_f which is the applied field voltage by exciter, and E_q of the generator. The control mode can dangerously affect the small signal stability of the system due to its high participation with the generator local modes.

To demonstrate the reduction in small signal stability due the control modes, another disturbance which excites the control mode is introduced. In the same SMIB system shown in Figure (2.2), the control modes can be excited by changing the set point voltage of the exciter from 1.1 pu to 1.0 pu at t= 1s. Figure (2.5) shows the

small signal instability of the SMIB system due to excitation of the control mode.

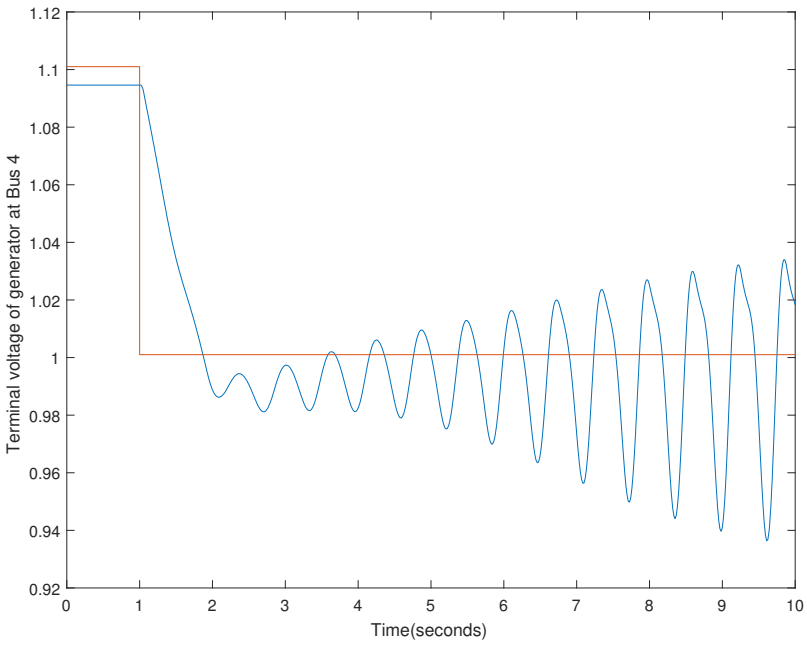

Figure 2.5: Terminal voltage oscillation of the generator at bus 4 with exciter system

The reduction in damping ratio in the case of transient stability and poor small signal stability is a characteristic of addition of exciter to the generator model. This is due to the gain of the exciter that changes the root locus of the overall system such that the eigenvalues move more closer to the origin. It could be seen that the addition of control modes are more prone to cause small signal instability than the transient instability because the small disturbances like the change in preset setting of exciter, HVDC components or even sudden change in load causes instability in the presence of less damped local mode which is highly coupled with the control modes.

2.7 Conclusion

In this chapter, classification on power system stability and various stability problems have been discussed with respect to the modes of oscillation. Various types of modes due to different components in the power system have also been studied. The local modes of a SMIB system are identified and the effect of addition of a exciter system producing control modes has been studied. Comparison between the small signal stability and transient stability is also made by exciting the system and reducing the voltage reference input to the exciter system. Thus, the relation of system response and its stability with various modes of system excited by the type of disturbance are studied in this chapter.

Chapter 3

Dynamic Modelling of Power System

3.1 Introduction

In this chapter, mathematical models that describe the dynamic behaviour of generator and exciter system are discussed. In Section 3.2, the dynamic model of synchronous generator and reduced order modelling of synchronous generator is discussed. In Section 3.3, the selection of reduced order models for stability studies is analyzed using a Single Machine Infinite Bus (SMIB) system. In Section 3.4, the modelling of IEEE AC1A exciter system is discussed and the effect of rotating excitation system is discussed. In Section 3.5, sensitivity analysis of the excitation system parameters on the small signal stability of the SMIB system is discussed. Section 3.6 concludes this chapter.

3.2 Modelling of synchronous generator

The dynamic modelling of the synchronous generator starts with the swing equation derived with the help of fundamental Newton's second law of motion substituted in terms of the synchronous motor parameters namely, the rotor angle and the net force in terms of electrical and mechanical power [9].

$$\frac{d^2\delta}{dt^2} = \frac{\omega_s}{2H}(P_m - P_e \sin\delta) \tag{3.1}$$

where, δ, ω_s, H are the rotor angle, synchronous speed and inertia constant of the generator, P_m and P_e are the input mechanical power and output electrical power of the generator. Equation (3.1) can also be written in terms of the rotor angle and speed deviation as follows:

$$\frac{d\Delta\delta}{dt} = \omega(t) - \omega_s = \Delta\omega \tag{3.2}$$

$$\frac{d\Delta\omega}{dt} = \frac{\omega_s}{2H}(P_m - P_e \sin\delta) \tag{3.3}$$

where,

$$P_e = real\left(\bar{V}\left(\frac{\bar{E} - \bar{V}}{(x_g + x_e)}\right)\right) \tag{3.4}$$

Equations (3.2) and (3.3) are referred to as the classical model of the synchronous generator which consists of two differential equation and one algebraic equation with $\Delta\delta$ and $\Delta\omega$ as the state variables. The parameters $\bar{E}$ and the $\bar{V}$ are the internal voltage of the generator and the voltage of the bus upto which the analysis is considered. x_g and x_e are the generator reactance and external network reactance respectively. In the classical model, only the mechanical dynamics are considered for the modelling of the synchronous generator and the electrical

dynamics are computed only by the algebraic equation of the power flow from the generator to a bus or load. The disturbance can be in the form of a change in the input mechanical power indicated with ΔP_m or with a change in the electrical power depending upon the x_e of the external network indicated by ΔP_m. Therefore equation (3.3) becomes

$$\frac{d\Delta\omega}{dt} = \frac{\omega_s}{2H}(P_m - P_e \sin\delta - D\Delta\omega) \tag{3.5}$$

where D is the generator load damping co-efficient when damping due to the damper winding is considered.

3.2.1 Addition of electrical dynamics to the classical model

In order to have an accurate model of the dynamic behaviour of the power system it is necessary to consider the non-linearity in the stator and the rotor circuits of the synchronous generator. The flux decay equations of stator winding, rotor winding with the damper winding is considered and the electrical dynamic equation is derived in detail [7] as follows:

$$T_{do}^{'}\frac{dE_q^{'}}{dt} = -E_q^{'} - (X_d - X_d^{'})\big[I_d - \frac{X_d^{'} - X_d^{''}}{(X_d^{'} - X_{ls})^2}(\psi_{1d} + (X_d^{'} - X_{ls})I_d - E_q^{'})\big] + E_{fd} \tag{3.6}$$

$$T_{do}^{''}\frac{\psi_{1d}}{dt} = -\psi_{1d} + E_q^{'} - (X_d^{'} - X_{ls})I_d \tag{3.7}$$

$$T_{qo}^{'}\frac{dE_d^{'}}{dt} = E_d^{'} + (X_q - X_q^{'})\big[I_q - \frac{X_q^{'} - X_q^{''}}{(X_q^{'} - X_{ls})^2}(\psi_{2d} + (X_q^{'} - X_{ls})I_q - E_d^{'})\big] \tag{3.8}$$

$$T_{qo}^{''}\frac{\psi_{2q}}{dt} = -\psi_{2q} + E_d^{'} - (X_q^{'} - X_{ls})I_q \tag{3.9}$$

and

$$\psi_d = -X_q^{''}I_q - \frac{(X_q^{''} - X_{ls})}{(X_q^{'} - X_{ls})}E_d^{'} + \frac{(X_q^{'} - X_q^{''})}{(X_q^{'} - X_{ls})}\psi_{2q} \tag{3.10}$$

$$\psi_q = -X_d^{''} I_d - \frac{(X_d^{''} - X_{ls})}{(X_d^{'} - X_{ls})} E_q^{'} + \frac{(X_d^{'} - X_d^{''})}{(X_d^{'} - X_{ls})} \psi_{2d} \tag{3.11}$$

where, X_d and X_q are the d-axis and q-axis synchronous reactance (pu) , $X_d^{'}$ and $X_q^{'}$ are the d-axis and q-axis transient reactance (pu) , $X_d^{''}$ and $X_q^{''}$ are the d-axis and q-axis sub-transient reactance (pu) , $T_{do}^{'}$ and $T_{qo}^{'}$ are the d-axis and q-axis transient open loop time constant (s) , $T_{do}^{''}$ and $T_{qo}^{''}$ are the d-axis and q-axis sub-transient open loop time constant (s) , $E_q^{'}$ and $E_d^{'}$ are the q-axis and d-axis internal voltages (pu) , ψ_{1d} and ψ_{2q} are the flux linkages of d-axis and q-axis damper winding (pu) ,I_d and I_q are d-axis and q-axis currents (pu) ,X_{ls} is the leakage reactance. Equations (3.6)-(3.11) adds 4 more differential equations (3.6)- (3.9) and 2 algebraic equations (3.10)-(3.11) to the classical model. Hence this model is called the 6th order model of the synchronous generator.

3.2.2 Reduced order modelling of synchronous generators

The 6th order model of the generator with 6 differential equations and 3 algebraic equations not only makes it complex to solve the differential equations but also difficult to maintain dynamic database for the whole power system under study. Although the 6th order model is better, the states with comparatively less participation factors when compared to other states can be neglected without any appreciable loss of accuracy.

Reduced 4th order model:

In a 4th order model, the sub-transient time constants which are less than one cycle are neglected as the response of the associated transfer function is almost instantaneous and the delay in the response is negligibly small [7]. Therefore

substituting $T_{do}^{''}$ and $T_{qo}^{''}$ equal to zero in equations (3.7) and (3.9),we get:

$$0 = -\psi_{1d} + E_q^{'} - (X_d^{'} - X_{ls})I_d \tag{3.12}$$

$$0 = -\psi_{2d} + E_d^{'} - (X_q^{'} - X_{ls})I_q \tag{3.13}$$

Now, substituting equation (3.12) and (3.13) into (3.6) and (3.8), we get

$$T_{do}^{'}\frac{dE_q^{'}}{dt} = -E_q^{'} - (X_d - X_d^{'})I_d + E_{fd} \tag{3.14}$$

$$T_{qo}^{'}\frac{dE_d^{'}}{dt} = -E_d^{'} + (X_q - X_q^{'})I_q \tag{3.15}$$

and

$$\psi_d = -E_q^{'} - X_d^{'}I_d \tag{3.16}$$

$$\psi_q = -E_d^{'} - X_q^{'}I_q \tag{3.17}$$

After the reduction of the states ψ_{2d} and ψ_{1d}, there are 2 electrical dynamic equations and 2 mechanical dynamic equations resulting in a 4^{th} order model. This model is also called two axis model of synchronous generator.

3rd order model:

The state due to the direct axis of the stator which is represented by $dE_d^{'}$ is still present in the 4th order model. For the power system under study, if the value of $T_{qo}^{'}$ is considerably small, then, a 3rd order model is possible. It is obtained by substituting $T_{qo}^{'}$ with zero in the equation (3.15) and the resulting 3rd order model is shown in equations (3.18) and (3.19).

$$E_d^{'} = (X_q - X_q^{'})I_q \tag{3.18}$$

and

$$T_{do}^{'}\frac{dE_q^{'}}{dt} = -E_q^{'} - (X_d - X_d^{'})I_d + E_{fd} \tag{3.19}$$

3.3 Selection of dynamic order of synchronous generator for stability studies

The order or number of differential equations considered for analyzing the dynamic behaviour of the synchronous generator is highly decided on the value of sub-transient and transient reactances and its time constants. If the time constant of that particular differential equation is very much less than the $\frac{1}{f}$ seconds of the system, then the differential equation is considered to be an algebraic equation that can be substituted in other differential equations. If the value of the d/q axis reactance of the generator is very small which causes very minute change,the particular reactance is considered to be zero. Consider the single machine infinite bus(SMIB) system shown in Figure (3.1) whose system data is shown in Appendix A.

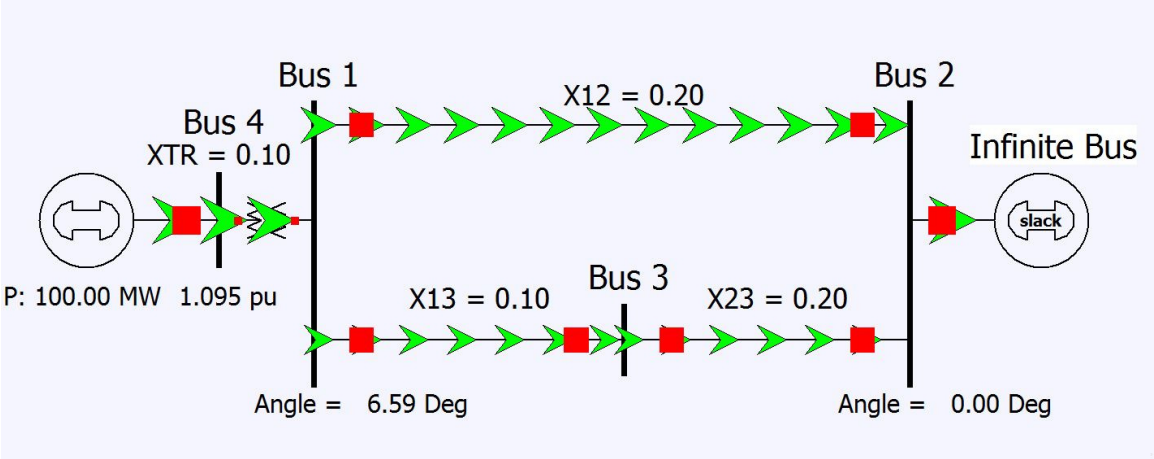

Figure 3.1: A SMIB power system

The generator in SMIB system shown in Figure (3.1) has very small sub-transient reactance and time constant, therefore the 6th order model is not necessary. In

this thesis, the response to the classical model and the effect of the addition of the electrical dynamics is studied and why the 3rd order model is not sufficient in this case is discussed. Figures (3.2) and (3.3) show the oscillation in the rotor angle and speed with a 3-phase fault occurring in bus 1 at t= 0s and then cleared at t=0.05s.

The differential equation solver ode45 in MATLAB [10] is used to numerically solve the classical model of generator for during and post fault conditions. In the classical model, the generator internal voltage is assumed constant, hence the oscillation is sustained and undamped.

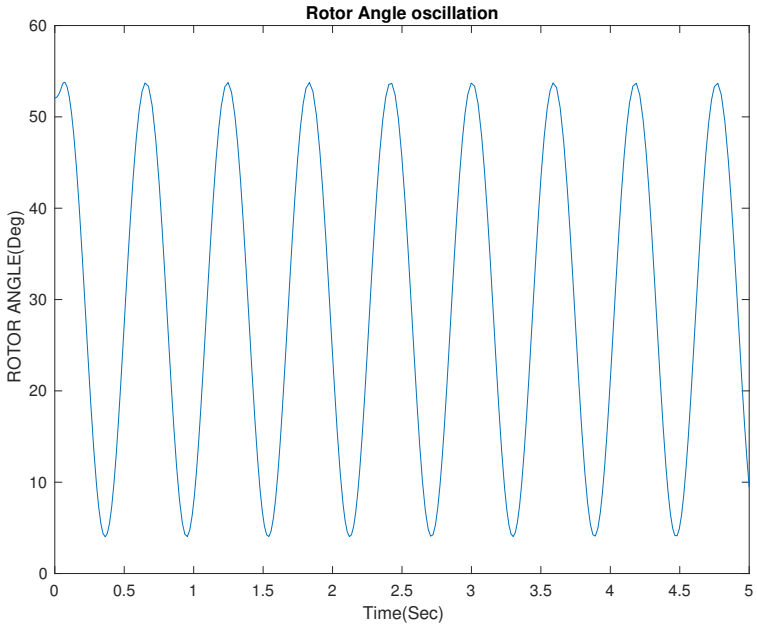

Figure 3.2: Rotor angle oscillation with classical Model

Figures (3.4) and (3.5) show the rotor angle and rotor speed after addition of the electrical dynamics to the classical model. It can be seen that the oscillation are now damped by generator internal voltages attaining a new equilibrium position in time

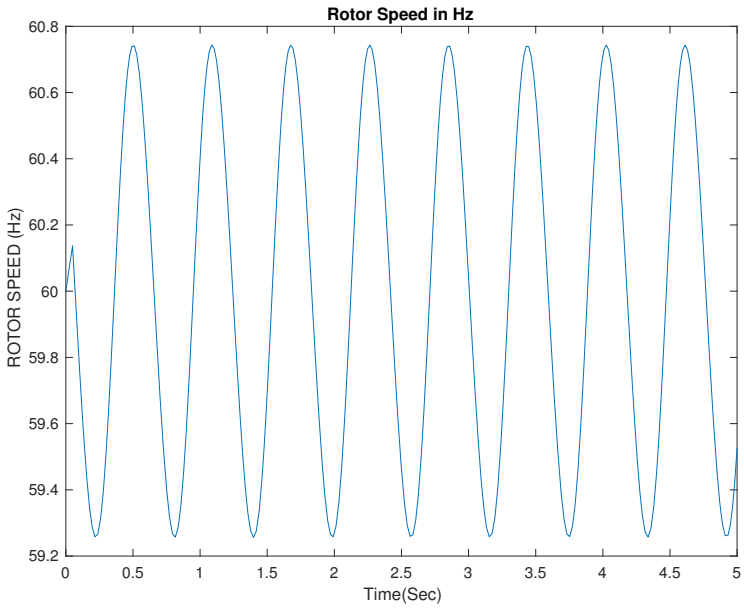

Figure 3.3: Rotor speed with classical model

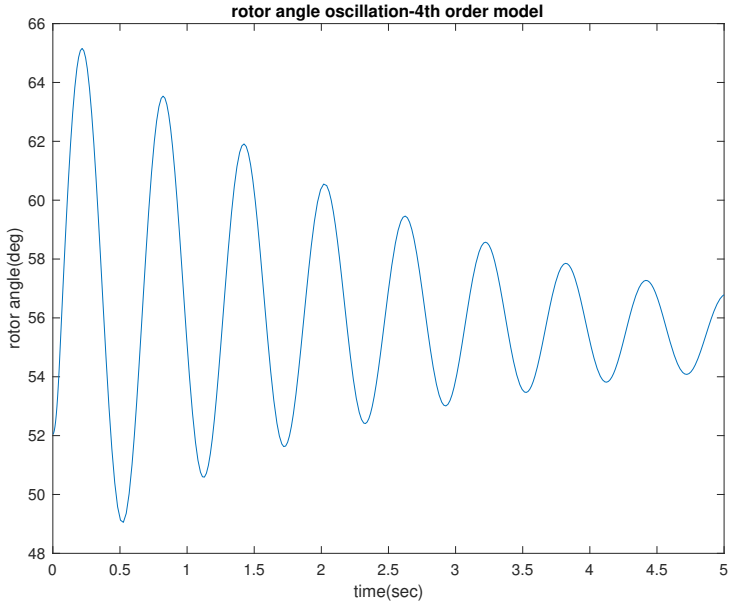

Figure 3.4: Rotor angle oscillation with 4th order modelling

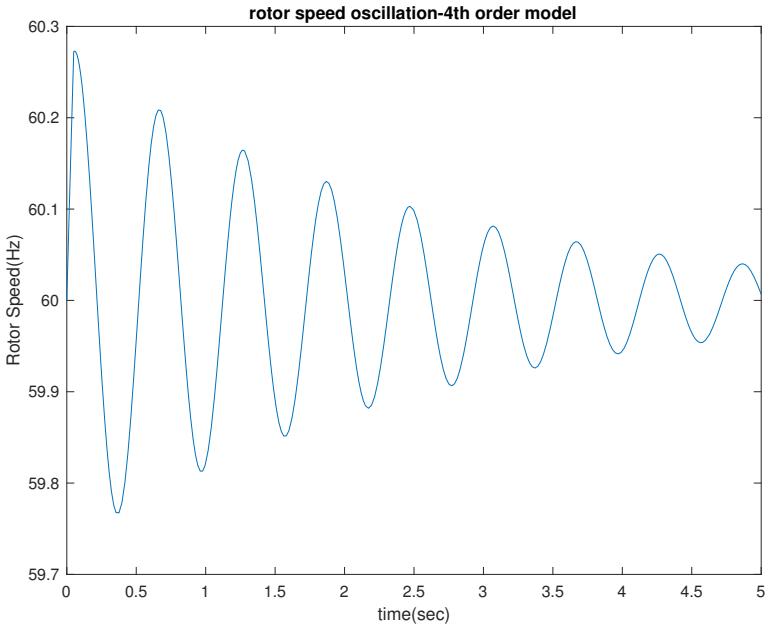

Figure 3.5: Rotor speed oscillation with 4th order modelling

$T'_{d0} = 7.0$s. As a comparison, Figure (3.6) shows the difference in response of a 3rd order model when compared with a 4th and 6th order model. This is because the time constant $T'_q = 0.75$s is far more higher than the time period of the system with f=60Hz which completes one cycle in 0.01667s. Therefore, both the 4th and 3rd order model is fairly the same at the initial integration times but has a phase shift with continued integration. This also explains the reduction in damping of the oscillations.

Therefore, for generators of small rating which has very small T'_{q0} and sub-transient reactance, a 3rd order model is sufficient. As the rating of the generator increases the value of T'_{q0} also increases with respect to the generation frequency and 3^{rd} order modelling would not accurately predict the response of the synchronous generator modelled. A 6th order model is not necessary unless the sub-transient reactances are large enough in which case cannot be neglected.

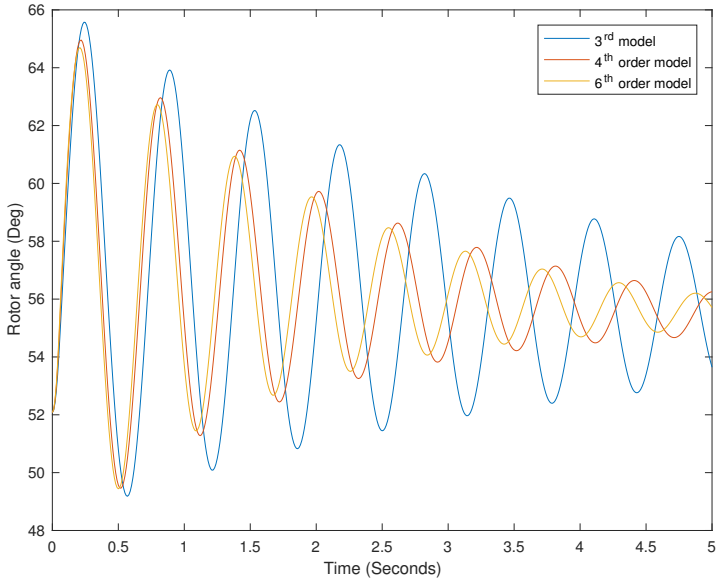

Figure 3.6: Comparison of 3rd, 4th and 6th order model of generator

Figure (3.6) also shows the 6th order model response where the change in damping ratio is very small when compared to 1.99%, 4.81% and 5.01% for 3rd, 4th and 6th order model respectively. This is explained by the Gibb's phenomenon [11] where increasing the order of the model makes the model response more representative of the actual system response with increasing damping but limited to a certain value. In the SMIB system, the maximum damping around 5% is achieved as explained by the Gibb's phenomenon due to increased leakage of energy from the higher frequencies.

In case of larger power systems with multiple generating stations, the overall order of the model is very high such that it increases the cost and time of such simulations. Therefore, it is necessary to choose appropriate order for generators so that the overall order of the system is low and the model response is closely represents the actual response of the system at the same time.

3.4 Modelling of IEEE type AC1A exciter system:

The automatic voltage regulator (AVR) is a power electronic based control device which is used to maintain a constant voltage at the generator's terminal by adjusting the internal voltage of the generator. This is done by adjusting the field current of the generator by adjusting the input field voltage achieved by power electronic devices. In short, during steady state, the AVR is used to provide constant reactive power support to the power system.

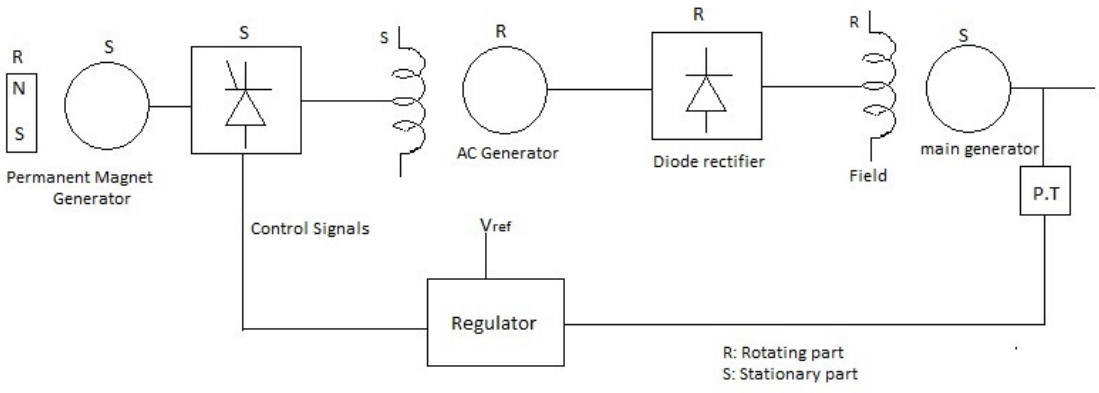

Figure 3.7: Block diagram of AVR and exciter system [12]

It is very important to model the dynamics of the AVR with the generator since E_{fd} is also present in the generator's dynamic equation. Figure (3.7) shows the brush-less excitation system in detail and voltage regulator in a block. A permanent magnet generator is used to provide the main supply to the exciter system which is connected to the shaft of the main generator. This is done to eliminate the external transients when the supply is taken from the generator terminal. Such an exciter system is called static system which is not commonly used.

3.4.1 Modelling of the AVR

The voltage regulator shown in the Figure (3.7) is a comparator with an amplifier circuit which instantaneously compares the value of the set-point voltage,V_{ref} with the terminal voltage of the generator measured by a potential transformer. The error value thus obtained is applied to a PI controller with a gain value to reduce the steady state error. The value of gain is set such that the rated voltage is obtained at the terminal of the generators. Thus the dynamic equation of the voltage regulator is essentially an equation of the PI controller with V_{ref} - $V_{measured}$ as the input. So we have,

$$T_A \frac{dV_R}{dt} = -V_R + K_A(V_{ref} - V_{measured}) \tag{3.20}$$

Where, V_{ref}, $V_{measured}$,V_R and K_A are the reference voltage, terminal voltage of generator, regulation voltage and gain of the AVR. The automatic voltage regulator also has limits governed by the thermal limitation and the loading of the separately excited AC generator used in the exciter system. In addition to the measured voltage, the regulator also has additional inputs for the Power System Stabilizer (PSS), stabilizer for the excitation system, frequency limiter etc.

3.4.2 Modelling of the exciter system

The brush-less excitation system shown in Figure (3.7) starts with the permanent magnet (PM) generator which generates constant voltage in the stator for the given input mechanical input provided by the turbine which is also coupled to the main generator. The PM generator produces AC voltage which is converted to DC using a controlled rectifier circuit to supply the field of a separately excited AC generator.

The controlled rectifier consists of gated thyristors or IGBT which can produce both DC output of both positive and negative polarities. Generally, while modelling the rectifier circuits the time constant is considered very small in the order of $\frac{1}{6}^{th}$ of the cycle. Here the dynamics of the PM generator does not greatly affect the response of the controlled rectifier connected to the generator. The controlled rectifier has direct control over the output of the self-excited AC generator which is again rectified using diode bridge and then fed to the main generator's field circuit. Since the field voltage can only be controlled using the controlled rectifier, it is necessary to model the dynamics of the separately excited generator.

Modelling of the separately excited AC generator: For any AC generator, the relation between the field voltage and the obtained armature voltage is given as

$$E_f = R_f I_f + \frac{dE_a}{dt} \tag{3.21}$$

where, E_f and E_a are the field and armature voltages, I_f and R_f are the field current and field resistance. Since, T'_{do} of the main generator is very high, we might need to apply more field voltage to minimize the rise time of the terminal voltage. There we need to consider the saturation effects of the separately excited AC generator, therefore equation (3.21) is modified by [13],

$$I_f = \frac{E_a}{R_g} + E_a S_e(E_a) \tag{3.22}$$

and,

$$E_a = K_a L_f I_f \tag{3.23}$$

where, $S_e(E_a)$ refers to the saturation function obtained from the open circuit characteristics of the generator. Substituting equations (3.22) and (3.23) in (3.21),

we get

$$E_f = \frac{R_f}{R_g}E_a + R_f S_e(E_a)E_a + \frac{1}{K_a}\frac{dE_a}{dt} \tag{3.24}$$

$$E_f = K_E E_a + S_E(E_a)E_a + T_E\frac{dE_a}{dt} \tag{3.25}$$

where,

$$K_E = \frac{R_f}{R_g} \qquad S_E(E_a) = R_f S_e \qquad T_E = \frac{1}{K_a} \tag{3.26}$$

Equation (3.25) represents the dynamic model of the AC generator used in the exciter system.

Modelling of the diode rectifier: Usually the dynamics of the rectifier is neglected since the time constant is very small. However, in the case of the diode rectifier the output voltage depends upon the input voltage and the output current. There is also appreciable drop in input voltage due to appreciable armature reaction reluctance in the self-excited AC generator. In addition, some value of inductance is introduced in the input terminals of the diode rectifier to reduce the commutation delay which results in furthur drop in the voltage. Therefore from [13],

$$E_{ed} = f(I_N)V_E \tag{3.27}$$

where,

$I_N = \frac{K_c I_{out}}{V_E}$, K_c is the commutation constant.

$f(I_N)$ is determined by the range of I_N.

Equations (3.20) - (3.27) refer to the dynamic equations of the AVR and excitation system. The IEEE Excitation system of Type AC1A can be obtained by taking the Laplace transform to obtain the individual transfer function of the blocks as shown in the Figure (3.8).

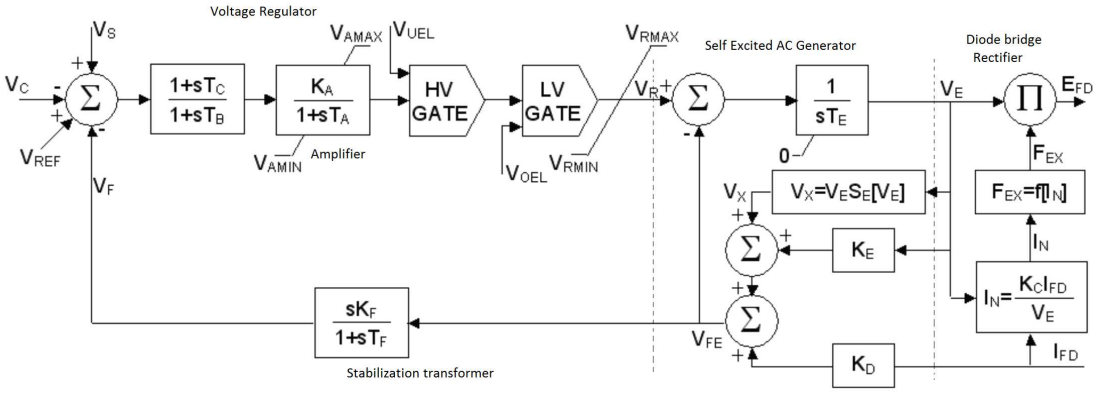

Figure 3.8: IEEE type AC1A AVR with exciter system [13]

It can be seen from the Figure (3.8) that the regulator has an input feed by the stabilizing transformer transfer function to stabilize the whole control system of the AVR and exciter system. The output of the regulator is influenced by limiter like under and over excitation limiters and the limiters for the whole output of the regulator block which is used to preserve thermal constraints of the AC generator and also to prevent dropping of voltage below a particular limit V_{Rmin} leading to insufficient field voltage to the main generator.

3.5 Effect of exciter model in the SMIB system

The addition of exciter model to the 4th order model of the synchronous generator results in system with 7 states. In the SMIB system, a 3 phase to ground fault is applied at bus 3 at t= 1s and cleared at t= 1.1s and the simulation is carried out for 10s using PowerWorld [8]. The removal of bus 3 from the system causes the system to attain a new equilibrium position due to the change of the external network topology. This causes the terminal voltage of the generator to be different than the voltage

before the fault. Figures (3.10) and (3.11) show the terminal voltage and rotor angle oscillation of the generator at bus 4 with and without a rotating excitation system. The parameter values used for the exciter system are shown in Appendix A.

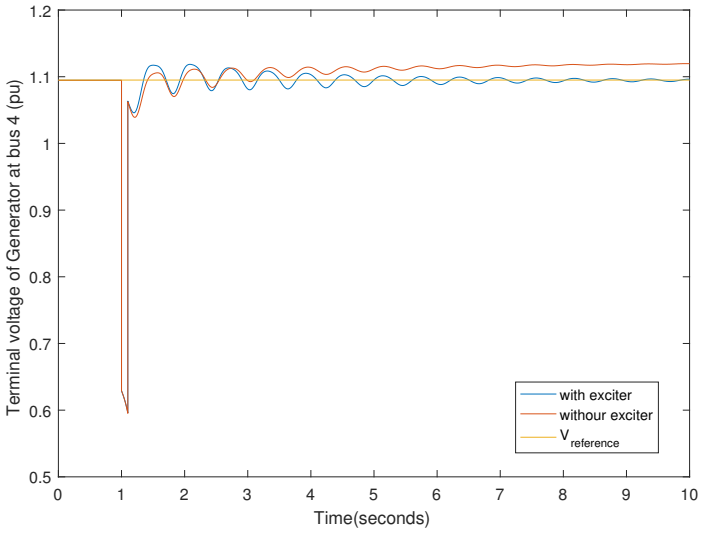

Figure 3.9: Terminal voltage oscillation of generator with and without exciter

From Figure (3.9), it can be seen that the exciter helps to maintain the same terminal voltage of the generator which tends to change due to change in system network without an exciter. Increasing the gain of the exciter helps to attain the V_{ref} faster with less steady state error which is the main purpose of adding exciter to the generator.

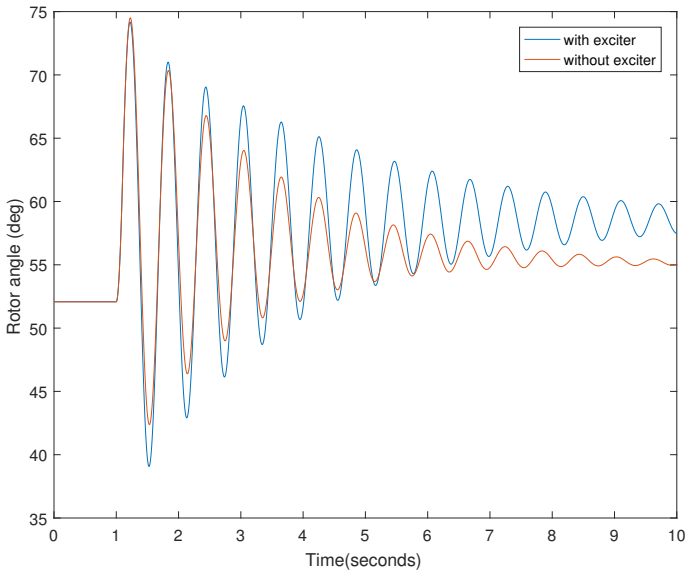

Figure 3.10: Rotor angle oscillation of generator at bus 4 with and without exciter

3.5.1 Sensitivity analysis of the excitation system parameters on small signal stability

The exciter system which is added to the synchronous generator needs to be tuned such that the system is stable in case of disturbance. From the simulation results from Section 3.2.3, it is to be noticed that the local mode is less damped due to the addition of the control modes introduced by the rotating exciter. This requires us to analyze the effect of various parameters of the exciter model affecting the damping of the local mode causing small signal and transient instability. The sensitivity of various parameters of the exciter model on the stability of the system can be analyzed by eigenvalue analysis.

Unlike the static exciter system, the amplifier/ voltage regulator gain, K_a variation does not cause instability in the rotating excitation system. It can be seen from the

Figure (3.11) that increase in the value of the amplifier gain substantially reduces the damping ratio of the local oscillation mode, but does not cause instability as the damping ratio does not reduce after Ka= 2000.

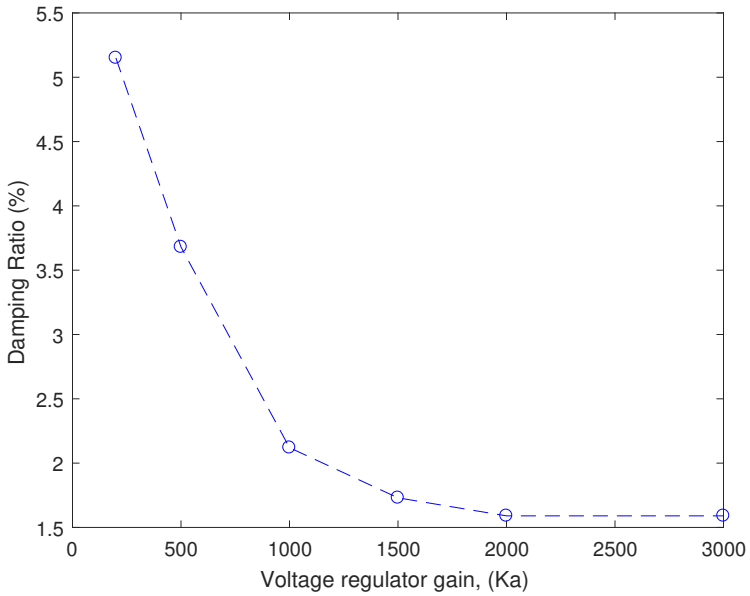

Figure 3.11: Effect of variation of damping ratio with amplifier gain K_a

The improved stability of the rotating excitation system is due to the feedback loop which consists of the stabilizer block. The stabilization of the exciter system is performed depending on the value of the stabilizer gain, K_f. This explains the declining nature of the damping ratio with the increase in the amplifier gain in Figure (3.11) with a minimum damping ratio of 1.59%. But, the rotating excitation system becomes vulnerable to instability with gain value of the stabilizing transformer used.

Figure (3.12) shows the change of damping ratio of the local mode corresponding to 1.667Hz with the variation of the stabilizer gain K_f with a fixed $K_a = 200$. Figure (3.13) shows the movement of the eigenvalues/ poles of the system with the variation

of K_f.

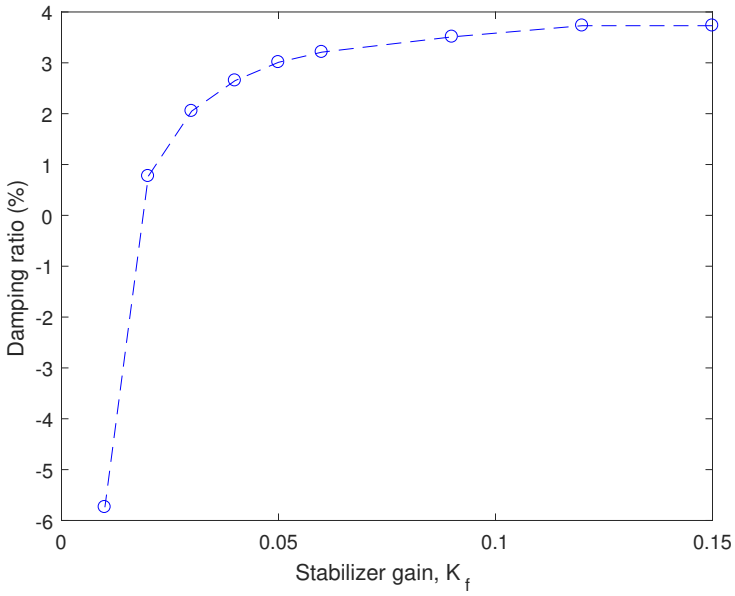

Figure 3.12: Effect of variation of damping ratio with stabilizer gain K_f

It can be noted from Figures (3.12) and (3.13) that $K_f = 0.01$ causes instability in the power system due to the presence of positive real part in the eigenvalue which causes negative damping ratio leading to instability. This is due to the stabilizing transformer not able to provide enough synchronous torque in the synchronous generator via the excitation system at amplifier gain, $K_a = 200$. Therefore, in rotating excitation system, the possibility of small signal instability is present when the K_f is small even though the value of amplifier gain is at a lower value. This indicates the system stability is highly affected by the gains of the excitation system which is a vital factor that needs to be taken into consideration in the model based modal analysis for stability purposes.

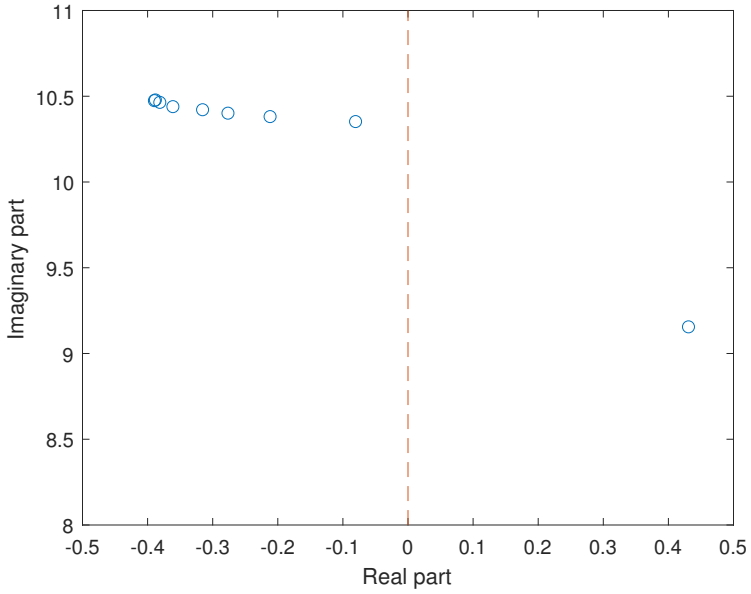

Figure 3.13: Movement of eigenvalues with variation in stabilizer gain K_f

3.6 Conclusion

In this chapter, the modelling of synchronous generator for dynamic studies is discussed and the reduced order modelling of synchronous generator has been studied. Selection of order for synchronous generator dynamic model has been explained using SMIB system as a case study. It is shown that the 4th order and 3rd order model shows significantly different results because of neglected T'_{q0} . The working of IEEE AC1A is discussed and the advantage of the rotating excitation over the static exciter is also discussed. Sensitivity analysis on various exciter parameters are also studied to understand the movement of eigenvalues for the same type of disturbance indicating the importance of the gains of the exciter in a model based modal analysis.

Chapter 4

Model based Assessment of Power System Small Signal Stability:

4.1 Introduction

In this chapter, eigenvalue based modal analysis using dynamic model of the power system is discussed. In Section 4.2, a generalized form of modal analysis for dynamic system is discussed using the process of linearization . In Section 4.3, conventional method of modal analysis for single bus equivalent of power systems is discussed. In Section 4.4, small signal stability of SMIB system is assessed by estimating the eigenvalues by linearization. Movement of eigenvalues with variation of operating parameters and network coupling are also discussed in Section 4.4. In Section 4.5, various difficulties in applying model based modal analysis to large power system are discussed. Section 4.6 concludes this chapter.

4.2 Generalized modal analysis based on eigenvalue estimation

The modes of vibration of any system can be obtained from the eigenvalue pairs possessed by the system. The eigenvalues of the system can be obtained from the differential equations that govern the system. In case of small disturbances to the system, the eigenvalues are obtained by linearizing the system equation around a point of equilibrium. This is applied to systems when the excitation reaches a new equilibrium position from a previous equilibrium point.

The linearization of system equation can be performed on previous equilibrium point which help to obtain modes and its associated damping before the disturbance. The eigenvalues obtained by linearizing around the new equilibrium point helps to obtain the present state of the system and estimation of system state for future disturbances. A system governed by differential algebraic equation can be represented in state space form as shown below:

$$\dot{x} = f(x, v, u) \tag{4.1}$$

$$0 = g(x, v, u) \tag{4.2}$$

where, x is the state variables of the system, v is the algebraic variable and u is the input to the system. If the response of the system is highly dependent on the initial condition attained at the new equilibrium position, the modal parameters after the new equilibrium point can be obtained by linearizing the above system of equations as follows:

$$\Delta\dot{x} = A\Delta x + B\Delta v + C\Delta u \tag{4.3}$$

$$0 = D\Delta x + E\Delta v + F\Delta u \tag{4.4}$$

where, A, B, C are the partial derivatives of equation (4.1) with respect to variables x, v, u respectively. Similarly, the matrices D, E, F are the partial derivatives of equation (4.2) with respect to variables x, v, u respectively.

The system characteristics can be obtained from the eigenvalues of the system matrix which can be calculated from the equations (4.3) and (4.4) as shown below:

$$A_{sys} = A - BE^{-1}D \tag{4.5}$$

The complex eigenvalues obtained from the system matrix, A_{sys} determines the stability of the system. A large negative value in the real part of a complex eigenvalue indicates the particular mode is highly damped. A negative real part close to zero indicates the mode is poorly damped and a consecutive disturbance of the system might cause instability. A positive real part with imaginary part indicates periodic instability, while a positive real without an imaginary part indicates aperiodic instability.

The state variable which contributes the most for a particular mode is used to decide the input signal to a stability controller. This can be obtained from participation factor of each state variable on all eigenvalue. A high value of participation factor indicates the most contribution of the state variable to the oscillation. The participation factor can be determined as follows:

$$p_{ki} = \psi_{ki}\phi_{ki} \tag{4.6}$$

where, ψ_{ki} and ϕ_{ki} are the right and left eigenvalues of the system matrix, A_{sys}.

4.3 Conventional modal analysis of power systems

Any power system network can be represented as a single bus equivalent circuit, where the generator under study is considered as a single machine and the rest of the network is replaced by infinite bus. The differential algebraic equations that govern the system response are represented in equations (4.7) and (4.8).

$$\begin{aligned}
\frac{d\delta}{dt} &= \omega_r - \omega_s \\
\frac{d\omega_r}{dt} &= \frac{\omega_s}{2H}(T_m - T_e) \\
\frac{dE_q^{'}}{dt} &= \frac{1}{T_{d0}^{'}}[-E_q^{'} - (X_d - X_d^{'})I_d + E_{fd}] \\
\frac{dE_d^{'}}{dt} &= \frac{1}{T_{q0}^{'}}[-E_d^{'} - (X_q - X_q^{'})I_q]
\end{aligned} \tag{4.7}$$

$$\begin{aligned}
-(X_q^{'} + X_t)I_q - E_d^{'} + E_b sin(\delta) = 0 \\
(X_d^{'} + X_t)I_q - E_q^{'} + E_b cos(\delta) = 0 \\
-X_t I_q + E_b sin(\delta) = V_d \\
X_t I_q + E_b cos(\delta) = V_q
\end{aligned} \tag{4.8}$$

Equation (4.7) represents the set of differential equations and equation (4.8) represents the set of algebraic equations. From [14], equations (4.7) and (4.8) can be linearized and written in state space form to obtain the A, B, C, D, E, F matrices as discussed in Section (4.2) are shown in equations (4.9)- (4.14).

$$A = \begin{bmatrix}
0 & 1 & 0 & 0 \\
0 & 0 & -\frac{\omega_s}{2H} I_{q0} & -\frac{\omega_s}{2H} I_{d0} \\
0 & 0 & -\frac{1}{T_{do}^{'}} & 0 \\
0 & 0 & 0 & -\frac{1}{T_{q0}^{'}}
\end{bmatrix} \tag{4.9}$$

$$B = \begin{bmatrix} 0 & 0 & 0 & 0 \\ 0 & 0 & -\frac{\omega_s}{2H}[E'_{q0}(X'_q - X'_d)I_{d0}] & -\frac{\omega_s}{2H}[E'_{d0}(X'_q - X'_d)I_{q0}] \\ 0 & 0 & 0 & -\frac{x_d - x'_d}{T'_{d0}} \\ 0 & 0 & -\frac{x_q - x'_q}{T'_{q0}} & 0 \end{bmatrix} \tag{4.10}$$

$$C = \begin{bmatrix} 0 & 0 \\ \frac{\omega_s}{2H} & 0 \\ 0 & \frac{1}{T'_{d0}} \\ 0 & 0 \end{bmatrix} \tag{4.11}$$

$$D = \begin{bmatrix} E_b cos\delta_0 & 0 & 0 & -1 \\ -E_b sin\delta_0 & 0 & -1 & 0 \\ E_b cos\delta_0 & 0 & 0 & 0 \\ -E_b sin\delta_0 & 0 & 0 & 0 \end{bmatrix} \tag{4.12}$$

$$E = \begin{bmatrix} 0 & 0 & -(X'_q + X_t) & 0 \\ 0 & 0 & 0 & X'_d + X_t \\ 0 & -1 & -X_t & 0 \\ -1 & 0 & 0 & X_t \end{bmatrix} \tag{4.13}$$

$$F = \phi_{2\times 4} \tag{4.14}$$

where, $x = \begin{bmatrix} \Delta\delta & \Delta\omega & \Delta E'_q & \Delta E'_d \end{bmatrix}^T$, $u = \begin{bmatrix} \Delta T_m & \Delta E_{fd} \end{bmatrix}^T$, $z = \begin{bmatrix} \Delta V_q & \Delta V_d & \Delta I_d & \Delta I_q \end{bmatrix}^T$ From equations (4.9)- (4.14), the eigenvalues of the system can be obtained for the equilibrium point for which the differential equations are linearized. For a network of more than one generator, the network matrix E changes accounting for the interaction between both the generators.

4.4 Small signal stability assessment of SMIB using eigenvalue analysis

Consider the SMIB system shown in the Figure (4.1), whose dynamic data is shown in Appendix A. A 3 phase to ground fault at bus 4 is considered as a disturbance for the estimation of eigenvalues of the system after the fault is cleared at t=0.5 seconds.

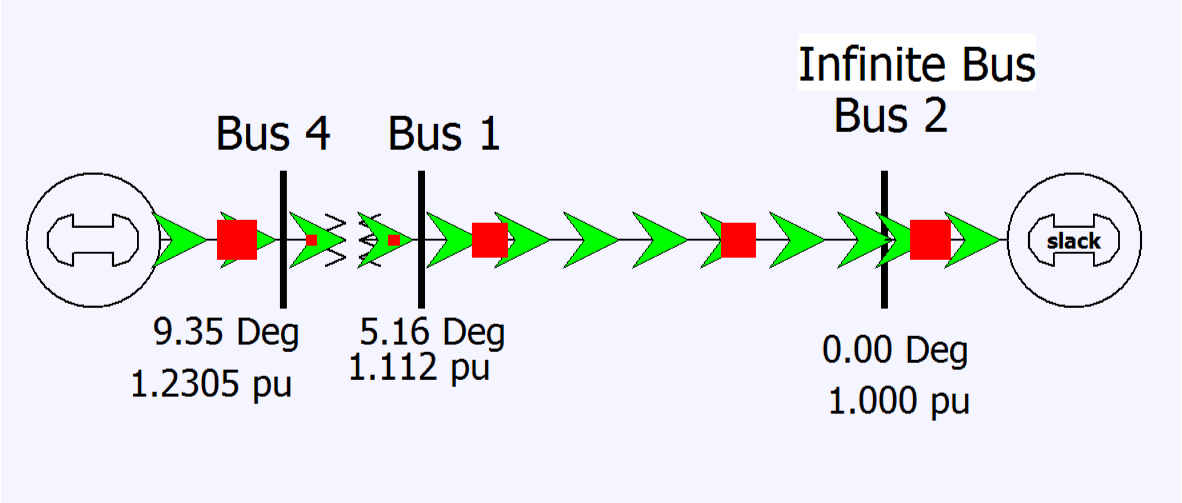

Figure 4.1: SMIB system considered for eigenvalue analysis

A 4th order model for the generator and a 2^{nd} order model for the exciter is considered for the calculation of the eigenvalues. Therefore, the resulting system matrix is a 6×6 matrix which results in 6 eigenvalues. The calculated system matrix, A_{sys} is shown in equation (4.15).

$$A_{sys} = \begin{bmatrix} 0 & 377 & 0 & 0 & 0 & 0 \\ -0.346 & -0.224 & -0.268 & 0.141 & 0 & 0 \\ -0.414 & -0.555 & -0.657 & 0 & 0.142 & 0 \\ 1.693 & -1.560 & 0 & -4.191 & 0 & 0 \\ 66.112 & -422.870 & -293.336 & -194.452 & -5 & -1000 \\ 0 & 0 & 0 & 0 & 0 & -1.000 \end{bmatrix} \tag{4.15}$$

where, $x = \begin{bmatrix} \Delta\delta & \Delta\omega & \Delta E_q^{'} & \Delta E_d^{'} & \Delta E_{fd} & \Delta V_f \end{bmatrix}^T$

Table 4.1: Eigenvalues of SMIB obtained from linearized dynamic model

	Eigenvalue	Damping ratio	Frequency
1	-0.3679+j11.0053	0.0334	1.7515
2	-0.3679-j11.0053	0.0334	1.7515
3	-3.2489+j6.6893	0.4369	1.0646
4	-3.2489-j6.6893	0.4369	1.0646
5	-2.8405	-NA-	-NA-
6	-1	-NA-	-NA-

Table (4.1) shows the list of eigenvalues with their damping ratios and frequencies which is also shown in Figure (4.2). From the participation factor table shown in Table (4.2), it can be seen that the 1.715 Hz component with least damping is due to $\Delta\delta$ and $\Delta\omega$. The 1.064 Hz component with highest damping is due to $\Delta E_q^{'}$ and ΔE_{fd} state variables.

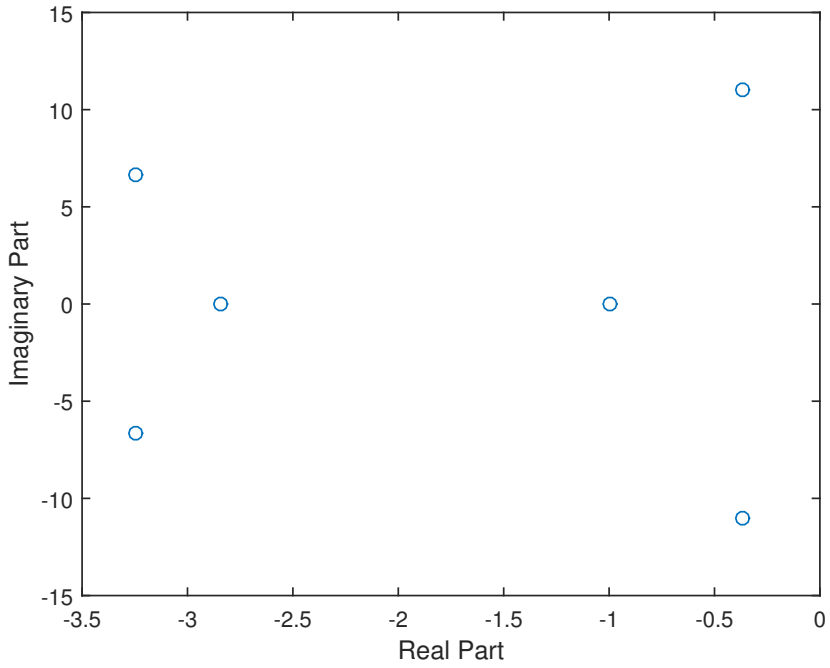

Figure 4.2: Eigenvalues on complex plane of considered SMIB system

Table 4.2: Participation factor on various state variable of the system.

Eigenvalue no.	$\Delta\delta$	$\Delta\omega$	$\Delta E_q^{'}$	$\Delta E_d^{'}$	ΔE_{fd}	ΔV_f
1	0.707	0.700	0.06	0.026	0.066	0
2	0.707	0.700	0.06	0.026	0.066	0
3	0.056	0.069	0.686	0.092	0.715	0
4	0.056	0.069	0.686	0.092	0.715	0
5	0.022	0.023	0.034	0.997	0.043	0
6	0	0	0	0	0	1

4.4.1 Sensitivity of reactive power support on small signal stability

From Section 4.3, it can be seen that matrices C and D are constant for a given generator parameters. The values of matrices B and E depend on the operation conditions of the system and system network. The generated reactive power can be varied to change the values of B matrix. The effect of reduction of reactive power from 50 Mvar to 0 Mvar is analyzed.

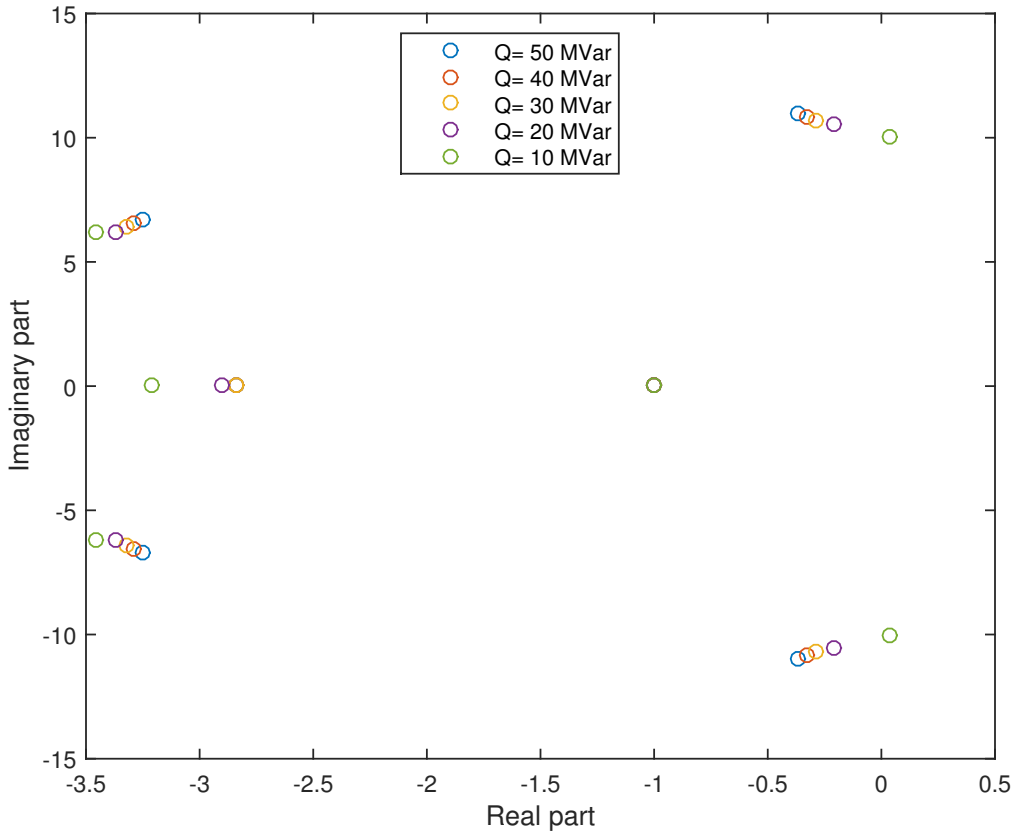

Figure 4.3: Movement of eigenvalues for varying Q_{gen}

From Figure (4.3), it can be seen that the reduction of reactive power causes the reduction of damping ratio of each mode causing the poles to move closer to the origin line. This is due to reduction of direct and quadrature currents in the B matrix which affects the values of the system matrix such that damping of the modes is reduced.

4.4.2 Sensitivity of system coupling on small signal stability

The stability of the system is also highly dependent on the network reactance represented by X_t. A higher value of X_t represents strong coupling of the generator with the rest of the network. A low value of X_t represents a weak coupling resulting in increased stability problems.

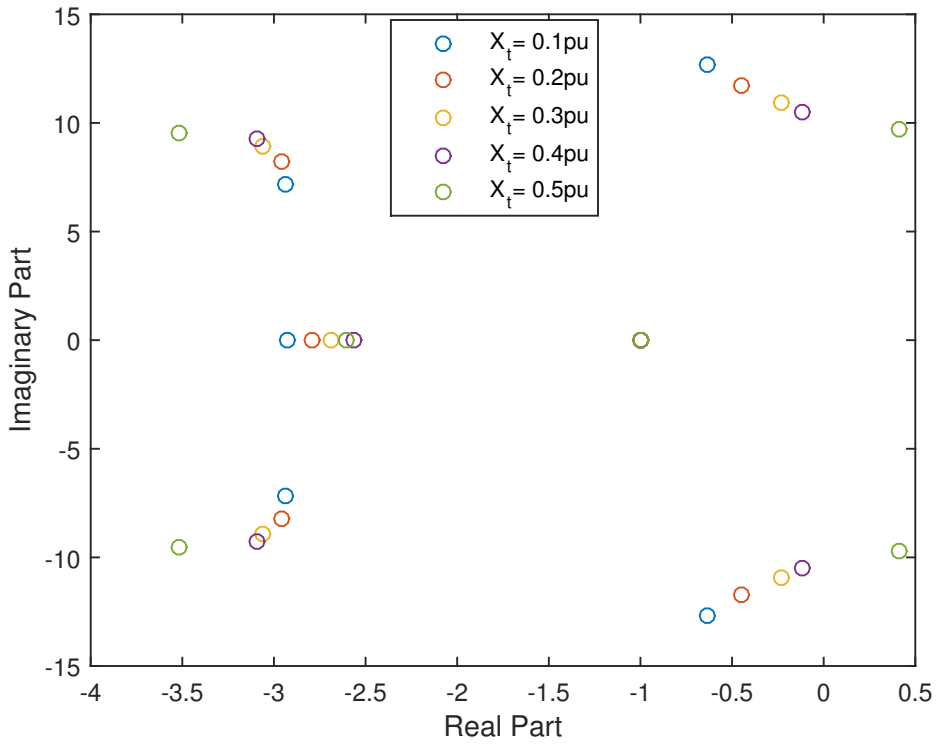

Figure 4.4: Movement of eigenvalues for varying coupling, X_t

Figure (4.4) shows the movement of eigenvalues for variation of X_t from 0.5 pu to 0.1 pu for a fixed value of $Q = 150MVar$. It can be seen that damping of the modes is greatly reduced similar to reducing reactive power generation. But reducing the coupling of the generator causes changes in network matrix, E which in turn causes changes in system matrix moving the poles closer to the origin line.

Thus from the sensitivity analysis of reactive power support and system coupling, it can be noted that the system stability is highly affected by changes in system operating parameter matrices A, B, D and system network matrix E. Therefore it is important to accurately calculate and maintain the values of the matrices A, B, C, D, E in order to estimate the modes that represent the actual response of system.

4.5 Difficulties in applying model based modal analysis to large power system

- Maintenance of dynamic database: Due to the linearization process, the initial values for every state variables and the other system variables need to be measured from the system to determine the modal properties. Also the system operating parameter matrices A, B, D and the system network matrix E is also need to be updated for every equilibrium point attained by the power system.

- For a larger order model, it requires a larger dynamic database that needs to maintained which is costly and time consuming.

- Models for power system characteristics like the ferro-resonance and skin effect might be negligible for large systems.
- The uncertainty in representing a constant current/ constant impedance model for loads in power system makes the model based modal analysis challenging.

4.6 Conclusion

In this chapter, eigenvalue based modal analysis has been discussed using a model based approach. The participation factor of every state variable on each eigenvalue is also discussed. The eigenvalue based modal analysis and the effect of participation factor of each state variable is explained using a SMIB system. Movement of main oscillatory mode causing instability with variation of generated reactive power and network coupling is analyzed with respect to the various model matrices.

Chapter 5

Modal Identification by Time Domain Techniques

5.1 Introduction

In this chapter, an alternative method of estimating the modal parameters of power system using measured oscillatory data is discussed. In Section 5.2, the concept of alternative approach to modal analysis and method of measurement based techniques are discussed. In Section 5.3, various types of signal processing methods to extract modal parameters from system responses are discussed. Prony analysis, Eigenvalue realization algorithm and matrix pencil method are discussed in Section 5.4. In Section 5.5, the measurement-based technique is illustrated using a SMIB system. In Section 5.6, the modal parameters of an IEEE 39 bus system are extracted using time domain techniques. In Section 5.7, disadvantages of time domain techniques are discussed. Section 5.8 concludes this chapter.

5.2 Alternative approach to traditional modal analysis

Modal analysis in power system has been performed using linearizing dynamic algebraic equations around an operating point. This provides important stability characteristics of the system that represent the system response to a disturbance. For small systems, the linearization technique can easily estimate the eigenvalues using numerical methods designed to solve full system matrices. For a large system, only a small number of modes with less accuracy are computed in the case of using reduced order sparse matrices [15]. Another approach which is being adopted is division of large order model into three small systems which is simulated simultaneously using tool called KLM- parallel with the help of 12 core super-computer [16]. This method is also not reliable due the global parameter which is shared for each small systems as shown in Figure (5.1).

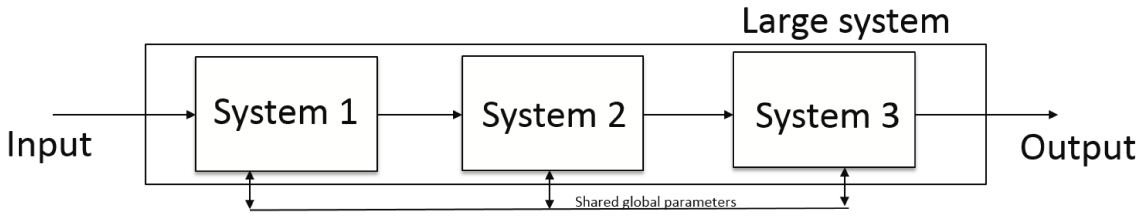

Figure 5.1: Cascaded modelling using KLM- parallel

Output based system identification is an alternative method for larger power systems where a reduced order linearization around an operating point produces erroneous results. These methods are a set of signal processing techniques which use

the time synchronized system measurements which became possible after the advent of phasor measurement units [17]. Since these methods are directly based on measured response, changes in modal parameters due to unknown characteristics can be tracked irrespective of the size of the system. The performance of these methods is affected and limited to availability of data with a required resolution under a certain noise level.

For example, in power systems, although an 8^{th} order model (4^{th} order model for generator, a 2nd order model for exciter, a 2^{nd} order model for governor) is linearized to obtain 8 eigenvalues, not all eigenvalues are responsible for oscillation in the system response. This is because a particular disturbance excites only one eigenvalue pairs called the main oscillatory mode. This holds true for large power systems where the oscillation and therefore the stability is predominately due to one or rarely at most 2 eigenvalue pairs. Table (5.1) shows the list of events that led to the Western North American blackout in 1996.

Table 5.1: List of events during 1996 Blackout [18]

Time/Event	Frequency	Damping ratio
10:52:19(brake insertion)	0.285 Hz	8.4%
14:52:37(John Day-Marion)	0.264 Hz	3.7%
15:42:03(Keeler-Allston)	0.264 Hz	3.5%
15:47:40(oscillation start)	0.238 Hz	-3.1%
15:48:50(oscillation finish)	0.216 Hz	-6.3%

It could be seen from table (5.1) that the inter-area mode with the 0.28Hz main oscillatory mode is the single eigenvalue pair whose damping ratio falls from positive to negative value causing the instability and blackout. In terms of measurement based modal analysis, the main oscillatory mode is identified in terms of amplitude and damping ratios relative to the natural frequency that each mode presents in the system response. Using extracted modal parameters, measurement based modal estimation techniques also provide a reduced order model for the large power system under study.

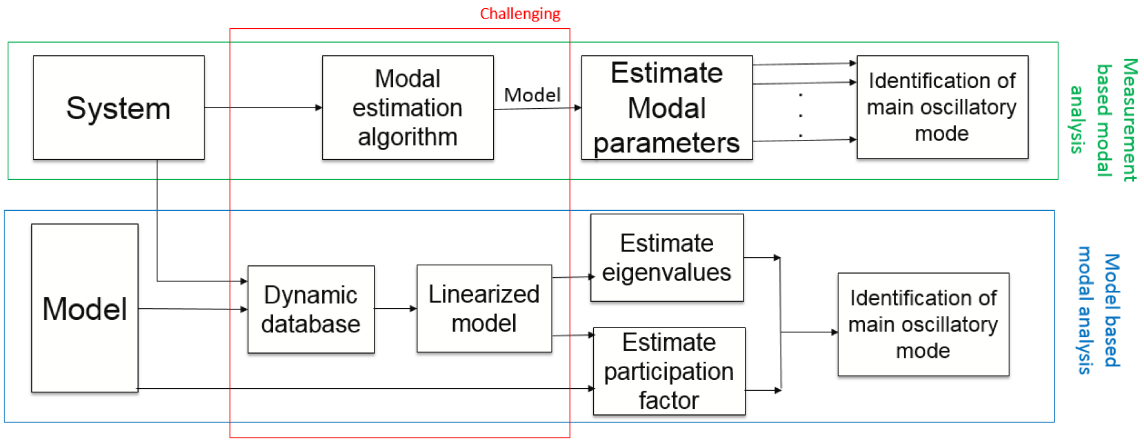

Figure 5.2: Cascaded modelling using KLM- parallel

Figure (5.2) shows the conventional method of modal analysis which is a model based approach that involves maintaining dynamic database and linearization process, whereas the measurement based technique involves modal extraction techniques from the system response.

5.3 Signal processing methods for modal extraction

The signal processing methods can be classified based on the approach to extract the modes from measured oscillatory response. The techniques can either use a model based approach, where a curve is fitted with the model and system response, or can be a direct analysis on a pre-processed form of the system response. A model-based approach is called parametric method and the latter being the non-parametric method. Usually, the time domain techniques are parametric based techniques which assume either a linear or non-linear model to obtain modal parameters [19]. Therefore, the parametric algorithms can be classified as Ringdown and Mode meter analysis.

5.3.1 Ringdown analysis

In this technique, according to [20], the modal parameters are obtained using N number of linearly superimposed damped sinusoids as shown in equation (5.1).

$$Y(t) = \sum_{i=1}^{N} A_i e^{-\Sigma_i t} \cos(\omega_i t + \phi_i) \tag{5.1}$$

where, A_i, is the amplitude of the i^{th} mode, Σ_i, is the damping constant of the i^{th} mode, ω_i, is the natural frequency of the i^{th} mode, ϕ_i, is the phase of the i^{th} mode, N, is the total number of modes.

Equation (5.1) is established based on the definition that oscillatory signals are obtained from the real part of the complex values obtained from the poles and zeros

of the transfer function which can be generally represented as:

$$Y(s) = \sum_{i=1}^{N} \frac{\beta_i}{s - \lambda_i} + \frac{\beta_i}{s - \lambda_i^{'}} \tag{5.2}$$

where, $Y(s)$, is the transfer function of the system to be identified. λ_i, $\lambda_i^{'}$ and β_i are the eigenvalue pairs and complex amplitude. The solution of equation (5.2) is written as

$$Y(t) = \sum_{i=1}^{N} \beta_i e^{\lambda_i t} + \lambda_i e^{\lambda_i^{'} t} \tag{5.3}$$

where the eigenvalue pairs can be expressed as $-\alpha_i \pm i\omega_i$ and the equation (5.3) becomes,

$$Y(t) = \sum_{i=1}^{N} \beta_i (e^{(-\alpha_i + i\omega_i)t} + e^{(-\alpha_i - i\omega_i)t})) \tag{5.4}$$

$$Y(t) = \sum_{i=1}^{N} 2\beta_i e^{-\alpha_i t} (\frac{e^{i\omega_i t} + e^{-i\omega_i t}}{2}) \tag{5.5}$$

The measured signals can be obtained by taking the real value of the equation (5.4) which can be simplified by substituting $\beta_i * 2$ as A_i and trigonometric identities to equation (5.5) to obtain equation (5.6).

$$Y(t) = \sum_{i=1}^{N} A_i e^{-\alpha_i t} \cos(\omega_i t + \phi_i) \tag{5.6}$$

The ringdown algorithm is widely used for analyzing transient response of the power system followed by a disturbance. All ringdown algorithms/ analysis are parametric including techniques like the Prony analysis, eigenvalue realization and matrix pencil method.

5.3.2 Mode meter analysis

The mode meter analysis is based on the analysis of ambient data assumed to be caused due to low-amplitude random variation like minute load changes. This

results in a system response of low amplitude depending on system dynamics [21]. The mode meter analysis is either a non-parametric(model-less) like the Welch periodogram or parametric method like the auto-aggressive moving average and Yule Walker technique. The mode meter analysis is not considered in this thesis.

5.4 Time domain techniques: Ringdown algorithm

5.4.1 Prony analysis

Prony analysis has been a viable technique to model a linear sum of damped complex exponentials with signals that are uniformly sampled. In Prony analysis curve fitting for a sum of exponentials is carried out at first and then extended models to interpolate intermediate points are obtained. Prony analysis is not only a signal analysis technique but also a system identification technique used to estimate modal parameters and mode shape in various fields including power system. Prony analysis is a parametric technique which involves three basic steps [22].

Step 1

From equation (5.6) a discretized form of equation (5.3) with sampling rate Δ_k can be written as

$$Y[k] = \sum_{i=1}^{N} C_i \mu_i^k \tag{5.7}$$

where, Y[k], is the sampled signal at sampling rate of Δ_k.

C_i, is $\frac{A_i e^{i\phi}}{2}$

μ_i^k, is $e^{\alpha_i \Delta_k}$

Equation (5.7) can be written as a linear prediction model as,

$$Y[N] = a_1 Y[N-1] + a_2 Y[N-2] + ... + a_N Y[0] \tag{5.8}$$

We can write equation (5.8) as a matrix form as

$$\begin{bmatrix} Y[N] \\ Y[N+1] \\ ... \\ Y[L-1] \end{bmatrix} = \begin{bmatrix} Y[N-1] & Y[N-2] & ... & Y[0] \\ Y[N] & Y[N-1] & ... & Y[1] \\ ... & ... & ... & ... \\ Y[L-2] & Y[L-3] & ... & Y[L-N-1] \end{bmatrix} \begin{bmatrix} a_1 \\ a_2 \\ ... \\ a_N \end{bmatrix} \tag{5.9}$$

Step 2

Equation (5.9) is of the form $Y = DA$ where the coefficients $a_1...aN$, are obtained by computing $A = D^{-1}Y$. The poles of the system can be obtained from equation (5.8) by taking root polynomial equation obtained from the coefficients in equation (5.8). The obtained poles contain the estimated damping co-efficient Σ_i and natural frequency ω_i of each mode.

Step 3

The amplitude and phase of each mode can be obtained from the known poles by writing equation (5.7) in matrix form as

$$\begin{bmatrix} Y[0] \\ Y[1] \\ Y[2] \\ ... \\ Y[L-1] \end{bmatrix} = \begin{bmatrix} 1 & 1 & ... & 1 \\ \mu_1^1 & \mu_2^1 & ... & \mu_N^1 \\ \mu_1^2 & \mu_2^2 & ... & \mu_N^2 \\ ... & ... & ... & ... \\ \mu_1^{L-1} & \mu_2^{L-1} & ... & \mu_N^{L-1} \end{bmatrix} \begin{bmatrix} C_1 \\ C_2 \\ C_3 \\ ... \\ C_N \end{bmatrix} \tag{5.10}$$

Equation (5.10) is of the form Y=UC and the value of $C_1...C_N$ can be obtained by computing $U^{-1}Y$.

From equation (5.7), the amplitude and the phase can be obtained as

$$\begin{aligned} A_i &= 2|C_i| \\ \phi_i &= args[C_i] \end{aligned} \tag{5.11}$$

5.4.2 Eigenvalue realization algorithm

The eigenvalue realization algorithm(ERA) uses the principles of minimum realization to obtain a state-space representation of the structure [23]. A realization is the estimation of the system matrices A, B, and C from the response of the structure. There can be infinite number of matrices A, B, C, and D each of different dimensions, that can be used to describe the input/output relationship of the system. However, the system should be realized with the least number of states or number of modes. This realization is called minimum realization [24]. The ERA starts with the discretized model of the system as shown in equation (5.12).

$$\begin{aligned} \dot{x}[k+1] &= Ax[k] + Bu[k] \\ y[k] &= Cx[k] + Du[k] \end{aligned} \tag{5.12}$$

Substituting $k = 0, 1, 2...$, we get $y[k]$ as shown in the equation bellow,

$$\begin{bmatrix} y[0] \\ y[1] \\ y[2] \\ y[3] \\ ... \\ Y[L-1] \end{bmatrix} = \begin{bmatrix} 0 \\ CB \\ CAB \\ CA^2B \\ ... \\ CA^{L-1}B \end{bmatrix} \tag{5.13}$$

The ERA technique starts with formation of Hankel and shifted Hankel matrix as shown below

$$H_0 = \begin{bmatrix} y[0] & y[1] & ... & y[L/2] \\ y[1] & y[2] & ... & y[(L/2)+1] \\ ... & ... & ... & ... \\ y[L/2] & ... & ... & Y[L-1] \end{bmatrix} \tag{5.14}$$

$$= \begin{bmatrix} CB & CAB & ... & CA^{L/2}B \\ CAB & CA^2B & ... & CA^{(L/2)+1}B \\ ... & ... & ... & ... \\ CA^{L/2}B & ... & ... & CA^{L-1}B \end{bmatrix} \tag{5.15}$$

$$= \begin{bmatrix} C \\ CA \\ CA^2 \\ ... \\ CA^{L/2} \end{bmatrix} \begin{bmatrix} B & AB & A^2B & ....A^{L/2}B \end{bmatrix} \tag{5.16}$$

$$H_0 = O_P C_P \tag{5.17}$$

where O_P and C_P are the controllability and observabilty matrix of the system.

In order to obtain the controllability and observabilty matrices, a singular value decomposition (SVD) of the Hankel matrix is performed. The SVD of H_0 yields,

$$H_0 = U_n \Sigma_n^2 V_n^T \tag{5.18}$$

where,

U_n, is the unit left eigenvector associated with the singular values.

Σ_n, is the singular values.

V_n, is the unit right eigenvector associated with the singular values.

Comparing equations (5.17) and (5.18), we can write,

$$O_p = U_n \Sigma_n C_p \quad = \Sigma_n V_n^T \tag{5.19}$$

The matrix can be obtained from a shifted Hankel matrix, H_1 which yields,

$$H_1 = O_P A C_P \tag{5.20}$$

Therefore,

$$A = O_P^{-1} H_1 C_P^{-1} \tag{5.21}$$

Finally we can write,

$$A = \Sigma_n^{-1} U_n^T H_1 V_n \Sigma_n^{-1} \tag{5.22}$$

From equations (5.16) and (5.17), the matrices B and C can be obtained from first elements of O_P and C_P and matrix $D = y[0]$.

5.4.3 Matrix pencil method

The matrix pencil method is based on numerical linear algebra. The matrix pencil method is also similar to ERA which works on the singular value decomposition [25]. While the ERA is better than Prony analysis in obtaining the state space model of the system, the matrix pencil method is a more robust technique producing better results from a signal with high level of noise.

In matrix pencil method, the problem of obtaining the poles of the system can be casted into a generalized linear eigenvalue problem as

$$[H_1 - \lambda H_0] \iff [H0^+ H_1 - \alpha[i]] \tag{5.23}$$

where,

H_0, is the Hankel matrix from ERA

H_1, is the shifted Hankel matrix from ERA

and the plus sign indicates the pseudoinverse of the matrix.

The SVD of the Hankel matrices H_0 and H_1 yields,

$$\begin{aligned} H_0 &= U\Sigma V_1 \\ H_1 &= U\Sigma V_2 \end{aligned} \tag{5.24}$$

and

$$\begin{aligned} V_1^{'} &= V_1[1:N] \\ V_2^{'} &= V_2[1:N] \end{aligned} \tag{5.25}$$

According to [26],

$$[[V_1]^H - \lambda[V_0]^H] \iff [[V_1^+]^H[V_2]^H - \lambda_i] \tag{5.26}$$

is equivalent to eigenvalues obtained by

$$[H_1 - \lambda H_0] \iff [H0^+ H_1 - \alpha[i]] \tag{5.27}$$

where,

the H denotes the complex conjugate of the matrix.

The A matrix of the system can be obtained from $V_1^{'}$ and $V_2^{'}$ as

$$[Y_1] = [V_1^{'}]^T[V_1^{'}] \tag{5.28}$$

$$[Y_2] = [V_2']^T [V_1'] \tag{5.29}$$

$$A = [Y_1]^{-1}[Y_2] \tag{5.30}$$

The eigenvalues can be obtained from the A matrix and the amplitude and phase can be obtained similar to Prony analysis. The difference between the matrix pencil and Prony analysis and the ERA is the increase robustness towards noise level since the matrix pencil method uses the unit vectors to obtain the elements of the A matrix. In the case of the Prony analysis,the curve is fitted directly on the noisy data and for ERA the A matrix is obtained using the singular values which is affected by the level of noise in the data.

5.5 Illustration using SMIB: System identification using measured data

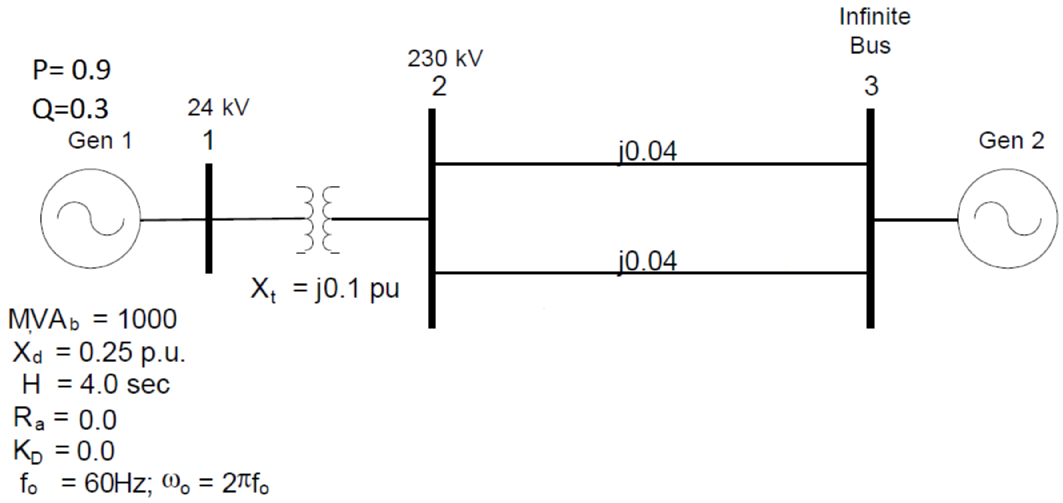

Figure 5.3: SMIB used for system realization

Consider the single machine infinite bus system shown in the Figure (5.3), which is used to show the relation between the participation factor in model based technique and main oscillatory mode in measurement based technique. The following are the generator parameters used in MATLAB used in control system toolbox for simulation.

Table 5.2: Generator parameters of SMIB system

Parameter	Value	Parameter	Value(pu)
H	3.5MWs/MVA	X_d	1.81
T'_{do}	7.5s	X_q	1.76
K_a	50	X'_d	0.3
t_a	0.2s	X'_q	0.16

The linearized state space representation of the SMIB is shown below:

$$\begin{bmatrix} \dot{\Delta\delta} \\ \dot{\Delta\omega} \\ \dot{\Delta E'_q} \\ \dot{\Delta E'_{fd}} \end{bmatrix} = \begin{bmatrix} 0 & \omega_0 & 0 & 0 \\ \frac{-K_1}{2H} & \frac{-D}{M} & \frac{-K_2}{2H} & 0 \\ \frac{-K_4}{T'_{do}} & 0 & \frac{-1}{K_3 T'_{do}} & \frac{1}{T'_{do}} \\ \frac{-k_A K_5}{T_A} & 0 & \frac{-k_A K_6}{T_A} & \frac{-1}{T_A} \end{bmatrix} \begin{bmatrix} \Delta\delta \\ \Delta\omega \\ \Delta E'_q \\ \Delta E'_{fd} \end{bmatrix} + \begin{bmatrix} 0 \\ 0 \\ 0 \\ \frac{K_A}{T_A} \end{bmatrix} u \qquad (5.31)$$

where K1- K6 are calculated from system operating parameters to be,

$K_1 = 0.84 \qquad K_3 = 0.38 \qquad K_5 = 0.1015$

$K_2 = 1.02 \qquad K_4 = 0.553 \qquad K_6 = 0.79$

Therefore, equation (5.31) becomes

$$\begin{bmatrix} \dot{\Delta\delta} \\ \dot{\Delta\omega} \\ \dot{\Delta E'_q} \\ \dot{\Delta E'_{fd}} \end{bmatrix} = \begin{bmatrix} 0 & 377 & 0 & 0 \\ -0.12 & 0 & -0.1457 & 0 \\ -0.0737 & 0 & -0.3509 & 0.1333 \\ -25.375 & 0 & -197.5 & -5 \end{bmatrix} \begin{bmatrix} \Delta\delta \\ \Delta\omega \\ \Delta E'_q \\ \Delta E'_{fd} \end{bmatrix} + \begin{bmatrix} 0 \\ 0 \\ 0 \\ 250 \end{bmatrix} u \qquad (5.32)$$

In order to obtain the change in rotor angle, the matrix C is [1 0 0 0] and D=0. The MATLAB [10] function lsim from control system toolbox is used to simulate change in the rotor angle of the generator from the obtained state space system as shown in Figure (5.4).

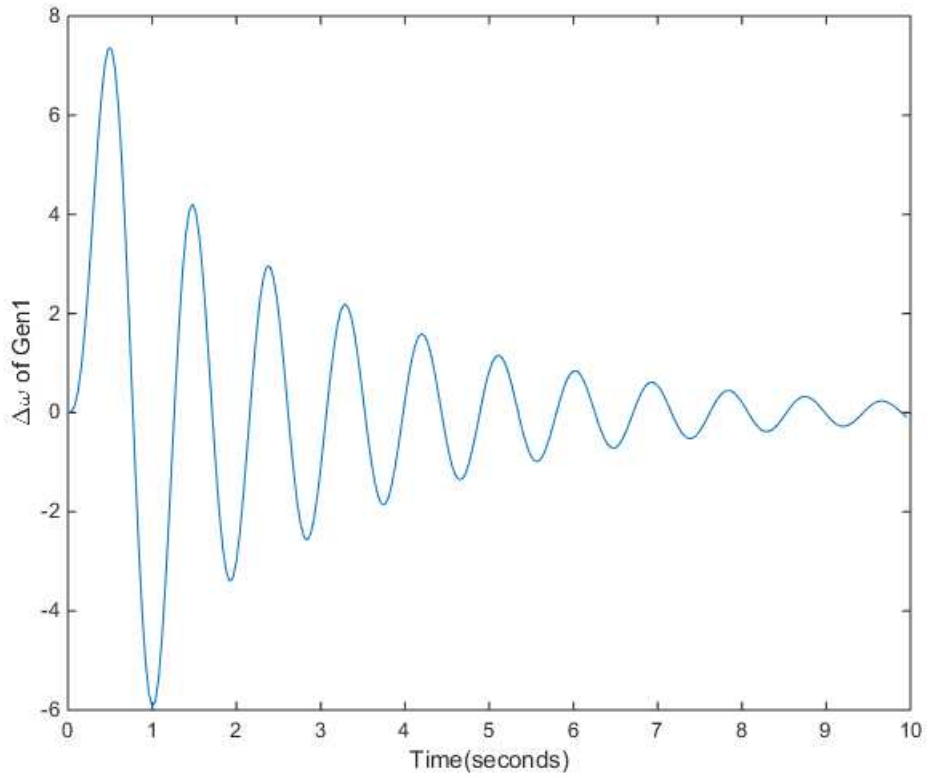

Figure 5.4: Oscillation of the generator rotor angle for impulse input

5.5.1 Modal analysis using linearized model

The modal parameters of the system can be easily obtained using the eigenvalues of the system matrix, A. The eigenvalues obtained using the linearized model of the SMIB are as follows:

$$\lambda = eig(\begin{bmatrix} 0 & 377 & 0 & 0 \\ -0.12 & 0 & -0.1457 & 0 \\ -0.0737 & 0 & -0.3509 & 0.1333 \\ -25.375 & 0 & -197.5 & -5 \end{bmatrix}) \tag{5.33}$$

Table 5.3: Modal parameters of SMIB system

Mode	Eigenvalue,λ	frequency	damping ratio
1	-2.3264 + j4.1051	0.653	0.566
1	-2.3264 - j4.1051	0.653	0.566
2	-0.3490 + j6.9061	1.099	0.050
2	-0.3490 - j6.9061	1.099	0.050

It can be seen from Table (5.3) that mode 2 is lightly damped and mode 1 is highly damped. In order to obtain the effect of each state variable on each mode, the participation factor is calculated.

It can be seen from Table (5.4), that δ, ω have higher participation factor of Mode 2 with 1.099 Hz and lower damping ratios. This implies that the time domain response of the rotor angle and speed will have higher oscillations because of mode 2 having very low damping ratio as seen in Figures (5.4) and (5.5). Whereas in E'_{fd}, E'_q, Mode

Table 5.4: Participation factors of each variables

	Mode 1	Mode 1	Mode 2	Mode 2
δ	-0.0294 + 0.0788i	-0.0294 - 0.0788i	-0.5790 + 0.1717i	-0.5790 - 0.1717i
ω	-0.0179 + 0.0604i	-0.0179 - 0.0604i	0.5179 - 0.2154i	0.5179 + 0.2154i
$E_q^{'}$	-0.2061 + 0.4594i	0.2061 + 0.4594i	0.0080 + 0.0758i	-0.0080 + 0.0758i
$E_{fd}^{'}$	-0.1587 - 0.4779i	-0.1587 - 0.4779i	0.0691 - 0.0320i	0.0691 - 0.0320i

1 has higher participation factor than mode 2 and since mode 1 is highly damped the time domain response has oscillations with lower amplitude due to lower participation factor as seen in Figures (5.6) and (5.7).

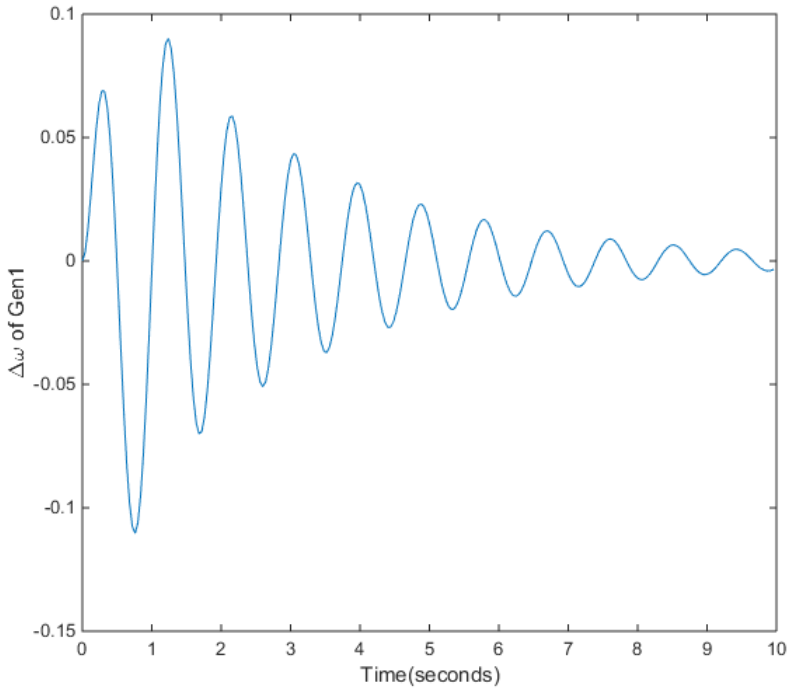

Figure 5.5: Oscillation of generator 1 speed for impulse input

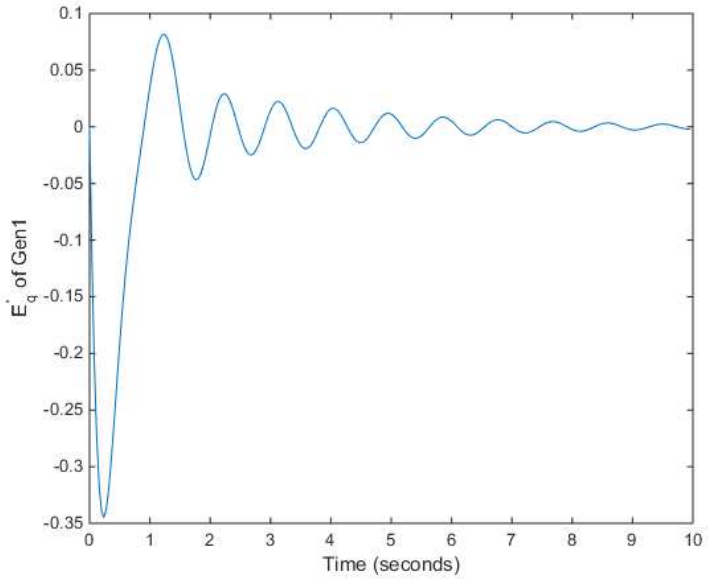

Figure 5.6: Oscillation of generator 1 q-axis voltage for impulse input

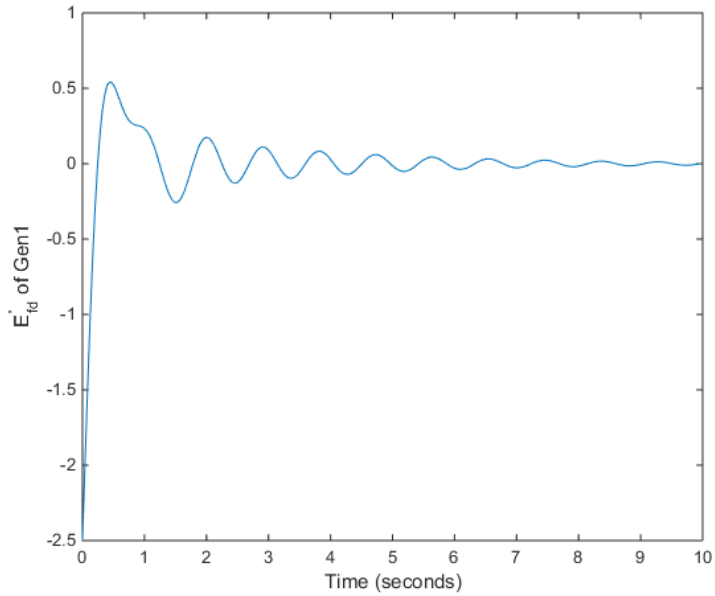

Figure 5.7: Oscillation of generator 1 field voltage for impulse input

5.5.2 System realization using eigenvalue realization technique.

The data for the change in rotor angle is collected from the simulation of the SMIB in order to obtain an output based model of the power system using ERA technique. 250 data points are collected with a time resolution of 0.04 seconds and ERA is applied on the data points. The SVD of the Hankel matrix reveals the presence of 4 eigenvalues in the data as shown below:

$$Singularvalues = \begin{bmatrix} 0.2804 & 0 & 0 & 0 \\ 0 & 0.2835 & 0 & 0 \\ 0 & 0 & 0.5181 & 0 \\ 0 & 0 & 0 & 0.8884 \end{bmatrix} \tag{5.34}$$

The system matrices A, B, C are obtained using equation (5.22) are as follows:

$$A = \begin{bmatrix} 0.9451 & 0.2589 & -0.0632 & 0.0177 \\ -0.2589 & 0.9653 & 0.0146 & -0.0070 \\ 0.0632 & 0.0146 & 0.8909 & 0.1575 \\ 0.0177 & 0.0070 & -0.1575 & 0.8941 \end{bmatrix} \tag{5.35}$$

$$B = [-0.0180; -0.0005; 0.0702; 0.0993] \tag{5.36}$$

$$C = [0.0180 - 0.00050.0702 - 0.0993]; \tag{5.37}$$

The discrete model obtained is based on the change in rotor angle data for the given input to the system. The discrete matrices, A, B, C can be converted to continuous state space system with zero order hold using d2c() in MATLAB and the

obtained continuous state space model is

$$A = \begin{bmatrix} -0.4706 & 6.6191 & -1.6697 & 0.6377 \\ -6.6191 & -0.0040 & 0.1502 & -0.1264 \\ 1.6697 & 0.1502 & -2.4506 & 4.3452 \\ 0.6377 & 0.1264 & -4.3452 & -2.4257 \end{bmatrix} \tag{5.38}$$

$$B = [-0.4266; -0.0689; 1.6305; 2.7613] \tag{5.39}$$

$$C = [0.0180 \quad -0.0005 \quad 0.0702 \quad -0.0993]; \tag{5.40}$$

The modal analysis of realized system matrix, A shows the same eigenvalues that was obtained from the linearized model of the power system. From equation (5.33)

$$eig(\begin{bmatrix} 0 & 377 & 0 & 0 \\ -0.12 & 0 & -0.145 & 0 \\ -0.073 & 0 & -0.351 & 0.133 \\ -25.375 & 0 & -197.5 & -5 \end{bmatrix}) = eig(\begin{bmatrix} -0.470 & 6.619 & -1.669 & 0.637 \\ -6.619 & -0.004 & 0.150 & -0.126 \\ 1.669 & 0.150 & -2.450 & 4.345 \\ 0.637 & 0.126 & -4.345 & -2.425 \end{bmatrix})$$

$$eig = \begin{bmatrix} -0.3490 + 6.906i \\ -0.349 - 6.906i \\ -2.326 + 4.105i \\ -2.326 - 4.105i \end{bmatrix} \tag{5.41}$$

Therefore, the system identified using ERA technique produces a model using the measured oscillatory data which has the same eigenvalue of the original model of the system. The participation of state variable can be obtained by extracting the individual modal parameters. The modal parameters of the rotor angle are shown in Table (5.5).

Table 5.5: Modal parameters of rotor angle of generator 1

	Amplitude	Phase	Natural frequency	Damping ratio
Mode1	11.629	115.04	0.653	0.5667
Mode2	6.91	-44.6	1.099	0.0505

It can be clearly seen from the Table (5.5), that the mode 2 with 1.09Hz component is the main oscillating energy. This is because, even though the amplitude of mode 2 is higher that mode 2, mode 2 has a very low damping compared to mode 1 which is in accordance with the highest participation factor in linearized model analysis.

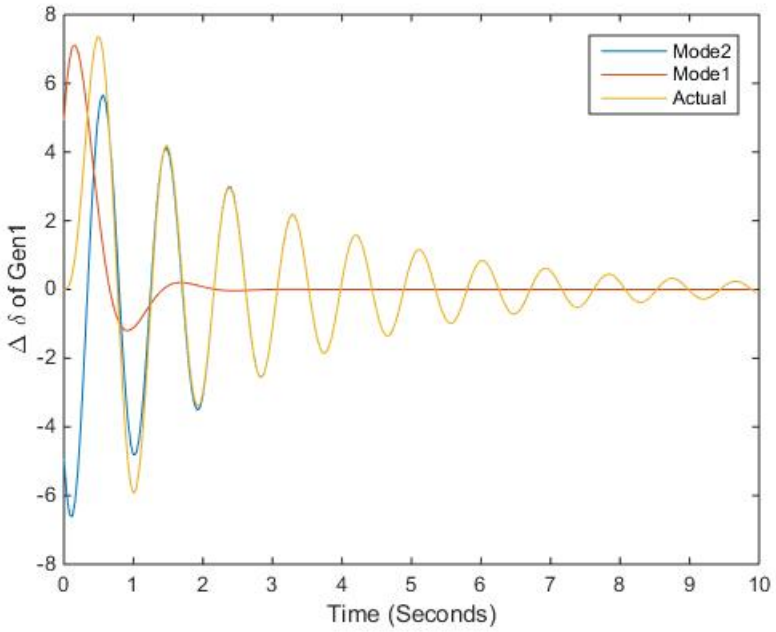

Figure 5.8: ERA fit showing individual modes of rotor angle oscillation

From Figure (5.8) it can be clearly seen that mode 2 is the main oscillatory mode contributing to the oscillatory energy in the rotor angle of the generator. Similar

results can also obtained for speed of the generator since both speed and rotor angle oscillation are due to a single eigenvalue pair.

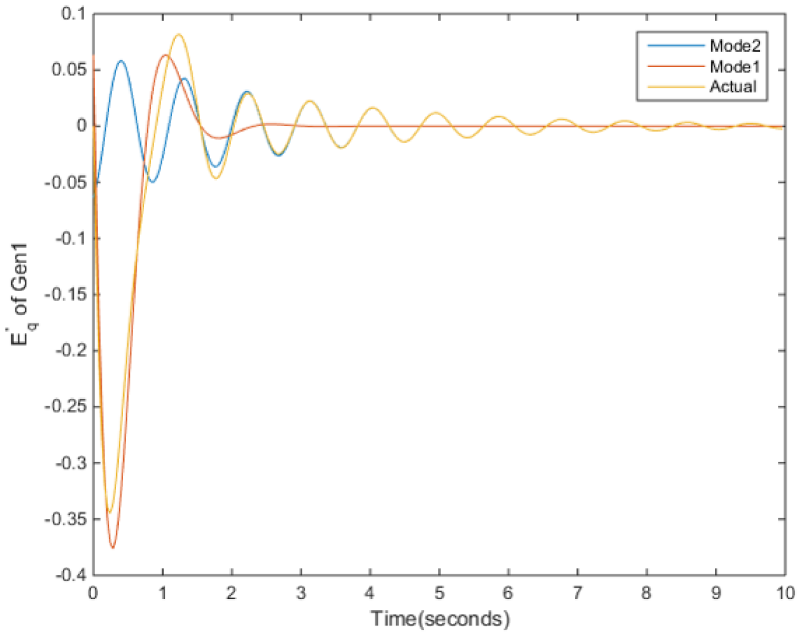

Figure 5.9: ERA fit showing individual modes of $E_q^{'}$ oscillation

Similarly, for q-axis voltage of the generator , it can be seen from the Figure (5.9) that mode 2 is the dominant mode due to very low damping compared to mode 1. Although mode 1 has the highest participation factor from Table (5.4), the effect of non- dominant mode 2 on q-axis voltage and field voltage is higher than mode 1 on the speed and rotor. This is because of the fact that mode 2 has very low damping relative to the frequency of oscillation. This indicates that a mode with higher participation factor obtained in a model-based technique need not necessarily be the mode of interest in stability studies. Since in this case the given disturbance excites the 1.099 Hz component only by decreasing the damping ratio.

5.6 Case study: 39 bus New England power system

The IEEE 39 bus network shown in Figure (5.10) is used to obtain a reduced order model of large systems using the measurement based time domain technique and to show the presence of single main oscillatory mode in a system with large number of generators. The parameters of each component in the 39 bus system is shown in Appendix C.

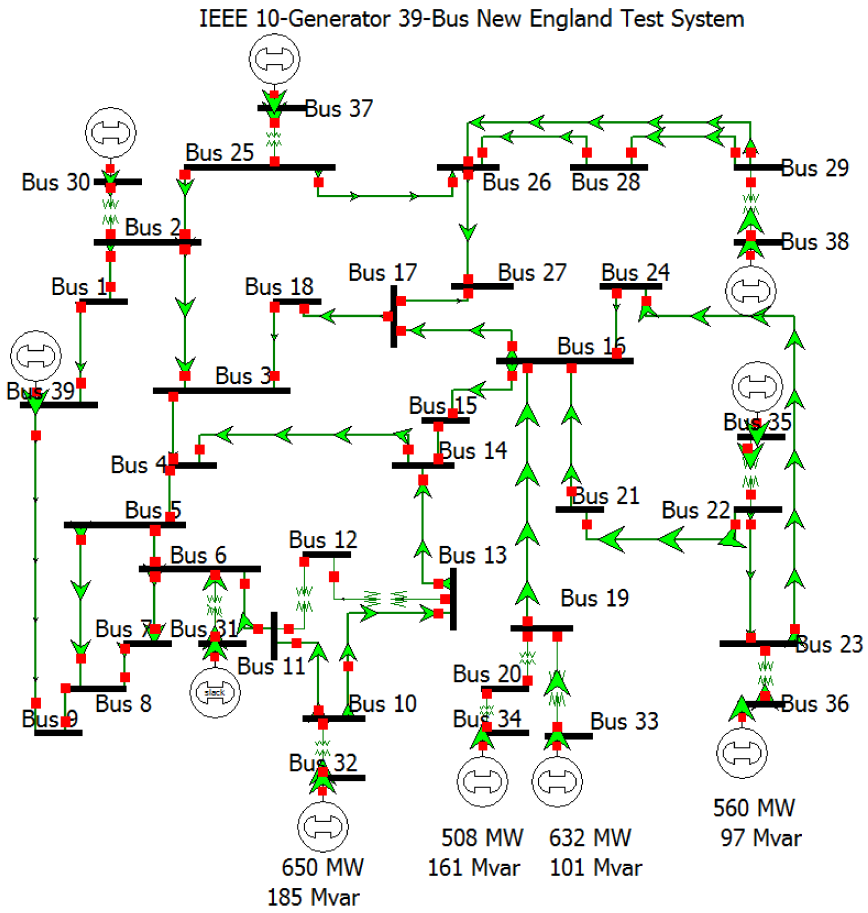

Figure 5.10: IEEE 39 Bus Network [27]

In order to analyze the small signal stability, the linearized system matrix A is obtained from the PowerWorld. The linearization is performed before the fault to obtain the eigenvalues of the healthy system and by applying the measurement based technique after the fault, the excited modes by the disturbance can be tracked by its movement towards the origin. The obtained matrix A is a 209 X 209 matrix with 209 state variable. The eigenvalues of the system, which is oscillatory in nature close to the origin, are shown in the Figure (5.11).

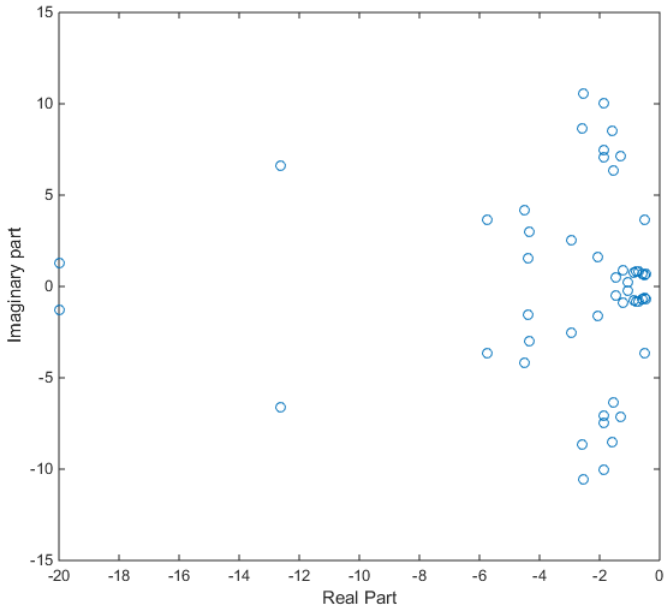

Figure 5.11: Eigenvalues of the 39 bus system before the fault

In order to perform an ERA/ Matrix pencil/ Prony analysis, a 3 phase to ground fault is introduced at bus 16 at 0.5 seconds and cleared at 0.7 seconds. The rotor angle and speed of generator 2, 5, 10 are chosen for analysis and shown in Figure (5.12). A 6th order model is fitted for the transient data after the fault is cleared

at t=0.7 seconds in MATLAB environment by importing the time domain data from PowerWorld.

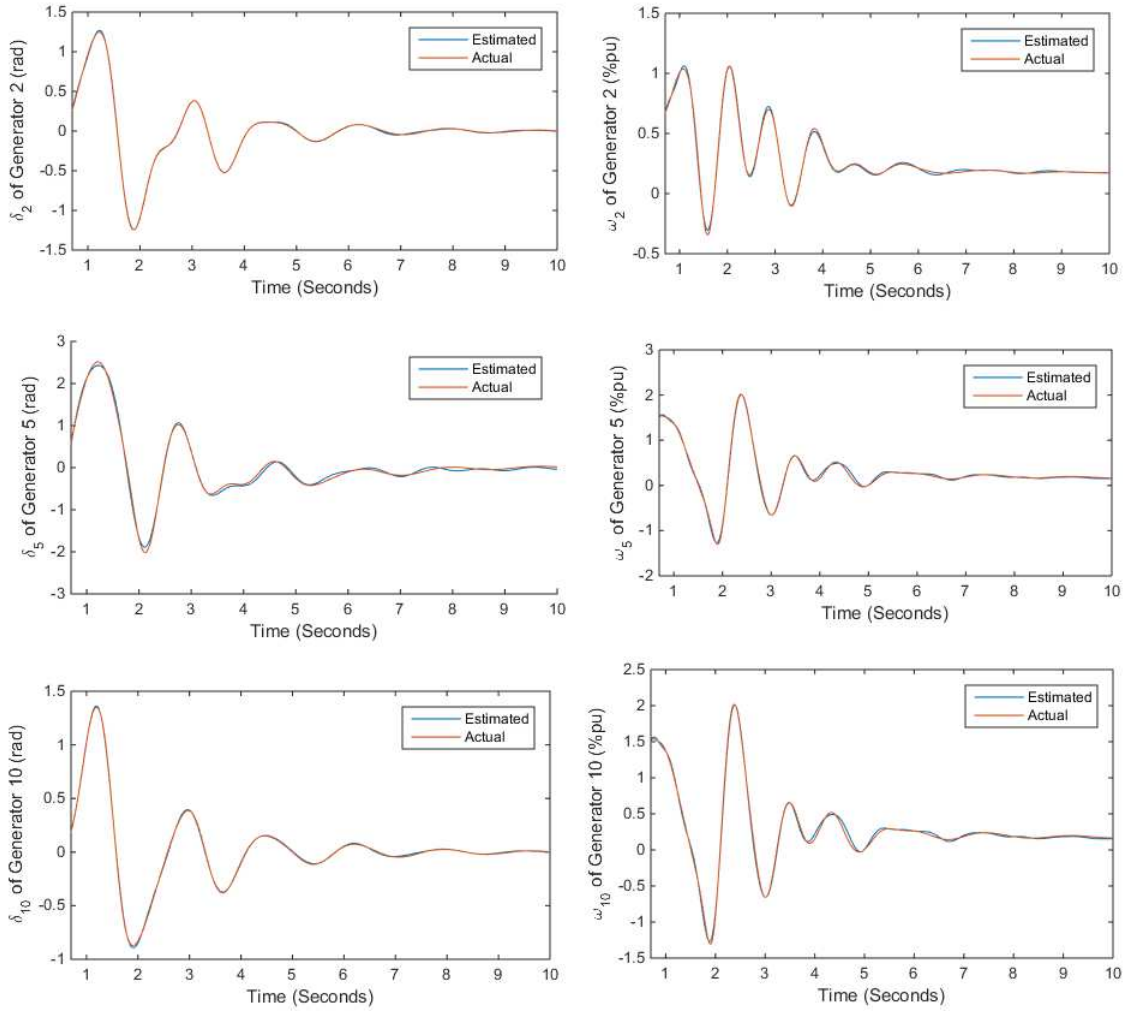

Figure 5.12: Eigenvalues of oscillatory nature of the 39 bus system

The realized system using the rotor angle and speed of the generators is of size 6 X 6 with three modes. The time domain fit of the realized model is shown in Figure (5.12) which indicates that the realized system modal parameters represent the actual system. The estimated modal parameters for rotor angle and speed of generator 2

Table 5.6: Modal parameters of speed of generator 2

	Amplitude	Phase	Natural frequency	Damping ratio
Mode1	4.19	164.73	1.18	0.1362
Mode2	3.05	56.5	1.001	0.141
Mode 3	1.14	-166.72	0.6063	0.265

Table 5.7: Modal parameters of rotor angle of generator 2

	Amplitude	Phase	Natural frequency	Damping ratio
Mode1	1.13	81.5	1.19	0.101
Mode2	0.85	-46.65	0.99	0.1037
Mode 3	2.388	99.06	0.599	0.2478

are shown in Tables (5.6) and (5.7). It can be seen from Tables (5.6) and (5.7) that mode 1 is the main oscillatory mode for both speed and rotor angle of generator 2 due to lower damping when compared to mode 3. The higher amplitude of mode 3 of rotor angle does not make it as a main oscillatory mode due to high damping relative to the natural frequency of mode 3.

Figures (5.13) and (5.14) show the movement of the eigenvalues before and after the disturbance in power system. The eigenvalues from the linearized model is used as eigenvalues before the fault and it can be seen that all the eigenvalues are towards the left half of the s-plane, indicating that the each mode is highly damped. The eigenvalues of the realized systems for rotor angle and speed of multiple generators 2, 5, 10 are shown in the Figures (5.13) and (5.14) respectively.

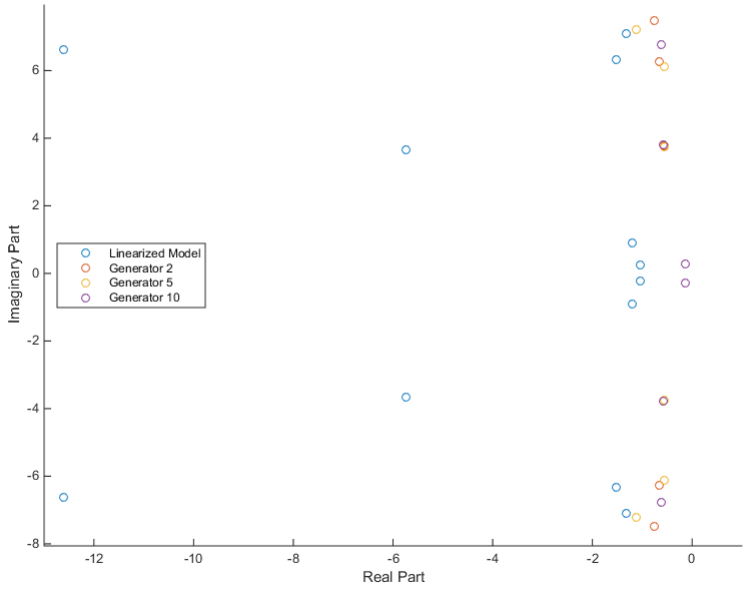

Figure 5.13: Movement of eigenvalues associated with rotor angle after fault.

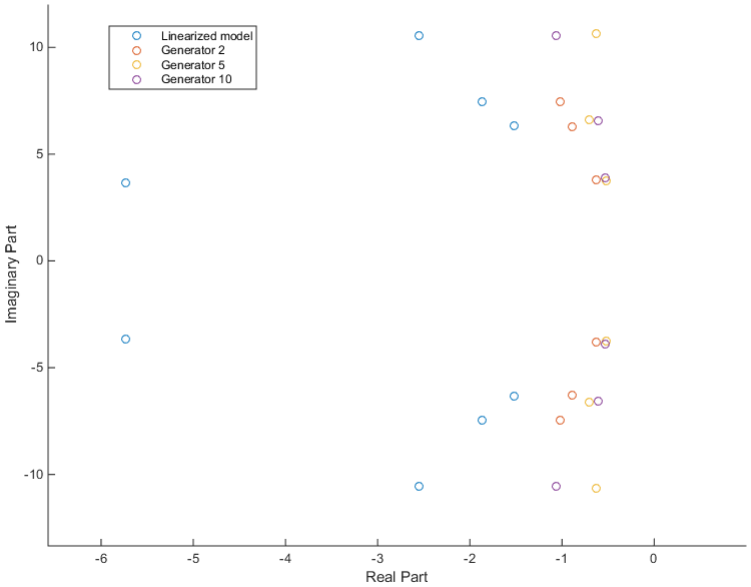

Figure 5.14: Movement of eigenvalues associated with generator speed after fault.

It can be seen that the realized system using the time domain techniques indicates the significant reduction of the damping ratios which causes the eigenvalues to move towards the right half of the s-plane, thus making the system vulnerable to instability. In addition, it can be seen that the main oscillatory mode of all the generators occurs along the same imaginary axis (around 1Hz) indicating that the main oscillatory mode is a single eigenvalue pair which is excited by the 3 phase fault in the system.

5.7 Disadvantage of time domain based technique

The algorithm of any time domain technique is based on the minimal error fit of the time domain model with the chosen system response. Therefore, the algorithm represents a single frequency mode as two modes as seen in Table (5.6) and (5.7) where mode 1 and 2 having more or less the same frequency and damping ratio are represented as two modes because of minimal error fit in time. This might make it difficult for identifying the main oscillatory modes present in the system response. On the other hand, the time domain techniques are always suitable for analyzing larger system where the system possesses a lot of closely spaced frequencies.

5.8 Conclusion

In this chapter, three types of time domain techniques are discussed to estimate the modal parameters from the obtained system response. System identification is performed for a SMIB system using the time domain techniques and compared with the modal analysis results from a calculated linearized model. System identification on a larger IEEE 39 bus network is performed for all 10 generators. The movement of the main oscillatory modes in the event of disturbance obtained from the time domain techniques is compared with the eigenvalues before the disturbance obtained from linearized model in view of stability monitoring.

Chapter 6

Modal Identification by Frequency Domain Techniques

6.1 Introduction

In this chapter, the method of extracting modal parameters by curve fitting in frequency domain using a frequency model is discussed. In Section 6.2, the concept of modal extraction in frequency domain and the types of frequency domain techniques with its disadvantages are discussed. In Section 6.3, the model used for frequency domain curve fitting is discussed. In Section 6.4, the method of extracting the modal parameters using curve fitting is discussed. In Section 6.5, the parametric discrete Fourier transform (p-DFT) is validated using synthetic signal with two levels of noise. In Section 6.6, IEEE 14 bus system is used as a case study and the modal parameters are obtained using p-DFT and the results are compared with results of traditional model based technique. In Section 6.7, the disadvantages of

frequency domain technique are discussed in comparison with time domain techniques. Section 6.8 concludes the chapter.

6.2 Modal identification in frequency spectrum

Similar to time domain techniques, both parametric and non-parametric methods can be used for frequency domain analysis to extract modal parameters from the measured system response. The graphical form of frequency domain analysis is one method of non-parametric Discrete Fourier Transform (DFT) technique where the modal parameters are directly obtained from the frequency domain plot of oscillatory signal. The modal parameters can be obtained by performing DFT of the time domain signal as indicated in the equation (6.1).

$$Y(j\omega) = \sum_{i=1}^{N} y[n] e^{-j2\pi in}, 0 \leq i \leq N \tag{6.1}$$

where,

$y[n]$ is the measured oscillatory signal

$Y(j\omega)$ is the DFT of the measured oscillatory signal.

According to [28], the modal parameters can be graphically obtained for k^{th} peak in DFT plot using the equations (6.2) - (6.4).

$$A_k = \frac{4|Y(\omega_k)|}{NT_s} \tag{6.2}$$

$$\phi_k = tan^{-1}\left[\frac{Im(Y(\omega_k))}{Re(Y(\omega_k))}\right] \tag{6.3}$$

$$\zeta_k = \frac{2}{\omega_k NT_s} ln\left(\frac{|Y(\omega_k)|}{Y(\omega_k)e^{-j\omega_k NT_s}}\right) \tag{6.4}$$

6.2.1 Shortcomings of non-parametric DFT technique

1. Leakage of energy due to rectangular windowing:

   As a property of the rectangular window used for the DFT, the leakage of energy due to Gibbs phenomenon is highest for a rectangular window with the lowest main-lobe width [29]. Therefore, the usage of other common windows like the hamming window, has higher side lobe attenuation(less leakage) but has higher main lobe width, which causes peaks to overlap with each other in frequency and hence the resolvability in frequency is compromised.

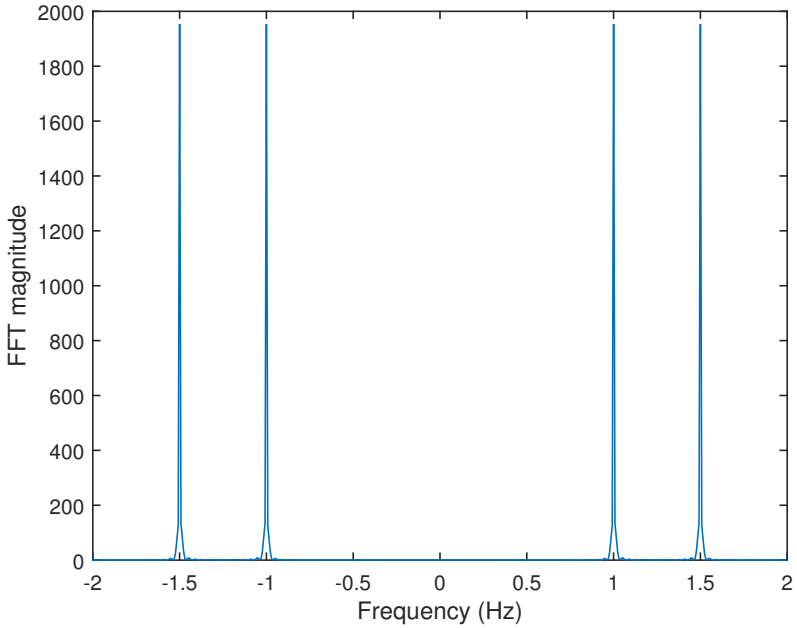

Figure 6.1: Infinite windowed/ undamped sinusoid with 1 and 1.5 Hz component

2. Significant aliasing in frequency:

   In applications like power system oscillations where several frequency

components are usually present along with the main frequency component, the leaked energy from other frequency components interferes with the main energy component of nearest mode and vice-versa. This causes the analysis of frequency spectrum to be harder even when the characteristic of a rectangular window is already known. But the usage of the rectangular window with lowest main-lobe width is enough to produce the peaks at the exact frequency location corresponding to the damped frequency of the input signal. Figures (6.1) and (6.2) show the DFT plot of undamped and damped sin wave consisting of 1Hz and 1.5Hz component.

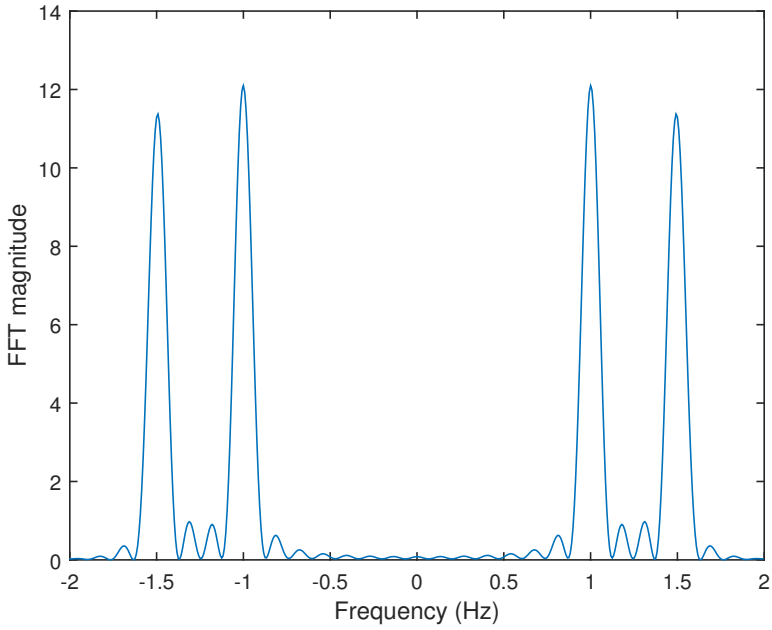

Figure 6.2: Windowed/ damped sinusoid with 1 and 1.5 Hz component

In addition, the damped sinusoids limit the number of samples or window size causing the significant leakage of energy and aliasing and giving rise to peaks

between 1 and 1.5 Hz component.

3. Type of window used:

   The analysis of a non parametric DFT technique is independent of the type of window used to produce the DFT plot. The usage of different types of windows produces different DFT plots and causes differences in the results of the non parametric DFT technique.

6.3 Modelling for parametric Frequency domain analysis

In order to overcome the short coming of non-parametric/ graphical method of frequency domain analysis, a model based frequency domain analysis called the parametric DFT is adopted. The response or the measured oscillatory data can be characterized by an impulse response of the system causing it to have N number of super-imposed sinusoidal modes which are exponentially decaying in nature as shown in equation (6.5).

$$y(t) = \sum_{k=1}^{N} A_k e^{-\zeta_k \omega_k t} sin(\omega_k \sqrt{1-\zeta^2} t + \phi_k) \tag{6.5}$$

where,

A_k is the amplitude of k^{th} mode.

ζ_k is the damping ratio of k^{th} mode.

ω_k is the damped frequency of k^{th} mode.

ϕ_k is the phase of k^{th} mode.

The time domain model shown in equation (6.5) is converted into frequency domain to make a least square fit in the frequency domain [30]. The Laplace transform of equation (6.5) can be written as shown in equation (6.6).

$$Y(jw) = \sum_{k=1}^{N} A_k \frac{(s + \zeta_k \omega_k) sin(\phi_k) + \omega_k \sqrt{1 - \zeta^2} cos(\phi_k)}{s^2 + 2\zeta_k \omega_k s + \omega_k^2} \tag{6.6}$$

$$Y(jw) = \sum_{k=1}^{N} A_k \frac{(s + \zeta_k \omega_k) sin(\phi_k) + \omega_k \sqrt{1 - \zeta^2} cos(\phi_k)}{(s - \alpha_{1k})(s - \alpha_{2k})} \tag{6.7}$$

where,

$\alpha_{1k,2k}$ is the poles of the s domain transfer function indicating the eigenvalues pairs responsible for the oscillation.

In order to perform a least square fit in the frequency domain, equation (6.7) can written in a generalized form as shown in equation (6.8).

$$Y(s) = \frac{b_1 s^{2N-1} + b_2 s^{2N-2} + ... + b_{2N}}{s^{2N} + a_1 s^{2N-1} + ... + a_{2N}} \tag{6.8}$$

$$Y(s) = \sum_{k=1}^{N} A_k \big(\frac{\beta_{1k}}{s - \alpha_{1k}} + \frac{\beta_{2k}}{s - \alpha_{2k}} \big) \tag{6.9}$$

By comparing equation (6.9) with equation (6.6) the modal parameters can be extracted [31] using the below equations:

$$\phi_k = cot^{-1}\big(\frac{1}{\sqrt{1 - \zeta_k^2}} \big(\frac{-Re(\beta_{1k}\alpha_{1k})}{-Re(\alpha_{1k})} - \zeta_k \omega_k \big) \big) \tag{6.10}$$

$$A_k = \frac{-Re(\beta_{1k})}{sin\phi_k} \tag{6.11}$$

$$\omega_k = |\alpha_{1k}| \tag{6.12}$$

$$\zeta_k = \frac{-Re(\alpha_{1k})}{\omega_k} \tag{6.13}$$

6.4 Least square fit of frequency domain model with DFT of system response

Mathematically, the discrete time Fourier Transform is written as,

$$Y[i] = \sum_{i=0}^{N} x(t) e^{\frac{-2\pi}{N} it}, i = 0, 1, ..., N \tag{6.14}$$

Where, $x(t)$ is the input signal for which the frequency response is to be obtained and N is the total number of samples in the input signal. The mapping of the resulting frequency response corresponding to frequency index, i to actual frequency can be written as $\omega_i = (2\pi i)$ where, $\omega_i \in [0, 2\pi]$.

According to the definition of the DFT, the plot of absolute value of the $Y[i]$ has peaks corresponding to the frequency component present in the input signal, which corresponds to particular frequency index, i mapped as $\omega_{i,k}$. From equation (6.5), the DFT producing peaks at $\omega_{i,k}$ are equal to the damped frequency of each mode in the measured data. The number of peaks in the DFT determines the order of the numerator and the denominator and number of its coefficients.

In order to capture the dominant energy of each of the mode, a curve is fitted for M points around each peak $\omega_{i,k}$ in the frequency spectrum of the input data. In [31], the value of M chosen should be a minimum odd integer nearest to $2f_cNT_s$, where f_c refers to the maximum frequency up to which the DFT can detect for peaks, usually 0.05Hz.

For the curve fitting to be performed and to capture dominant energy of each mode with M points can be done using (6.8) as

$$Y(j\omega_{i,M}) = \frac{b_1(j\omega_{i,M})^{2N-1} + b_2(j\omega_{i,M})^{2N-2} + ... + b_{2N}}{((j\omega_{i,M})^{2N}) + a_1(j\omega_{i,M})^{2N-1} + a_2(j\omega_{i,M})^{2N-3} + ... + a_{2N}} \tag{6.15}$$

$$(-\omega_{i,M})^N = \frac{b_1(j\omega_{i,M})^{2N-1} + b_2(j\omega_{i,M})^{2N-2} + ... + b_{2N}}{Y(j\omega_{i,M})} - a_1(j\omega_{i,M})^{2N-1} - a_2(j\omega_{i,M})^{2N-3} - ... - a_{2N} \quad (6.16)$$

Let

$$B_{i,M} = \frac{b_1(j\omega_{i,M})^{2N-1} + b_2(j\omega_{i,M})^{2N-2} + ... + b_{2N}}{Y(j\omega_{i,M})} \quad (6.17)$$

$$A_{i,M} = -a_2(j\omega_{i,M})^{2N-3} - ... - a_{2N} \quad (6.18)$$

From equating the real and imaginary parts of equation (6.16) around each point in M, the numerator and denominator coefficients a and b can be extracted as

$$W = CX \quad (6.19)$$

where,

$$W = \begin{bmatrix} -\omega_{1,1}^2 & 0 & -\omega_{1,2}^2 & 0 & ... & -\omega_{1,M}^2 & 0 \end{bmatrix} \quad (6.20)$$

$$C = \begin{bmatrix} C_a & C_B \end{bmatrix} \quad (6.21)$$

and

$$C_b = \begin{bmatrix} Re(B_{1,1}) & Im(B_{1,1}) & ... & Re(B_{1,M}) & Im(B_{1,M}) & ... & Re(B_{k,M}) & Im(B_{k,M}) \end{bmatrix} \quad (6.22)$$

$$C_a = \begin{bmatrix} Re(A_{1,1}) & Im(A_{1,1}) & ... & Re(A_{1,M}) & Im(A_{1,M}) & ... & Re(A_{k,M}) & Im(A_{k,M}) \end{bmatrix} \quad (6.23)$$

$$X = \begin{bmatrix} a_1 & a_2 & ... & a_{2k} & b_1 & b_2 & ... & b_{2k} \end{bmatrix} \quad (6.24)$$

The main advantage of applying frequency domain technique in general is the ease of identifying the main oscillatory modes based on highest peak in the DFT plot of the system response, provided that the modes are not closely spaced to each other.

6.5 Application of parametric DFT on synthetic signal

For validating the parametric DFT technique, a synthetic signal is generated using equation (6.5) with the modal parameters as shown in Table (6.1):

Table 6.1: Synthetic signal modal parameters

Mode	Amplitude	Phase	Natural Frequency(Hz)	Damping ratio
1	0.5	0	0.5	0.08
2	0.7	0	0.6	0.08

For this simulation, the value of $M = 9$ with an $f_c = 0.1Hz$ and then data is synthesized for 30 seconds and sampled at 0.1 seconds. In order to have better resolution in frequency in the DFT, the data is zero padded and the DFT is carried out for N =1000 points. The synthetic signal is added with random white Gaussian noise with zero mean. Figure (6.3) shows the DFT of synthetic signal and Figure (6.4) shows the synthetic signal generated for 30 seconds with 20 dB of noise.

It can be seen from the Figure (6.3) that there are two distinct peaks occurring at $\omega_1 = 0.49$ rad and $\omega_2 = 0.59$ rad which indicates the presence of two modes, therefore N =2. Note that the ideal DFT of a sine or cosine is an impulse occurring at their corresponding frequencies, in this case at 0.49 and 0.59 radians. However, Figure (6.3) shows that a part of the energy from impulses is lost across various frequencies due to poor side lobe attenuation of the rectangular window.

Figure (6.3) also shows the fitted frequency spectrum with M =9 points around

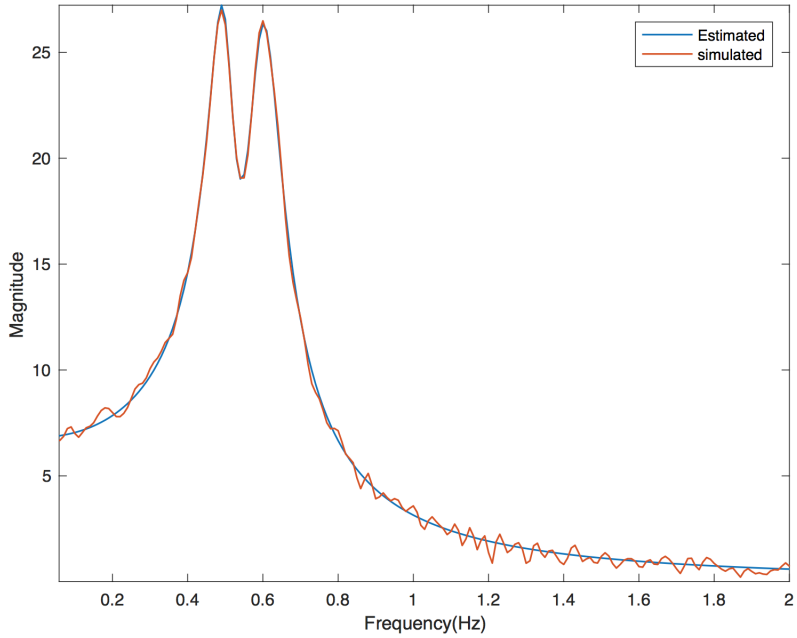

Figure 6.3: Frequency spectrum of the synthesized signal with 20db noise

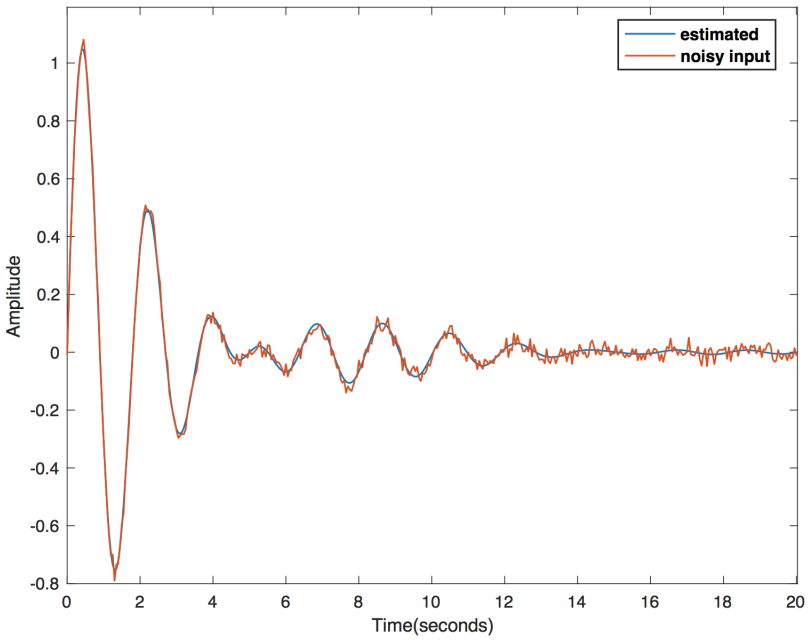

Figure 6.4: Frequency spectrum of the synthesized signal with 20db noise

each peak in the frequency spectrum and the least square fit is performed as discussed in Section (6.4). Tables (6.2) and (6.3) show the estimated mode parameters for mode 1 and 2 respectively with a noise level of 20 dB and 10 dB.

Table 6.2: Mode 1 parameters in synthetic signal

Mode	Amplitude	Phase	Natural Frequency(Hz)	Damping ratio
No noise	0.503	0.002	0.499	0.0805
20 db[1]	0.501/0.006	0.007/0.03	0.501/0.001	0.0801/0.001
10db[1]	0.507/0.02	0.005/0.03	0.499/0.002	0.0806/0.002

Table 6.3: Mode 2 parameters in synthetic signal

Mode	Amplitude	Phase	Natural Frequency(Hz)	Damping ratio
No noise	0.695	0.001	0.599	0.0795
20 db[1]	0.704/0.01	0.005/0.03	0.599/0.001	0.0803/0.001
10db[1]	0.688/0.02	0.004/0.03	0.599/0.003	0.0789/0.001

Comparing Tables (6.2) and (6.3) with the actual modal parameters from Table (6.1), it can be seen that the modal parameters are estimated within acceptable ranges for noisy signal. During the application to actual system, the estimated modal parameters obtained by fit in frequency domain are verified by time domain fit with the considered system response.

[1]Represented as Mean/ SD for 20 simulations

6.6 Case study: IEEE 14 bus system

Figure (6.5) shows the IEEE 14 bus with 5 generator system which is considered as a case study for frequency domain technique. In this illustration, different system responses are chosen to track different eigenvalue pairs as the main oscillatory mode for stability purposes. The dynamic model parameters of all the generators is shown in Appendix B.

A 3-phase to ground fault is applied at bus 6 at time t =1s and cleared at t =1.1s and the simulation is carried out till t =5s using PowerWorld simulator.

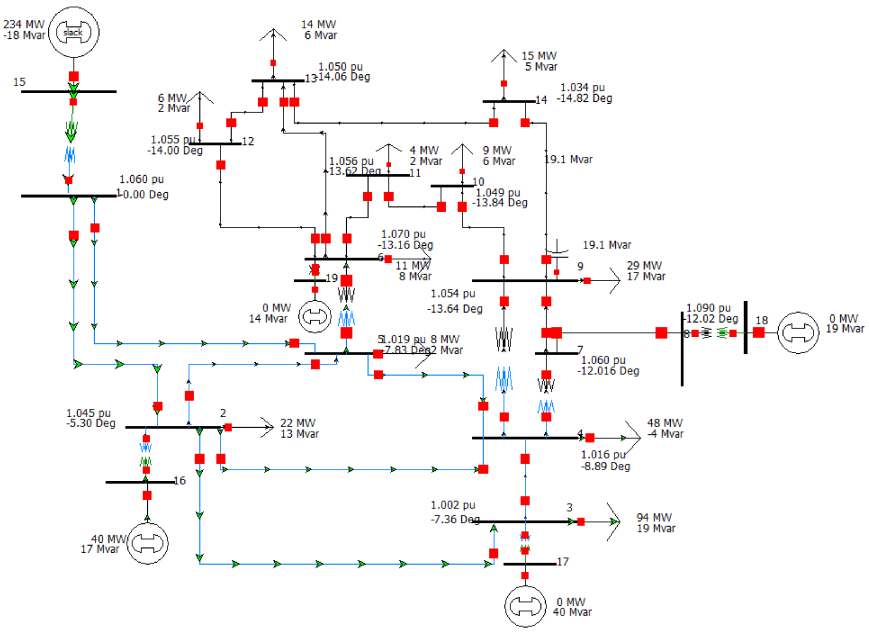

Figure 6.5: IEEE 14 bus 5 generator system [32]

The terminal voltage and generated power of generator 19 are selected for analysis and the obtained data is shown in Figure (6.6) and Figure (6.7).

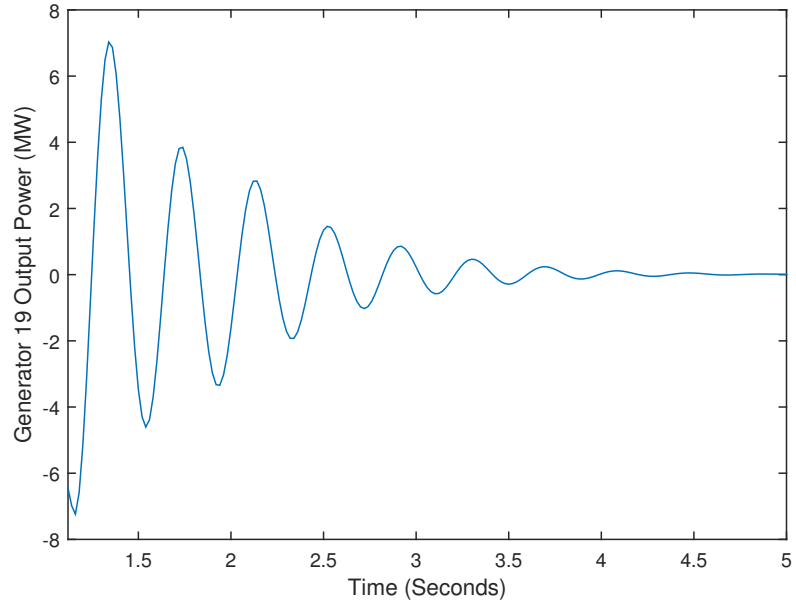

Figure 6.6: Simulated output power of Generator 19

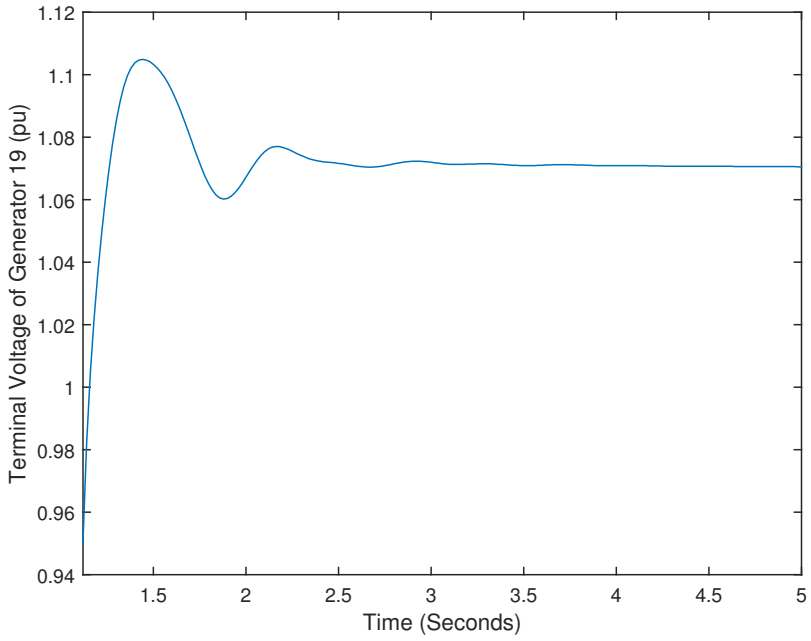

Figure 6.7: Simulated terminal voltage of Generator 19

The simulated data produced from the simulator is generated with a sample time of 0.04s, and before the DFT is carried out, the dc component is removed with the known steady state value of each signal followed by zero padding to have better frequency resolution. Figures (6.8) and (6.9) show the DFT of the terminal voltage and output power generated by generator 19 with the fitted frequency response using the parametric DFT technique.

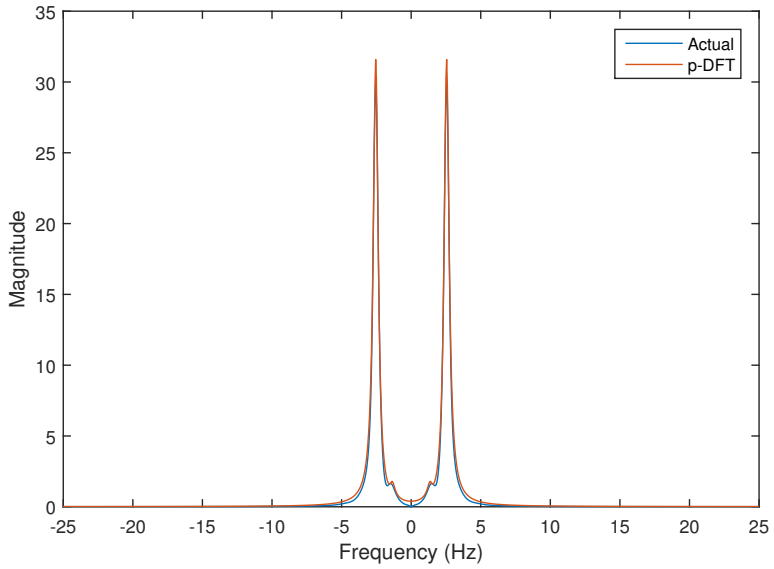

Figure 6.8: Fitted frequency spectrum of output power

For the terminal voltage, the curve fitting is performed around the two peaks at $\omega_{1,1}$=1.3Hz and $\omega_{1,2} = 2.5Hz$ with M =11 points and for the generated power at $\omega_{2,1}$=1.45Hz and $\omega_{2,2}$= 2.5Hz with M = 11 points. Figures (6.10) and (6.11) show the actual data and that the estimated response from the modal parameters obtained by fitting in frequency domain indicating the estimated modal parameters provide better fit in time and preserve the frequency properties of the signal.

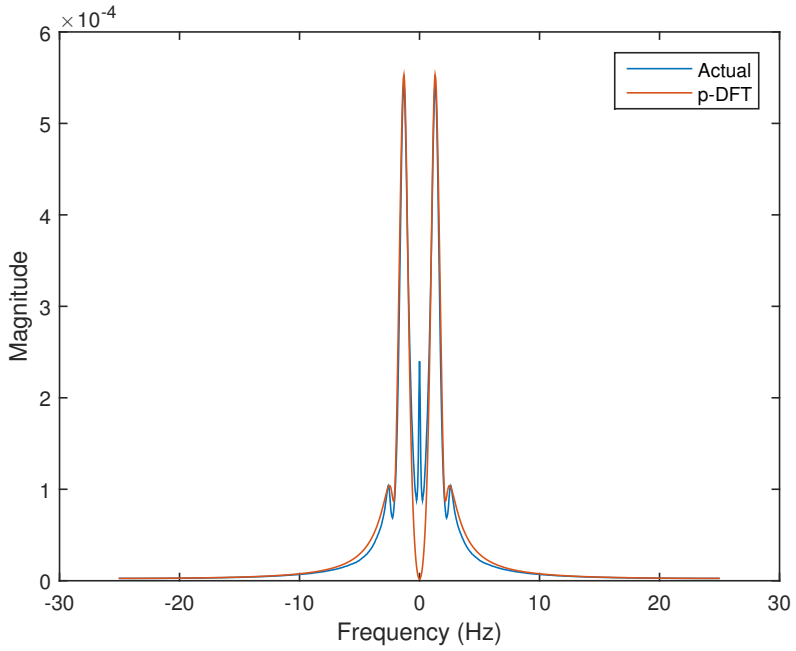

Figure 6.9: Fitted frequency spectrum of terminal voltage

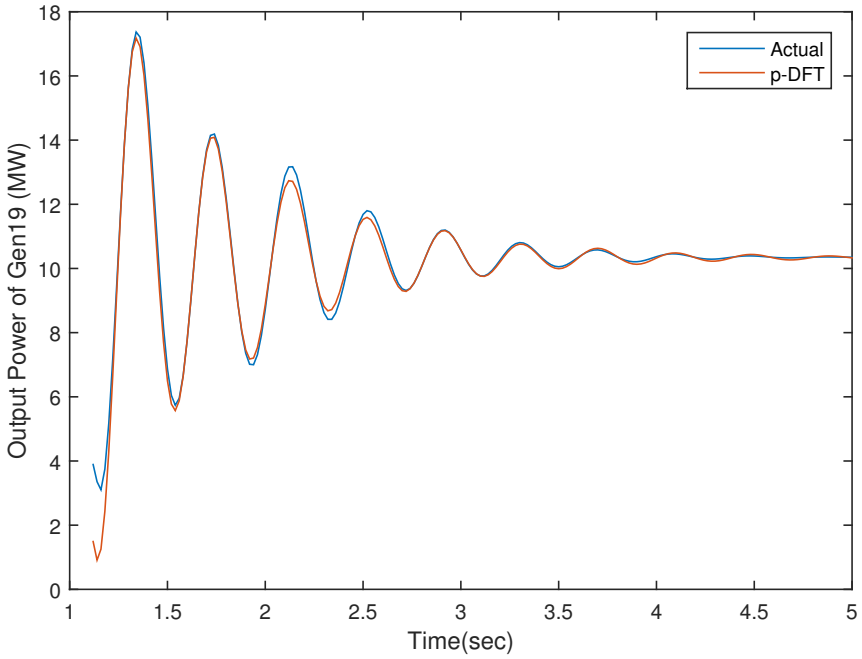

Figure 6.10: Output power fit in time

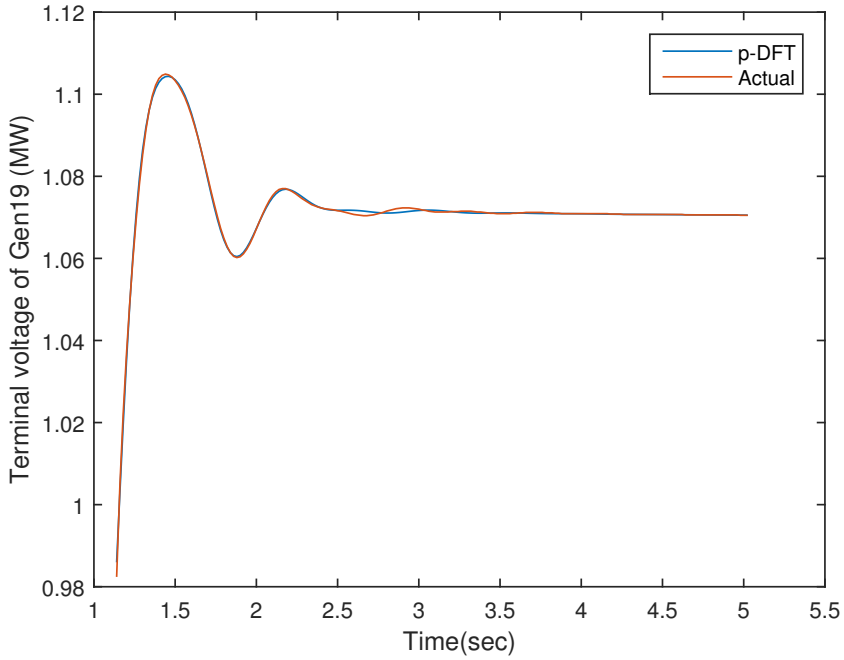

Figure 6.11: Terminal voltage fit in time

6.6.1 Analysis of extracted modal parameters

The extracted modal parameters of the output power of Generator 19 are shown in Table (6.4).It is observed that mode 1 has very high amplitude and low damping ratio, which indicates that mode 1 is the main dominating mode causing oscillation. Since mode 2 has very low amplitude and high damping ratio, it lasts less than a second and therefore cannot be the main dominating mode.

Similarly, for modal parameters from the voltage shown in Table (6.5), it can be seen that mode 1 has very high amplitude but very high damping ratio when compared to mode 2. However, mode 2 has very low amplitude relative to its frequency, which indicates that mode 1 is the main dominating mode and mode 2 is the less critical mode.

Table 6.4: Modal parameters of output power using p-DFT

Mode	Amplitude	Phase	Natural Frequency(Hz)	Damping ratio
1	42	-150.91	2.541	0.0713
2	3	-19.01	1.374	0.1501

Table 6.5: Modal parameters of terminal voltage using p-DFT

Mode	Amplitude	Phase	Natural Frequency(Hz)	Damping ratio
1	4.742	-41.77	1.264	0.4135
2	0.367	-154.63	2.411	0.1829

Therefore, by choosing the output power and terminal voltage as the input signal for measurement based analysis, the 2.541 Hz and 1.374 Hz components can be tracked for monitoring/ stability studies.

6.6.2 Comparison of results with model based modal analysis

In order to verify the obtained modal parameters and estimated main oscillatory mode, the 12×12 linearized system model of the IEEE 14 bus system is obtained using PowerWorld and modal parameters with their participation factors are calculated for both output power and terminal voltage using MATLAB. Table (6.6) and Table (6.7) show the obtained modal parameters for output power and terminal voltage respectively.

It can be seen from Table (6.6) that 94% of the energy of the measured signal is made up of the 2.539 Hz component with a damping of 0.081 whereas only 3% for

Table 6.6: Modal parameters of output power using model based modal analysis

Mode	Natural Frequency(Hz)	Damping ratio	Weighted % of mode
1	2.539	0.081	94.47
2	1.578	0.147	3.65

Table 6.7: Modal parameters of terminal voltage using model based modal analysis

Mode	Natural Frequency(Hz)	Damping ratio	Weighted % of mode
1	2.448	0.143	14.55
2	1.367	0.345	71.481

1.57 Hz component which indicates that the majority of the oscillation in the signal is made up of the 2.539 Hz component which is the main oscillatory mode.

Similarly from Table (6.7), 71% of the energy of the 1.367 Hz component and 14% of the 2.448 Hz component can be seen as oscillation in the terminal voltage. Therefore 1.367 Hz component is the main oscillatory mode with the highest contribution and 2.448 Hz with 14% component can be considered as relatively critical mode when compared to the 3% of 1.578 Hz component.Therefore, the extracted modal parameters analyzing oscillatory data is the same as the results of the model based modal analysis.

The knowledge of tracking a particular eigenvalue pair by selecting different system responses can be obtained using the eigenvalues participating with each of the state variable. Therefore, the model based modal analysis is important in order to study the frequency properties of the system in order to effectively track modes

using measurement based technique.

6.7 Disadvantages of frequency domain techniques

Frequency domain techniques is mainly based on the number of distinct peaks in the DFT of the system response. In the case of larger system with several frequency components, the peaks occurs with larger width due to aliasing. Figure (6.12) shows the DFT of the rotor angle of generator 39 from the larger IEEE 39 bus system, where the width of lobes is too wide indicating the possible overall of closely spaced frequencies. Since the p-DFT is based on the magnitude of the DFT, the estimated modal parameters shows better fit in time.

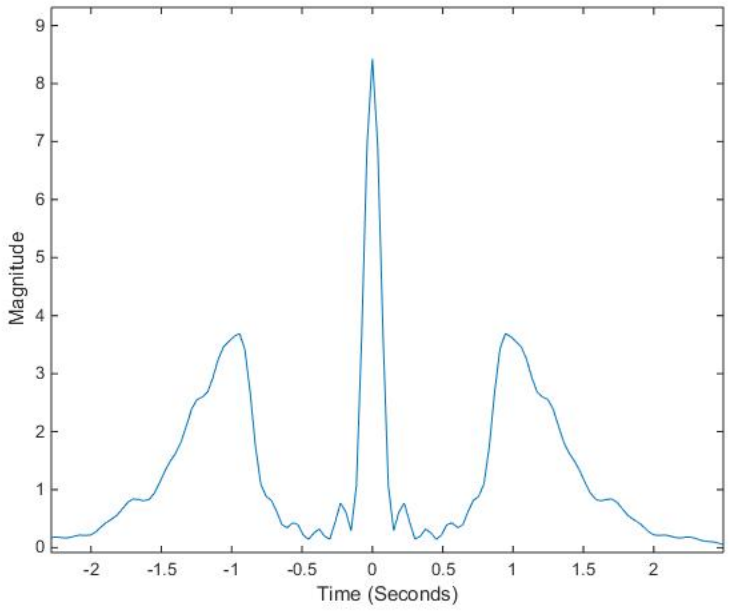

Figure 6.12: DFT plot of rotor angle oscillation of Generator 39 from IEEE 39 bus system

On the other hand, the frequency domain technique could be applied to relatively less larger systems and the main oscillatory modes can be simultaneously identified by the highest peak in DFT plot unlike a time domain technique where the modes are usually split for better in time domain. However, the time domain technique is suitable for larger systems where frequency domain techniques cannot be applied.

6.8 Conclusion

In this chapter, the method of extracting modal parameters in frequency domain using parametric DFT techniques is discussed. The p-DFT is validated using a synthetic signal with two levels of noise and then illustrated using IEEE 14 bus system. Using IEEE 14 bus system it is also shown that different eigenvalue pairs can be tracked by choosing different system responses for monitoring. The results of the extracted modal parameters of Generator 19 are also compared with the model based modal analysis and it is found that both results are more or less the same. The frequency domain techniques are compared and contrasted with the time domain techniques and the disadvantage of frequency domain techniques are discussed.

Chapter 7

Measurement based Power System Stabilizer Tuning

7.1 Introduction

In this chapter, the method of tuning/ re-tuning a power system stabilizer (PSS) based on extracted modal parameters is discussed and illustrated using the IEEE 39 bus system. In Section 7.2, the parameters in PSS transfer function are discussed and the method of tuning a PSS is discussed. In Section 7.3, the measurement based PSS tuning for a single machine infinite bus (SMIB) system is applied. The effect of exciter and stabilizer gain in terms of damping ratio of the resulting main oscillatory mode is also analyzed in Section 7.3. In Section 7.4, IEEE 39 bus system is considered as a case study and PSS of all the 10 generators are re-tuned using measurement based technique and it is shown that the re-tuned PSS provides better damping compared to the PSS of IEEE 39- bus system. Section 7.5 concludes the chapter.

7.2 Measurement based PSS re-tuning

Based on the output only model obtained using Prony/ ERA/ Matrix pencil method, the PSS of each generator can be re-tuned in order to obtain better performance [33]. Equation (7.1), shows the parameters in the transfer function of a PSS to be tuned.

$$H(s) = K\left(\frac{T_W s}{1+T_W s}\right)\left(\frac{1+T_1 s}{1+T_2 s}\right)\left(\frac{1+T_3 s}{1+T_4 s}\right) \tag{7.1}$$

where,

T_W is the washout time constant and is usually set to 10 seconds to allow for inter-area modes and filter out torsional modes.

K is the gain of the PSS.

T_1, T_2, T_3, T_4 are the lead compensator time constants which needs to be calculated based on the modes in the oscillation.

With the known output only transfer function of the system, $G(s)$, the closed loop transfer function can be represented as,

$$G_0(s) = \frac{G(s)}{1 - G(s)H(s)} \tag{7.2}$$

Using the pole placement method, the mode with the least damping ratio λ, can be replaced with a mode with higher damping ratio λ_0, by satisfying the stability criterion as,

$$1 - G(\lambda_0)H(\lambda_0) = 0 \tag{7.3}$$

The above technique does not change the frequency of oscillation but increases the damping ratio by moving the eigenvalue towards the left half of the s-plane. The

time constants of the PSS can be calculated by

$$T_2 = \frac{1}{2\pi f\sqrt{\alpha}} \tag{7.4}$$

$$T_1 = \alpha T_2 \tag{7.5}$$

where, α is the scaling factor which is usually chosen to be a value 6-10. To have a scaling factor for a desired damping ratio, scaling factor can be obtained from the compensation phase computed from (7.3) as,

$$\phi = arg(\frac{1}{G_0(\lambda_0)}) \tag{7.6}$$

A single phase lead block can compensate up to 45 degrees, therefore, a number of compensation blocks can be connected in series if the compensation angle is greater than 45 degree [34]. The scaling factor for each phase lead block can be calculated as

$$\alpha = \frac{1 - sin(\phi)}{1 + sin(\phi)} \tag{7.7}$$

The gain of the PSS can be calculated either by choosing $1/3^{rd}$ of the least maximum gain causing instability or can be calculated using root locus for achieving a specific damping ratio.

7.3 PSS tuning for single machine infinite bus system

Figure (7.1) shows the single machine infinite bus system with an exciter system parameters shown in Appendix A. A fault is introduced at bus 3 at t =0 and line 2-3 is removed at t =0.5s.

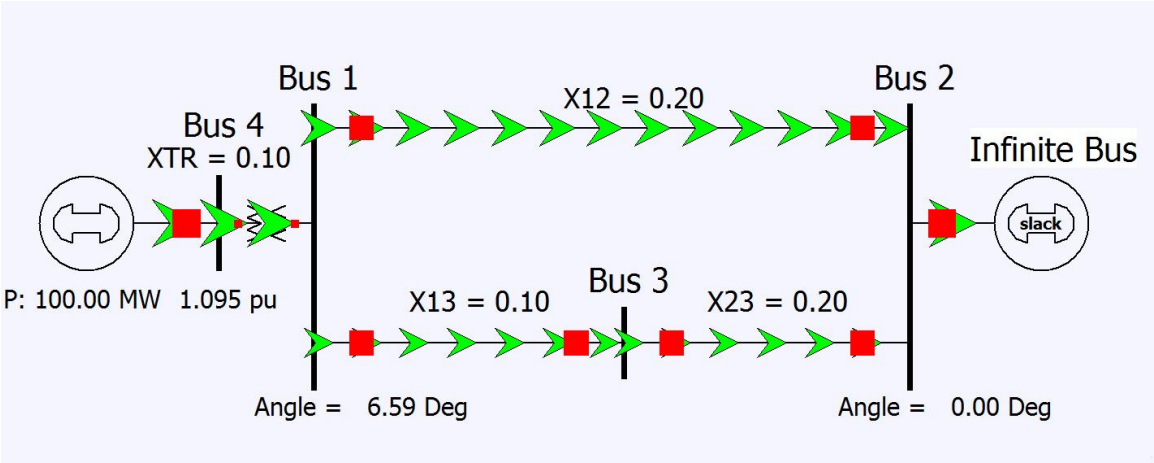

Figure 7.1: Single machine infinite bus system

The oscillation of the rotor angle of the SMIB without the PSS is calculated as 1.602 Hz with a damping ratio of 3.5%. Using eigenvalue realization technique and the output only model, the PSS parameters are calculated using the method discussed in Section (7.2) and shown in Table (7.1).

Table 7.1: Parameters of measurement based tuning of PSS

K	4.65
T_1, T_3	0.2499
T_2, T_4	0.0395

The PSS is tuned to have 15% damping of the 1.602 Hz component with $\alpha = 6.328$. The generator rotor angle and speed with and without PSS are shown in Figures (7.2) and (7.3) respectively. It can be seen that the first half cycle is required for PSS to detect the presence of oscillation and improve the damping. In addition, it can be seen that there is no change in frequency of oscillation as discussed in Section (7.2).

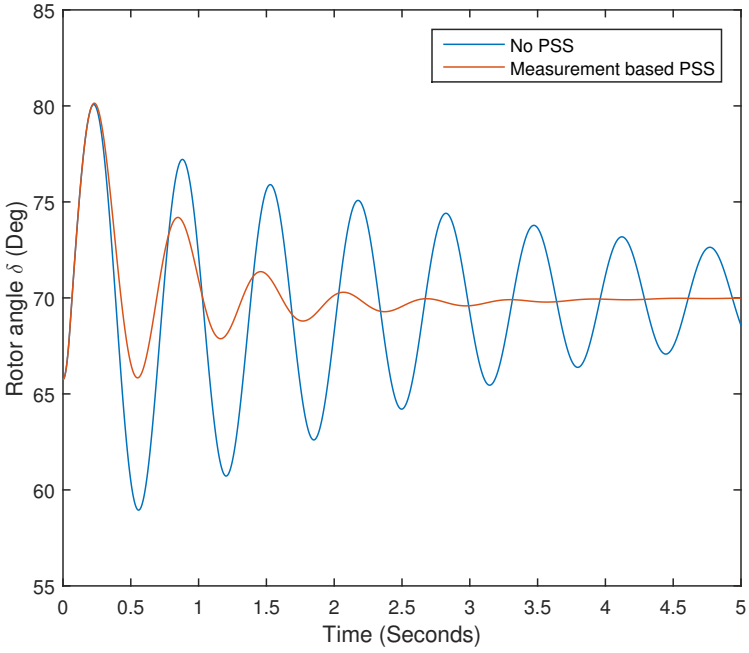

Figure 7.2: Rotor angle of generator with and without PSS

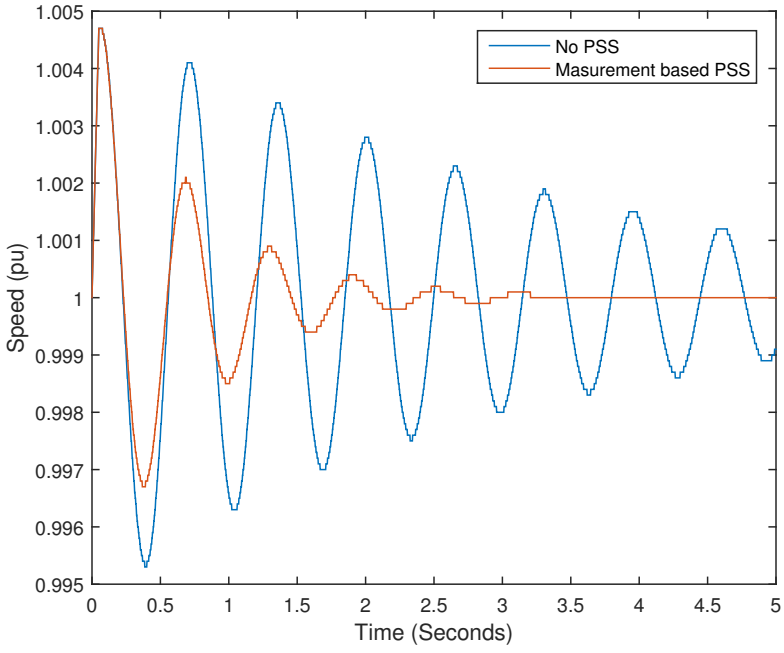

Figure 7.3: Speed of generator with and without PSS

7.3.1 Effect of exciter gain and stabilizer gain

With the addition of PSS, the increase in exciter gain does not cause instability. Instead it increases the damping ratio of the oscillation to a maximum value co-responding to the stabilizer gain as illustrated in Figure (7.4) and Table (7.2). Therefore, a PSS gain calculated for a set point damping ratio using an output only model with a reduced exciter gain will not result in a desired damping ratio in the actual system.

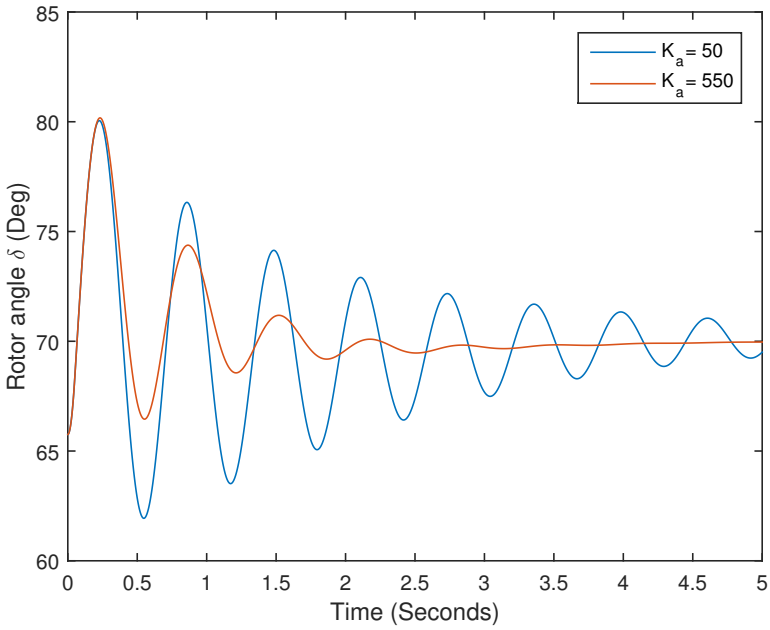

Figure 7.4: Effect of exciter gain on PSS performance/ stability

With the increase in the stabilizer constant, the damping is increased up to a particular value beyond which additional control modes are introduced. A further increase in stabilizer gain causes a reduction of control mode damping ratios as shown in Figure (7.5) and Table (7.3).

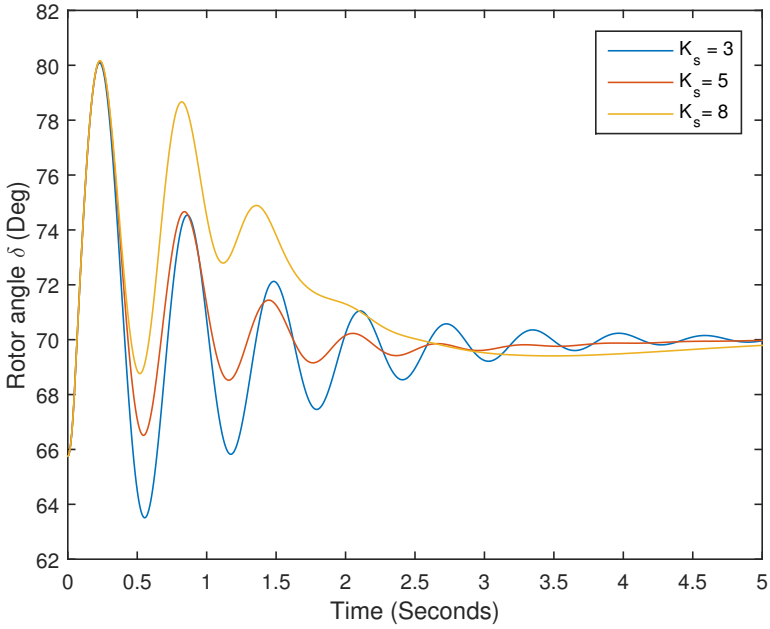

Figure 7.5: Effect of change in PSS gain on stability

Table 7.2: Effect of damping ratio of main oscillatory mode on exciter gain

K_a	Frequency(Hz)	Damping ratio
50	1.602	5.087%
150	1.602	8.886%
350	1.586	16.607%
550	1.524	16.905%

Table 7.3: Effect of damping ratio of main oscillatory mode on PSS gain

K_s	Frequency(Hz)	Damping ratio
3	1.608	9.384%
5	1.605	15.826%
8	1.55	30.175%
	0.14	15.32%

7.4 Case study: IEEE 39 bus system

The IEEE 39 bus system shown in Figure (7.6) is considered for re-tuning of the PSS parameters of all the 10 generators using the method discussed in Section (7.2). The system parameters are shown in Appendix C and the time domain simulations are carried out using PowerWorld. A 3-phase to ground fault in bus 16 at $t = 0$ is cleared at $t = 0.5$ seconds and the simulation is carried out for 10 seconds.

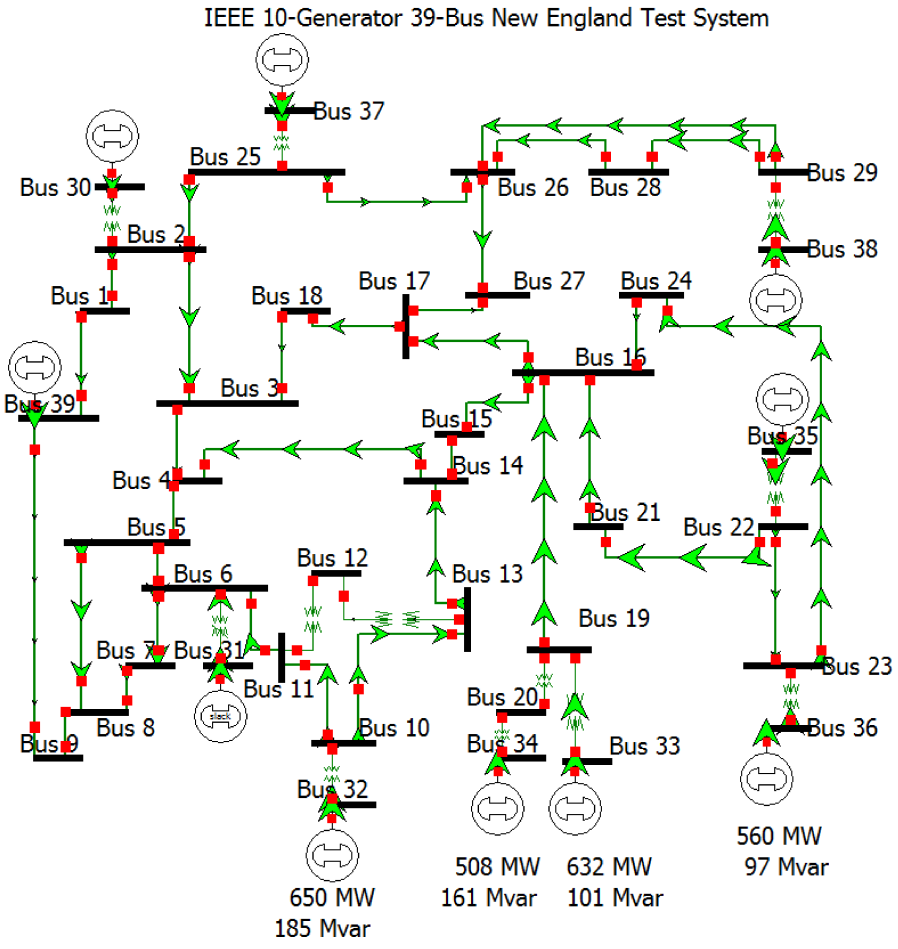

Figure 7.6: IEEE 39 bus test system [27]

For each of the 10 generators present in the 39 bus system, the PSS is tuned with a preset value of time constants and gains such that the center frequencies of each lead block are present in low frequency (0.1 - 0.5 Hz) and local frequency (0.9 - 1.5 Hz). In order to have optimal PSS tuning using the actual measurement of the system response, the time domain simulation is carried out without any PSS which resulted in instability. The obtained modal properties for each generator are shown in Table (7.4).

Table 7.4: Main dominating mode and unstable mode without PSS

Generator no.	Largest residue mode (Hz)	Unstable mode (Hz)
30	0.474	0.366
31	0.946	0.268
32	0.802	0.156
33	0.969	0.514
34	0.67	0.4
35	1.127	0.42
36	1.14	0.419
37	1.16	0.274
38	1.041	0.801
39	0.685	0.875

The lead blocks of the PSS of each generator are tuned such that the center frequencies are equal to the main dominating mode and unstable mode. For generators 30, 34 and 39 both the lead blocks are tuned to the unstable mode due to very high compensation angle required to move it to the left half of the s-plane. The parameters of the exciter and generators are unchanged. Table (7.5) shows the PSS time constants after re-tuning.

Table 7.5: Re-tuned PSS parameters

Generator no.	T_1	T_2	T_1	T_2	K_s
30	1.06	0.160	1.375	0.137	3.46
31	1.878	0.222	0.5320	0.053	4.8
32	3.226	0.036	0.629	0.076	3.78
33	2.978	0.338	0.629	0.063	5.0
34	1.258	0.153	0.534	0.067	3.8
35	1.198	0.119	1.198	0.119	7.0
36	1.198	0.119	1.198	0.119	4.5
37	1.837	0.229	0.434	0.0434	5.5
38	0.628	0.079	0.503	0.053	3.0
39	5.0000	0.6	0.7190	0.0808	8.0

The time domain simulation is carried out using PowerWorld and the rotor angle and speed oscillation are shown in Figures (7.7)- (7.10).

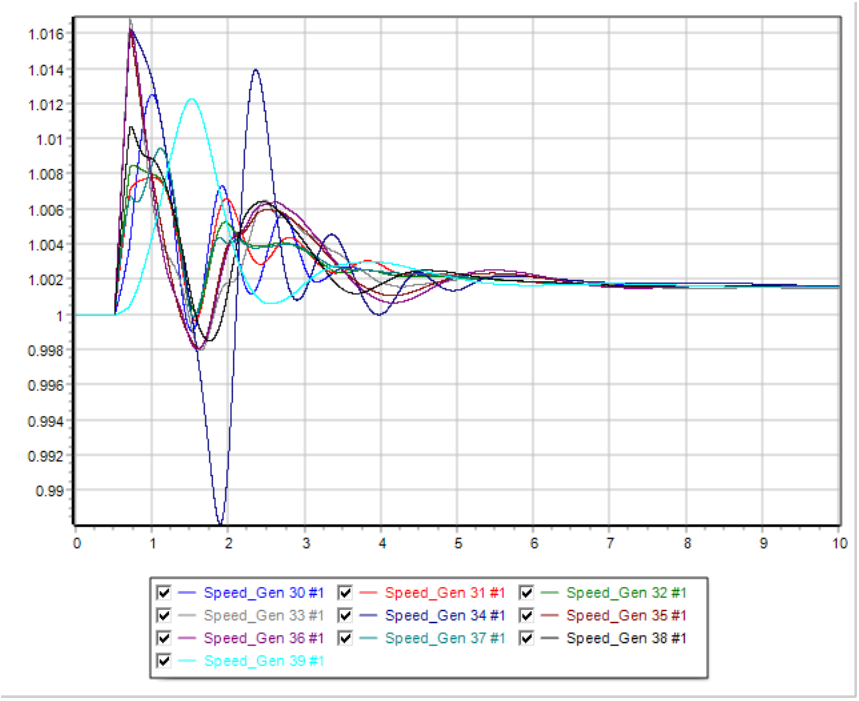

Figure 7.7: Speed of generators with measurement based PSS tuning

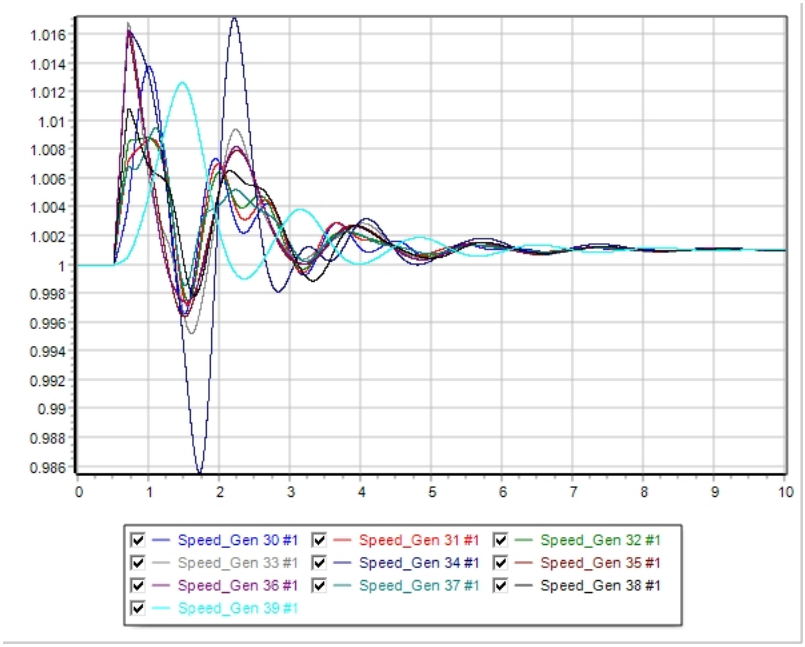

Figure 7.8: Speed of generators with PSS parameters of 39 bus test system

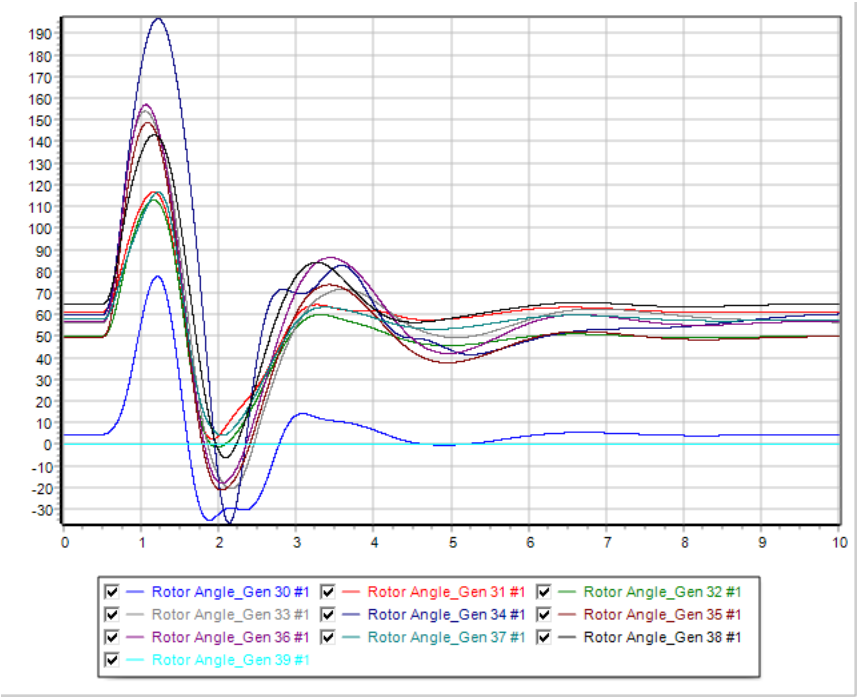

Figure 7.9: Rotor angle of generators with measurement based PSS tuning

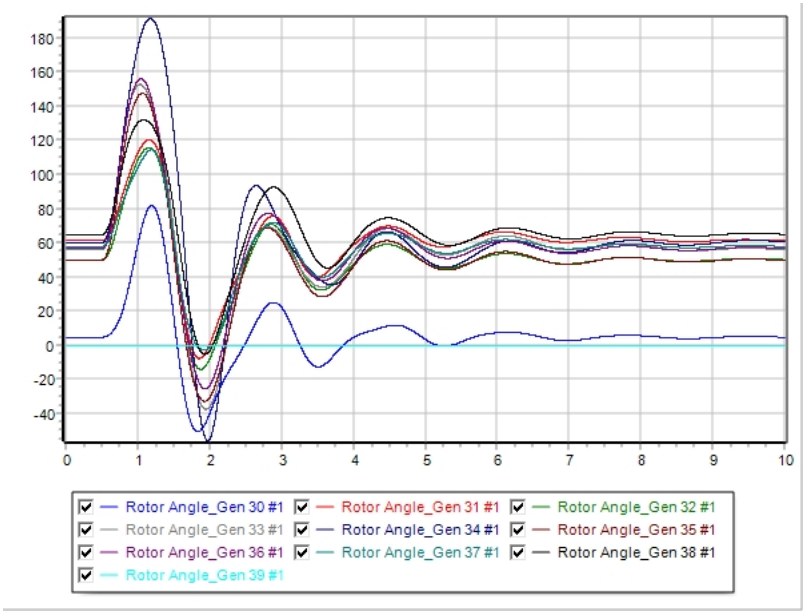

Figure 7.10: Rotor angle of generators with PSS parameters of 39 bus test system

It can be seen that the oscillation in frequency are highly damped in Figure (7.7) when compared to the performance of the conventional PSS of 39 bus system shown in Figure (7.8). Moreover the rotor angle oscillations of the re-tuned PSS is of low frequency oscillation with higher damping as shown in Figure (7.9) and the conventional PSS produces poor damping with higher frequency of oscillation.

Table 7.6: Performance comparison of 39 bus PSS and measurement based PSS on speed of Generator 39

	Mode no.	Mode frequency(Hz)	Damping ratio(%)
39 Bus PSS	1	0.598	17.38
parameters	2	1.272	12.609
Measurement based	1	0.353	35.35
PSS tuning	2	0.923	18.44

Table 7.6 shows the main oscillatory modes of the slack generator 39. It can be seen that measurement based PSS tuning have main dominating modes with higher damping ratio than the modes produced by the PSS in the 39 bus system. The decrease in the frequency is due to the movement of the pole along the real axis (damping ratio) also causes movement of the pole along the imaginary axis (frequency) depending on the root locus of the overall pole and zero of the system and the corresponding gain of the PSS.

The improved damping is due to the resulting eigenvalues on the far left of the s-plane indicating the power system is more stable for the same type of disturbance. This is one of the important application in power system stability using the modal

parameters extracted from the measurement based modal analysis.

7.5 Conclusion

In this chapter, the method of measurement based PSS tuning/ re-tuning is discussed and illustrated using SMIB system. The effect of exciter gain and stabilizer gain are analyzed in terms of damping ratio of the resulting eigenvalues of the system with a stabilizer. The PSS of IEEE 39 bus system is re-tuned using measurement based technique. It is shown that tuning the PSS to specific frequencies based on the obtained modal parameters from measurement-based techniques showed better damping when compared to that of the damping provided by the PSS of the 39 bus system.

Chapter 8

Conclusion and Future Work

8.1 Conclusion

In this thesis, an alternative approach is proposed to extract modal parameters of the power system using the obtained time domain response of the system. Three types of time domain techniques namely, Prony analysis, eigenvalue realization and matrix pencil method are discussed and applied on IEEE 39 bus system. The extracted modal parameters were compared with the parameters obtained using conventional model based technique. As a frequency domain based technique, parametric DFT technique is discussed and compared with non-parametric form of DFT technique and illustrated with IEEE 14 bus system. The shortcomings of frequency domain technique over the time domain techniques are also discussed.

Lastly, with the extracted modal parameters, tuning/ re-tuning of PSS is illustrated and it is shown that the re-tuned PSS provides better damping when compared to the nominal PSS of IEEE 39 bus system.

8.2 Contribution of the research

- Various types of power system stability problems and importance of the system operating parameters, system network parameters and gain of the exciter system on the stability of the system are studied in detail.

- Three types of time domain techniques namely Prony analysis, eigenvalue realization and matrix pencil method are studied and illustrated using IEEE 39 bus system.

- A parametric form of DFT technique is studied and illustrated using IEEE 14 bus system and its shortcomings on time domain technique is discussed.

- Using a special case SMIB, it is shown that a mode with high participation factor is not the main mode of interest in stability studies at all times. Using the larger 39 bus system, it is shown that only one eigenvalue pair out of many eigenvalues is excited by a particular disturbance. Using a 14 bus system, monitoring/ tracking of different main oscillatory mode by choosing different system responses for measurement based technique is shown.

- A method of PSS tuning/ re-tuning is discussed and it is shown that the performance of re-tuned PSS from the extracted modal parameter is better than that of default PSS of test system.

8.3 Future work

In this thesis, extraction of modal parameters from the system response and re-tuning of PSS has been effectively discussed. The following study can be a possible future research related to the area of this thesis.

- Selection of proper probing signal for optimally extracting modal parameters.
- Extracting specific modes from the given probing signal with the knowledge of participation factors.
- Consider the differences in the dynamics of the PMU in capturing the transient region of the oscillation.
- Resolution limitation of PMU and its effect of different time and frequency domain techniques.
- A machine learning algorithm can be created for specific systems to identify main oscillating mode with a given preset value of damping ratio and amplitude.
- Application of these techniques and analysis on real power system oscillatory data.

References

[1] N. K. Dmitry, C. W. Taylor, and W. A. Mittelstadt, "Model validation for August 10, 1996 WSCC outage," *IEEE Transactions on Power Systems*, vol. 14, no. 3, Aug. 1999.

[2] P. Hunter, "India blackout highlights: Power gap, opportunities," *ENR: Engineering News-Record*, vol. 269, no. 5, pp. 12–17, Aug. 2012.

[3] P. Kundur, *Power system stability and control*. 1st edition, McGraw-Hill, NY, 1994.

[4] A. R. Messina, *Inter area oscillation in power system*. 1st edition, Springer publication, NY, 2009.

[5] P. Kundur *et al.*, "Definition and classification of power system stability ieee/cigre joint task force on stability terms and definitions," *IEEE Transactions on Power Systems*, vol. 19, no. 3, pp. 1387–1401, Aug. 2004.

[6] M. Gibbard, P. Pourbeik, and D. Vowles, *Small-signal stability, control and dynamic performance of power systems*. The University of Adelaide press, Adelaide, 2015.

[7] P. W. Sauer, and M. A. Pai, *Power system dynamics and stability.* 1st edition, Prentice Hall, NJ, 1998.

[8] PowerWorld simulator, Version 19, PowerWorld Corporation, Champaign, IL, USA, 2016.

[9] J. Glover, T. Overbye, and M. Sharma, *Power system analysis and design,* 5th edition, Cengage Learning, MA, 2012.

[10] Matlab version R2016b. Natick, Massachusetts: The MathWorks Inc, 2016.

[11] A. J. Jerri, *Advances in the gibbs phenomenon.* 1st edition, Sampling Publishing, NY, 2011.

[12] R. Bhaskar, M. L. Crow, E. Ludwig, K. T. Erickson, and K. S. Shah, "Nonlinear parameter estimation of excitation systems," *IEEE Transactions on Power Systems*, vol. 15, no. 4, pp. 1225–1231, Nov. 2000.

[13] "IEEE recommended practice for excitation system models for power system stability studies," IEEE *Std 421.5-2005 (Revision of* IEEE *Std 421.5-1992)*, pp. 1–93, Apr. 2006.

[14] A. Roth, D. Ruiz-Vega, D. Ernst, C. Bulac, M. Pavella, and G. Andersson, "An approach to modal analysis of power system angle stability," *2001 IEEE Porto Power Tech Proceedings*, vol. 2, no. 2, pp. 2–6, Sep. 2001.

[15] M. Parashar and J. Mo, "Real time dynamics monitoring system: Phasor applications for the control room," *42nd Annual Hawaii International Conference on System Sciences*, pp. 1–17, Jan. 2009.

[16] K. Bertels, *Hardware/ software co- design for hetero-genous multi-core platforms*. 1st edition, Springer Publishing, Delft, NL, 2012.

[17] D. Trudnowski, "Estimating electromechanical mode shape from synchrophasor measurements," *IEEE Transactions on Power Systems*, vol. 23, no. 3, pp. 1188–1195, Apr. 2008.

[18] North American Electric Reliability Council, *Review of selected 1996 electric system disturbances in north america*. [Online]. Available: `https://www.nerc.com/pa/rrm/ea/System%5C%20Disturbance%5C%20Reports%5C%20DL/1996SystemDisturbance.pdf`.

[19] Technical report: PES-TR15, "Identification of electro-mechanical modes in power systems," *IEEE power and energy society*, Jun. 2012.

[20] N. Zhou *et al.*, "Algorithm summary and evaluation: Automatic implementation of ringdown analysis for electromechanical mode identification from phasor measurements," *Pacific Northwest National Laboratory*, Feb. 2010.

[21] G. Liu and V. Venkatasubramanian, "Oscillation monitoring from ambient pmu measurements by frequency domain decomposition," *IEEE International Symposium on circuits and systems*, pp. 2821–2824, May. 2008.

[22] J. F. Hauer, "Application of prony analysis to the determination of modal content and equivalent models for measured power system response," *IEEE Transactions on Power Systems*, vol. 6, no. 9, pp. 1048–1056, Aug. 1991.

[23] J. N. Juang and R. S. Pappa, "An eigensystem realization algorithm for modal parameter identification and model reduction," *Journal of Guidance, Control, and Dynamics*, vol. 8, no. 9, Jul. 1985.

[24] I. Kamwa, R. Grondlin, E. J. Dickinson, and S. Fortin, "A minimal realization approach to reduced order modelling and modal analysis for power system response signals," *IEEE Transactions on Power Systems*, vol. 8, no. 3, pp. 1020–1029, Aug. 1993.

[25] J. Sanchez-Gansca and J. Chow, "Computation of low order models from time domain simulations using hankel matrix," *IEEE Transactions on Power Systems*, vol. 12, no. 4, pp. 1461–1467, Nov. 1997.

[26] T. K. Sarkar and O. Pereira, "Using the matrix pencil method to estimate the parameters of a sum of complex exponentials," *lEEE Antennas and Propagation Magazine*, vol. 37, no. 1, pp. 48–55, Feb. 1995.

[27] University of Cyprus, *Dynamic ieee test systems*. [Online]. Available: `http://icseg.iti.illinois.edu/ieee-14-bus-system/`.

[28] J. K. Hwang and Y. Liu, "Noise analysis of power system frequency estimated from angle difference of discrete fourier transform coefficient," *IEEE Transactions on Power Systems*, vol. 29, no. 4, pp. 1533–1541, Aug. 2014.

[29] A. V. Oppenheim and R. W. Schafer, *Discrete time signal processing*. 3rd edition, Pearson publication, NJ, 2010.

[30] Z. Tashman, H. Khalinia, and V. Venkatasubramanian, "Multi-dimensional fourier ringdown analysis for power systems using synchrophasors," *IEEE Transactions on Power Systems*, vol. 29, no. 2, pp. 731–741, Oct. 2014.

[31] J. K. Hwang and Y. Liu, "Identification of inter-area modes from ringdown data by curve-fitting in the frequency domain," *IEEE Transactions on Power Systems*, vol. 32, no. 4, pp. 842–851, Mar. 2017.

[32] University of Cyprus, *Dynamic ieee test systems*. [Online]. Available: `http://icseg.iti.illinois.edu/ieee-14-bus-system/`.

[33] G. Chen, Y. Sun, L. Cheng, J. Lin, W. Zhao, and C. Lin, "A novel pss-online re-tuning method," *Electric Power Systems Research*, vol. 91, pp. 87–94, Oct. 2012.

[34] S. Vemuri and B. Chowdhury, "Performance improvement of power system stabilizers using prony analysis," *International Journal of Power and Energy Systems*, vol. 28, no. 2, pp. 177–185, Oct. 2008.

Appendix A

Single machine infinite bus system data:

Steady state data:

Bus data:

Table A.1: Generator parameters used

Bus	Type	Voltage(pu)	Gen Power(MW)	Load power (MW)	load power (Mvar)
4	PV	1.095	100	0	0
1	Slack	1	-	0	0

Dynamic data:

Generator data:

H =3, D = R_a =0, X_d =2.1pu, X_q =0.5pu, $X_d^{'}$ =0.5pu, $X_q^{'}$ =0.2pu,$T_{d0}^{'}$ =7 seconds, $T_{q0}^{'}$ =0.75 seconds, X_l =0.15pu.

Exciter data: (IEEE AC1A)

Following is the exciter data used in chapter 2:

K_a =200, T_a =0.1 seconds, V_{rmax} =3pu, V_{rmin} =-3pu,T_e =0.08 seconds, K_e =0.01,K_f =0.01, T_f =1.0 seconds, E_1 =3.00, E_2 =4.00, $S(E_1)$ =0.03, $S(E_2)$ =0.1

Following is the exciter data used in chapter 3:

K_a =200, T_a =0.1 seconds, V_{rmax} =3pu, V_{rmin} =-3pu,T_e =0.06 seconds, K_e =0.05,K_f =0.15, T_f =1.0 seconds, E_1 =2.5, E_2 =2.5, $S(E_1)$ =0.03, $S(E_2)$ =0.1

Appendix B

IEEE 14 bus system data:

Figure (B.1) shows the IEEE 14 bus system considered for the frequency domain based modal extraction using parametric DFT technique.

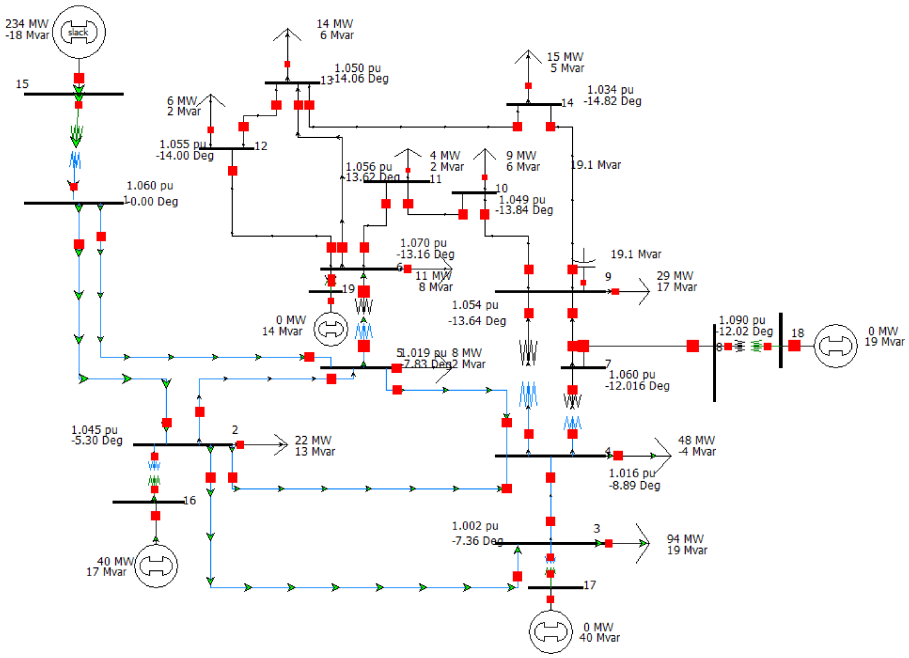

Figure B.1: IEEE 14 bus 5 generator system

The IEEE 14 bus system is a single area system with 14 buses, 5 generators generating 274.2 MW and 71.6 Mvar, 11 loads consuming 250 MW and 73.5 Mvar, 1 switched shunt generating 19.1 MW, 11 transmission lines. The base MVA and base voltages of the system are 100 MVA and 132 KV respectively.

The system load flow and dynamic data are obtained from the following online source: http://icseg.iti.illinois.edu/ieee-14-bus-system/

Appendix C

IEEE 39 bus data:

Figure (C.1) shows the IEEE 39 bus system considered for the time domain based modal extraction using eigenvalue realization technique.

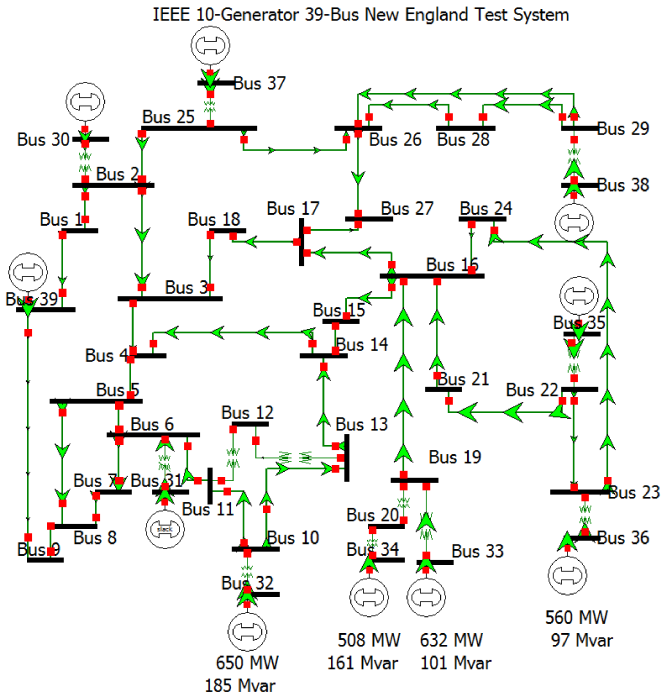

Figure C.1: IEEE 39 bus test system

The IEEE 39 bus system is a single area system with 39 buses, 10 generators generating 6191.3 MW and 837.3 Mvar, 31 loads consuming 6141.4 MW and 1408.9 Mvar, 34 transmission lines. The base MVA and base voltages of the system are 100 MVA and 1 KV respectively.

The system load flow and dynamic data are obtained from the following online source: http://icseg.iti.illinois.edu/ieee-39-bus-system/

Publications:

Conferences:

S. Rajmurugan and B. Jeyasurya, "*Identification of Power system electro-mechanical modes using time domain techniques*", 26th Newfoundland Electrical and Computer Engineering Conference, St. Johns, NL, Nov 2017.

S. Rajmurugan and B. Jeyasurya, "*Modal Identification of Power System Oscillation using parametric DFT technique*", Electrical Power and Energy Conference, Saskatoon, SK, Oct 2017.

Posters:

S. Rajmurugan and B. Jeyasurya, "*Power system stability enhancement using measurement based modal parameter estimation*", FEAS annual research poster day, 30th May 2018.

S. Rajmurugan and B. Jeyasurya, "*Oscillation monitoring technique for pre-detection of power system instability*", FEAS annual research poster day, 26th April 2017.